

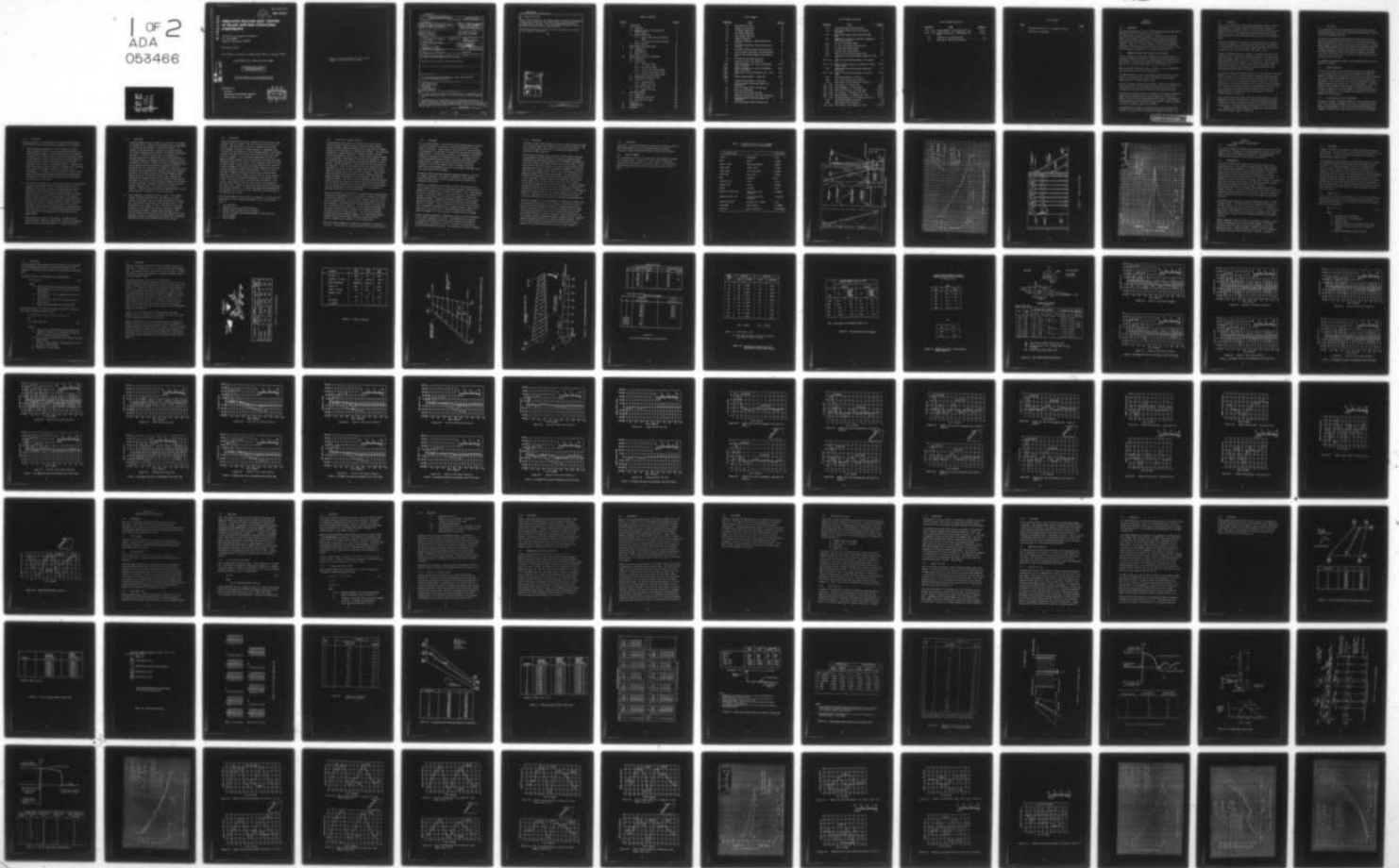
AD-A053 466

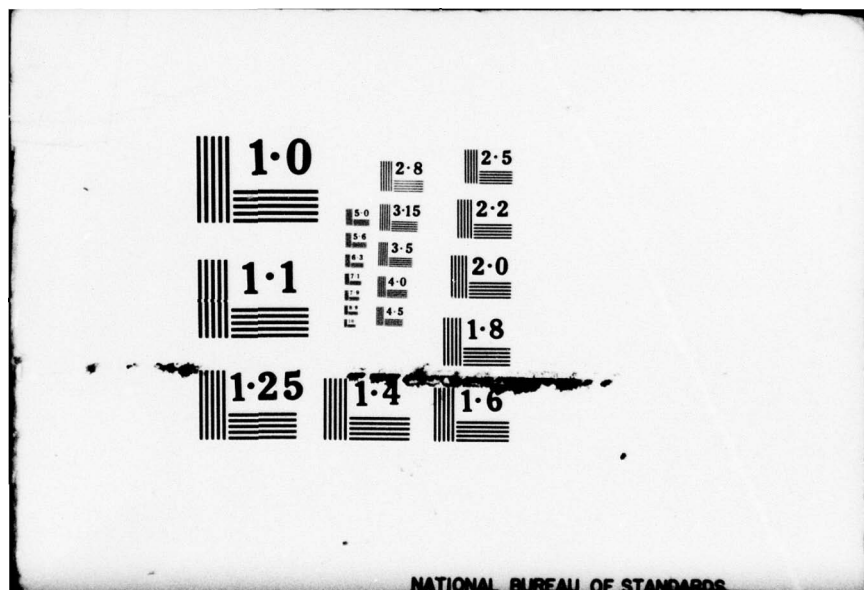
BOEING AEROSPACE CO SEATTLE WASH
SIMULATED NUCLEAR GUST TESTING OF MAJOR AIRPLANE STRUCTURAL COM--ETC(U)
JAN 77 D M ECKBLAD, N E FUNSTON

F/G 19/4
DNA001-76-C-0367
DNA-4243F
NL

UNCLASSIFIED

1 of 2
ADA
053466





NATIONAL BUREAU OF STANDARDS

AD-E300187

12 SC

DNA 4243F

AD A 053466

SIMULATED NUCLEAR GUST TESTING OF MAJOR AIRPLANE STRUCTURAL COMPONENTS

The Boeing Aerospace Company
P.O. Box 3999
Seattle, Washington 98124

28 January 1977

Final Report for Period 1 September 1976—31 January 1977

CONTRACT No. DNA 001-76-C-0367

APPROVED FOR PUBLIC RELEASE;
DISTRIBUTION UNLIMITED.

THIS WORK SPONSORED BY THE DEFENSE NUCLEAR AGENCY
UNDER RDT&E RMSS CODE B34207T464 B88QAXAE50206 H2590D.

AD NO. _____
DDC FILE COPY

Prepared for
Director
DEFENSE NUCLEAR AGENCY
Washington, D. C. 20305

DDC
RECEIVED
MAY 3 1978
B

Destroy this report when it is no longer
needed. Do not return to sender.



UNCLASSIFIED

SECURITY CLASSIFICATION OF THIS PAGE (When Data Entered)

REPORT DOCUMENTATION PAGE		READ INSTRUCTIONS BEFORE COMPLETING FORM
1. REPORT NUMBER DNA 4243F [✓]	2. GOVT ACCESSION NO.	3. RECIPIENT'S CATALOG NUMBER
4. TITLE (and Subtitle) SIMULATED NUCLEAR GUST TESTING OF MAJOR AIRPLANE STRUCTURAL COMPONENTS.	5. AUTHOR(s) David M. Eckblad Nelson E. Funston	6. TYPE OF REPORT & PERIOD COVERED Final Report for Period 1 Sep 76-31 Jan 77
7. PERFORMING ORGANIZATION NAME AND ADDRESS The Boeing Aerospace Company [✓] P.O. Box 3999 Seattle, Washington 98124	8. CONTRACT OR GRANT NUMBER(s) DNA 001-76-C-0367 ^{hu}	9. PROGRAM ELEMENT, PROJECT, TASK AREA & WORK UNIT NUMBERS Subtask B88QAXAE502-06
10. CONTROLLING OFFICE NAME AND ADDRESS Director Defense Nuclear Agency Washington, D.C. 20305	11. REPORT DATE 28 January 1977	12. NUMBER OF PAGES 146
13. MONITORING AGENCY NAME & ADDRESS (if different from Controlling Office) DNA, SBIE	14. SECURITY CLASS (of this report) UNCLASSIFIED	15. SECURITY CLASS (of this report) UNCLASSIFIED
16. DISTRIBUTION STATEMENT (for this Report) Approved for public release; distribution unlimited.	17. DISTRIBUTION STATEMENT (of the abstract entered in Block 20, if different from Report)	15a. DECLASSIFICATION/DOWNGRADING SCHEDULE
18. SUPPLEMENTARY NOTES This work sponsored by the Defense Nuclear Agency under RDT&E RMSS Code B34207T464 B88QAXAE50206 H2590D.	19. KEY WORDS (Continue on reverse side if necessary and identify by block number) Blast Damage Testing Nuclear Gust Loading Test Methods Airplane Blast Test Mission Completion	
20. ABSTRACT (Continue on reverse side if necessary and identify by block number) This report contains the results of an investigation as to the feasibility of simulating nuclear gust loading on a B-52 fin or wing by a mechanical dynamic test. The investigation was accomplished by use of a mathematical simulation of mechanical test setup. The results show that a test simulating nuclear gust loads is feasible and the resulting bending moments in the critical areas of		

DD FORM 1 JAN 73 1473 EDITION OF 1 NOV 65 IS OBSOLETE

UNCLASSIFIED
SECURITY CLASSIFICATION OF THIS PAGE (When Data Entered)

059 610

JOB

next page

UNCLASSIFIED

SECURITY CLASSIFICATION OF THIS PAGE(When Data Entered)

20. ABSTRACT (Continued)

the fin and wing compare well with bending moments calculated using the VIBRA-4 computer code. Two possible test setups for a B-52 fin test are described. In one method, the loading is input by fast acting pneumatic actuators attached to the fin main spar. In the other method, the loading is induced by rapid acceleration of the fin support structure.

The report also contains a discussion of basic consideration for an aircraft mission completion investigation.

ACCESSION for	
NTIS	White Section <input checked="" type="checkbox"/>
DDC	Buff Section <input type="checkbox"/>
UNANNOUNCED	<input type="checkbox"/>
JUSTIFICATION	
BY	
DISTRIBUTION/AVAILABILITY CODES	
Dist. AVAIL. and/or SPECIAL	
A	

UNCLASSIFIED

SECURITY CLASSIFICATION OF THIS PAGE(When Data Entered)

TABLE OF CONTENTS

<u>Section</u>	<u>Page No.</u>	
I	INTRODUCTION	7
	1.0 BACKGROUND	7
	1.1 SUMMARY OF DYNAMIC GUST FEASIBILITY INVESTIGATION	7
	1.2 MISSION COMPLETION	9
	1.2.1 Mission Completion User Requirements	9
	1.2.2 Aircraft Gust Encounter Approach	13
	1.3 UNITS OF MEASURE	16
II	BLAST LOADING ON B-52H AIRCRAFT	22
	2.0 INTRODUCTION	22
	2.1 CONFIGURATION	22
	2.2 VIBRA-4 RESULTS	23
III	DYNAMIC ANALYSIS OF TEST SIMULATION	53
	3.0 INTRODUCTION	53
	3.1 DYNAMIC MODEL	53
	3.1.1 Fin Dynamic Model	53
	3.1.2 Wing Dynamic Model	53
	3.1.3 Fin Pull Test Dynamic Model	54
	3.1.4 Fin Base Shake Dynamic Model	55
	3.1.5 Wing Pull Test Dynamic Model	56
	3.2 COMPARISON OF VIBRA-4 AND DATS	57
	3.3 SIMULATION OF FIN TEST	60
	3.3.1 Base Shake Test	60
	3.3.2 Dynamic Pull Test	61
	3.4 SIMULATION OF WING TEST	62
	3.4.1 Dynamic Pull Test	62
IV	TEST CONFIGURATION	133
	4.0 INTRODUCTION	133
	4.1 DYNAMIC PULL TEST SETUP	133
	4.2 BASE SHAKE TEST SETUP	134
V	CONCLUSION	138
VI	RECOMMENDATIONS	139
VII	REFERENCES	140

LIST OF FIGURES

<u>Figure No.</u>	<u>Title</u>	<u>Page No.</u>
1-1	Base Shake Test Setup	18
1-2	Dynamic Pull Test Setup	19
1-3	Fin Moment Comparison	20
1-4	Wing Moment Comparison	21
2-1	Test Loading Conditions	26
2-2	VIBRA-4 Conditions	27
2-3	B-52H Fin Aerodynamic Loading Distribution for Test	28
2-4	B-52H Wing Aerodynamic Loading Distribution for Test	29
2-5	Location of Bending Moment and Load Stations	30
2-6	Wing Pre-Blast Steady State Lift Distribution	31
2-7	Wing Pre-Blast Bending Moment B-52H Wing and Fin	32
2-8	Ultimate Bending Moment Capability	33
2-9	Wing Tested Limit Load Capability	34
2-10 - 2-19	VIBRA-4 (30 modes) Test Load and Aerodynamic Load - B-52H Wing	35-39
2-20 - 2-29	VIBRA-4 (8 Modes) Test Load and Aerodynamic Load - B-52H Wing	40-44
2-30 - 2-37	VIBRA-4 Test Load and Aerodynamic Load - B52H Fin	45-48
2-38 - 2-42	VIBRA-4 Bending Moments - B-52H Wing	49-51
2-43	VIBRA-4 Bending Moments - B-52H Wing	52
3-1	B-52H Fin Dynamic Model Node Numbers and Coordinates	65
3-2	B-52H Fin Dynamic Model Stiffness Data	66
3-3	Mass Data Terminology	67
3-4	B-52H Fin Dynamic Model Mass Data	68
3-5	Comparison of B-52H Fin Cantilever Frequencies	69
3-6	B-52H Wing Dynamic Model Node Number and Coordinates	70
3-7	B-52H Wing Dynamic Model Stiffness Data	71

LIST OF FIGURES (Continued)

<u>Figure No.</u>	<u>Title</u>	<u>Page No.</u>
3-8	B-52H Wing Dynamic Model Mass Data	72
3-9	B-52H Dynamic Model Nacelle and External Mass Data	73
3-10	B-52H Dynamic Model Nacelle Cantilever Mode Data	74
3-11	Comparison of B-52H Wing Cantilever Frequencies - 230 Kip Gross Weight	75
3-12	Fin Pull Test Dynamic Model	76
3-13	Fin Pull Test Loading Characteristics	77
3-14	Fin Base Shake Dynamic Model	78
3-15	Wing Pull Test Dynamic Model	79
3-16	Wing Pull Test Loading Characteristics	80
3-17	VIBRA-4/DATS Peak Bending Moment Comparison B-52H Fin	81
3-18, 3-19	VIBRA-4 and DATS Bending Moments Time History - Fin	82
3-20 - 3-27	DATS Fin Bending Moment for 10 Modes and 1 Mode, VIBRA-4 Input	83-86
3-28	VIBRA-4/DATS Peak Bending Moment Comparison - B-52H Wing	87
3-29 - 3-33	VIBRA-4 and DATS Bending Moment Time History - Wing	88-90
3-34	Peak Bending Moments - B-52H Fin	91
3-35	Peak Lateral Acceleration B-52H Fin	92
3-36	Peak Lateral Relative Deflection B-52H Fin	93
3-37 - 3-44	Test Loading - Fin-Base Shake	94-97
3-45 - 3-52	Bending Moments - Fin Base Shake	98-101
3-53 - 3-60	Relative Deflections - Fin Base Shake	102-105
3-61 - 3-68	Test Loading - Fin Dynamic Pull Test	106-109
3-69 - 3-76	Bending Moments - Fin Dynamic Pull Test	110-113
3-77 - 3-84	Relative Deflections - Fin Dynamic Pull Test	114-117
3-85	Peak Bending Moments B-52H Wing	118
3-86	Peak Acceleration B-52H Wing	119
3-87 - 3-96	Test Loading - Wing Dynamic Pull Test	120-124

LIST OF FIGURES (Continued)

<u>Figure No.</u>	<u>Title</u>	<u>Page No.</u>
3-97 - 3-101	Bending Moments - Wing Dynamic Pull Test	125-127
3-102 - 3-111	Relative Deflections - Wing Dynamic Pull Test	128-132
4-1	Dynamic Pull Test Actuator Data	136
4-2	Base Shake Prime Mover Performance	137

LIST OF TABLES

<u>Table</u>		<u>Page</u>
1	Conversion factors for U.S. customary to metric (SI) units of measurement	17

SECTION I INTRODUCTION

1.0 BACKGROUND

This document presents the results of work accomplished under DNA Contract DNA 001-76-C-0367 Simulated Nuclear Blast Testing of Airplane Major Structural Components." The results of the primary tasks I and II which are concerned with evaluating the feasibility of gust testing are summarized in Section 1.1 and detailed in Sections 2 through 6. Task III, a review of current aircraft hardness assessment activities is not directly related to Tasks I and II but is part of the same contract and is reported in this document under Section 1.2.

1.1 SUMMARY OF DYNAMIC GUST FEASIBILITY INVESTIGATION

In the assessment of an aircraft's vulnerability to nuclear effects, the structural responses to the nuclear induced gust winds are perhaps the most dramatic. And when major structural components such as the wing or the tail fail the aircraft and mission are most certainly lost.

Many of the other effects will cause a failure of a single component and not necessarily cause the loss of the aircraft.

For these reasons it is vital to know the threshold of failure of major parts of the airplane due to nuclear induced gusts when evaluating effectiveness of an airplane weapon system.

The current method of gust failure prediction is based on calculating the loads theoretically and then comparing these loads to static failure allowables derived from test and analysis of the aircraft structure.

The object of the current effort is to develop a test approach whereby the major aircraft components could be tested dynamically. With such a dynamic test not only could the dynamic failure levels of the components be established but also the response could be used as a check on response calculation in computer codes such as VIBRA-4.

In development of a dynamic test approach where only a portion of the aircraft is involved, there are three major problems to overcome. The

1.1 (Continued)

first is the establishment of the external aerodynamic forces as felt by the components. The second problem is to account for the change in boundary conditions between a wing or a fin in the test fixture and the wing or the fin as it is attached to the aircraft body in free flight. The third problem is simulating these forces and constraints by mechanical means.

In the work completed, the external air loads and responses on a B-52H wing and fin have been calculated using the VIBRA-4 code. See Reference 1. These external loads and airplane responses have been used to derive an equivalent test load to be applied in the dynamic test.

A number of different mechanical methods of simulating these test loads have been modeled. These models have been programmed in a computer code named DATS (Dynamic Analysis of the Test Simulation). The code has been used to predict what would happen in a simulated test. From a comparison with this predicted test response bending moments and bending moments calculated in VIBRA-4 and the static failure bending moments of the various test approaches have been evaluated.

As a result of this bending moment comparison, two test approaches show good promise for a fin test. The first approach is the base shake where the fin is attached to a moving base and forced through a prescribed acceleration pulse. This test configuration is shown in Figure 1-1. This test approach has the advantage of simplicity of test control and the advantage of no external forces applied directly to the aerodynamic surfaces of the fin. The comparison of bending moments predicted for this test and bending moments calculated using VIBRA-4 are compared with the fin ultimate moments in Figure 1-2.

The second approach is the dynamic pull test shown in Figure 1-3. This method while it lacks the simplicity of the base shake does provide for a better load simulation and more flexibility in the type of loads that can be applied. The bending moments predicted for this test are Figure 1-2 compared to the VIBRA-4 moments, the moments for a base shake and the ultimate moments capability of the fin.

1.1 (Continued)

For the wing test, only the dynamic pull test was simulated since the base shake appeared to require more motion from the prime mover than the existing test hardware capability.

The results of the bending moment comparison on the wing figure 1-4 shows good comparison in the critical area in the outboard wing section, but does not give a good match in the less critical root area. A better bending moment comparison could be obtained with an increased number and increased complexity of dynamic load generators attached to the wing. An alternate approach could be to test only the outboard wing segment since this is the critical area and a test of a smaller portion of the wing would simplify the test.

The alternate test approaches needs further refinement before the final approach is selected.

1.2 MISSION COMPLETION

Initial effort on this task was directed to assessing the requirements of various using groups for aircraft mission completion information. Methods for determining the response of aircraft to nuclear gust encounters were then examined to see whether they were suitable for meeting user requirements. It was found that none of the existing methods (primarily computer programs) were suitable for all user requirements. A two step approach using two types of existing computer programs does appear suitable for meeting all user requirements. Other environments have not yet been examined but it is anticipated that combinations of existing methods will prove suitable.

1.2.1 Mission Completion User Requirements

The types of technical information needed for mission completion evaluations will be strongly influenced by the users. Discussions have been held with several members of the aircraft survivability/vulnerability community to determine their past experiences in providing information

1.2.1 (Continued)

to other agencies and their expectations for potential future users. From these discussions current users can be placed in four categories.

- A. Those making system comparisons. This is typically a system analysis approach in which aircraft vulnerability assessments are used to determine whether a given aircraft system can be expected to complete its assigned mission in spite of various defense systems it must penetrate. Closely related activities include comparison of one system with another to determine which has the better capability under various offense/defense scenarios. Extremely fine grain detail does not appear warranted for these kinds of simulation since only a finite number of options and scenarios can be investigated. It is important to cover the entire range of damage versus performance and particularly important to have comparable information on different (often competing) systems if the results of comparisons are to be valid.
- B. Those making operational plans. Operational planners use survivability/vulnerability assessment results for mission planning to select payloads, mission profiles, routes, alternate targets and routes, and single aircraft versus multiple aircraft formations. The operational planners are faced with an enormous number of possible targets, routes, mission profiles and payloads. They require a quick method of determining which routes and mission profiles are best for various potential weapon encounters. Either a very rapid assessment technique or a precalculated catalog will be needed. The entire range of damage versus performance is important since a given damage level early in a mission might mandate an abort while later in the mission the degradation would not prevent mission accomplishment.
- C. Those developing criteria for new systems. The development of nuclear hardness criteria for a new aircraft system is an iterative process by several government agencies. It requires trade offs

1.2.1 (Continued)

(either by engineering trade studies or by intuition) of the impact of hardness on cost, schedules and performance against improvements in survivability and therefore in system effectiveness. The accuracy of cost predictions is improved as a system progresses from concept through preliminary design, final design and prototype production. For the next several years it is doubtful that accurate predictions of hardening costs will be available early in the concept formulation stage when decisions on hardening criteria are beginning to be made. Tentative criteria can be selected and the design process initiated provided that reasonably "balanced" evaluations for gust, overpressure and thermal are made and that new evaluations can be generated and examined by each of the concerned agencies as the iterative process of system development proceeds. Tentative decisions on hardening criteria, costs, schedules and performance can converge towards the final design provided each of the agencies have equally valid assessment procedures and the ability to examine the range of parameter variations associated with their agencies responsibilities. Fast availability of results is essential. Comparable mission completion assessment outputs for the several agencies is necessary for realistic decisions.

- D. Those responsible for meeting hardening criteria. This category includes the System Program Offices, the contractors, and the technical review agencies who are jointly responsible for assuring that the operational system meets the established criteria. One requirement of this category of users is the ability to evaluate the impact of minor changes in materials, structure, or external configuration on hardness. Another major requirement is the ability to make accurate evaluations that review agencies will find acceptable in order to preclude costly overdesign that is sometimes necessary to provide high confidence that criteria are met.

1.2.1 (Continued)

From the discussions held to date, it appears that in the future a new category of user will emerge. This will be the aircraft crew during missions. When the ability of aircraft to complete missions after partial damage is included in systems analyses, in operational plans, in criteria for new systems and in the acceptance process it will become essential that the flight crews make the correct decisions after their aircraft is damaged. If the crew aborts unnecessarily or fails to modify altitude, airspeed, routes, and maneuvers to maximize the changed performance capability the aircraft mission completion capability may be seriously reduced. Before the crew can take effective action they must be able to diagnose the damage and have preset guidelines for selecting alternate degraded performance operating modes. This will require a great deal of advance evaluations considering many potential weapon encounters, a wide range of damage, and the effect of various changes in flight conditions on the degraded performance at each segment of the mission. This large catalog of situations must be reduced to a realistically small number of decisions that the crew can be expected to make under stress. Methods of training the crews, possibly by simulators, will need to be developed. It appears that adding simulated damage into the characteristics of existing flight simulators could provide much of the necessary crew training.

When the requirements of all the users are compared, it is clear that the major needs of mission completion assessments will not be met unless there is:

1. Fast turnaround
2. Equivalent results for different systems
3. Complete range of damage versus performance
4. Ability to consider many weapon encounters, mission types and mission segments
5. High confidence

1.2.2 Aircraft Gust Encounter Approach

High confidence can be obtained at present only by using the best available computer simulation programs combined with test results. Generally the best computer programs require a large amount of computer running time for each point on a vulnerability envelope. The calculations required for a complete envelope for a number of yields, altitudes and aircraft speeds are prohibitive. The fast running computer programs that can generate a large number of vulnerability envelopes for a range of situations embody simplifications that decrease confidence in their outputs. The two requirements, high confidence and fast turnaround are not compatible. Short cuts and simplifications are necessary for any method that can be used to determine damage levels leading to mission completion criteria for all the situations of interest. These simplifications preclude incorporating all the aircraft response and nuclear weapon environment information that is now available. This leads to lowered confidence. The users of mission completion evaluations need the highest possible confidence since they must make decisions which affect the cost, design, performance, and system capability of aircraft systems. They also need mission completion evaluations for a large number of potential situations - all at high confidence.

Nuclear gust encounter was selected as an exemplary topic to determine how to resolve the requirements for a large number of vulnerability envelopes, all with high confidence. There are several methods, both hand calculations and computer programs for calculating aircraft response to nuclear gust encounters. After examination of several methods it was found they fall into three distinct categories: (1) Hand calculation methods that are useful for calculating a few points on a vulnerability envelope. Calculating many points becomes tedious. (2) Fast running computer programs that calculate complete envelopes, (3) Sophisticated computer programs that provide the highest confidence currently available. Excessive computer time is needed to calculate many points.

None of the three categories are completely acceptable for the needs of all users. The most practical method currently available appears to be to

1.2.2 (Continued)

use a two step approach. First one of the sophisticated computer programs is used to calculate aircraft gust vulnerability envelopes for a small number of conditions. Second, inputs to one of the fast running programs are adjusted until a good match is obtained with the sophisticated computer program results. The fast running program is then employed to calculate vulnerability envelopes for additional conditions. Confidence declines as the new conditions deviate farther from the baseline sophisticated program results. However, by judicious selection of the baseline situations, a fairly large range of yields, altitudes, and flight conditions can be encompassed with only a few envelopes calculated on the long running sophisticated programs.

The best aircraft nuclear gust encounter computer programs now available are VIBRA-4 (reference 1) and VIBRA-6 (reference 10). Both programs require detailed inputs of aircraft structure, mass distribution, and aerodynamic coefficients.

VIBRA-6 is an updated version of VIBRA-4 and while little experience is yet available on running time it is expected the computer running time for VIBRA-6 will be approximately the same as for VIBRA-4. This is approximately 20 minutes of CDC-6600 computer time for each point on a gust vulnerability envelope. On the order of 8 to 16 points are needed for a single gust encounter envelope. A separate envelope may be needed for each altitude, weapon yield, damage criteria, aircraft gross weight and aircraft speed that are of interest. Clearly the number of points to be calculated would lead to extremely high computer costs. Computer programs or hand calculations which are a factor of 10 or 100 more economical than VIBRA-4 or VIBRA-6 are needed if all the situations of interest are to be examined.

Several inexpensive methods of calculating aircraft nuclear gust encounters are available (references 8, 9 and 11). These methods can be utilized to calculate large numbers of aircraft gust vulnerability envelopes at acceptable cost. Confidence in results is low until correlation with a high confidence method can be shown. The easiest way to increase confidence

1.2.2 (Continued)

is simply to adjust input parameters to the fast running computer programs until the output agrees with VIBRA results for a baseline situation. The fast running program is then used to calculate gust vulnerability envelopes for other situations.

From examination of VIBRA-4 gust envelopes, forced fitting of envelopes from the Boeing Aircraft Vulnerability Volume (AVV) computer program (reference 8) to the VIBRA-4 contours for 1 MT at 5000 ft. and comparison of AVV gust contours with VIBRA-4 contours for 1 MT at 20,000 ft. it was found that less than five percent error in gust envelope dimensions were introduced by using AVV to scale from 5000 ft. to 20,000 ft. Errors for yield scaling or changed flight conditions could not be checked as the appropriate VIBRA-4 contours were not available. Scaling with yield is expected to be relatively error free since gust wave scaling with yield is well understood. Changed aircraft flight conditions, such as gross weight, speed, center of gravity location and wing and tail angles of incidence are expected to introduce larger errors. To insure acceptable confidence the procedure would be to calculate VIBRA gust vulnerability envelopes for the two extremes of aircraft flight conditions. Interpolation between the extremes by using a fast running program such as AVV is then realistic. Accuracy of the interpolation can be assessed by scaling from each extreme VIBRA case all the way to the other extreme VIBRA case.

The least trustworthy of scaling parameters is expected to be damage level. Calculations of the extreme values of interest, sure safe and sure kill, does not provide good guidance to selecting intermediate damage levels. Specific structural loads which cause specified damage levels can become a new baseline envelope once they are calculated, but estimating the relationships from gust velocity to aerodynamic load to structural load to structural damage to aerodynamic changes to impact on mission completion appears beyond the capability of any existing computer programs. This will be a step by step iterative process until the effect on mission completion of a selected structural load (with resultant damage) is

1.2.2 (Continued)

established. The gust envelopes which produce that structural load can then be determined by the two step computer approach, baseline envelopes by VIBRA, intermediate envelopes by fast running programs.

1.3 UNITS OF MEASURE

This investigation and all of the input data to the mathematical models are in English units. Distance is in inches, force in pounds and acceleration in multiples of 32.2 ft/sec^2 . Table 1 is a tabulation of relevant conversion factors to convert from English units to metric units.

Table 1. Conversion factors for U.S. customary to metric (SI) units of measurement

To convert from	To	Multiply by
inches	centimeters	2.54
feet	meters	0.3048
square inches	square centimeters	6.4516
square feet	square meters	0.0929
cubic inches	cubic centimeters	16.38706
cubic feet	cubic meters	0.0283
Kips	kilograms	454.0
gallons (U.S.)	liters	3.785
pounds force	newtons	4.44822
pounds	kilograms	0.454
pounds per square inch	newtons per square centimeter	0.6894757
pounds per cubic inch	kilograms per cubic centimeter	27,679.90
inches per second	centimeters per second	2.54
inch-pounds	meter-newtons	0.1129848
inch-kips	meter-kilonewtons	0.0001129848

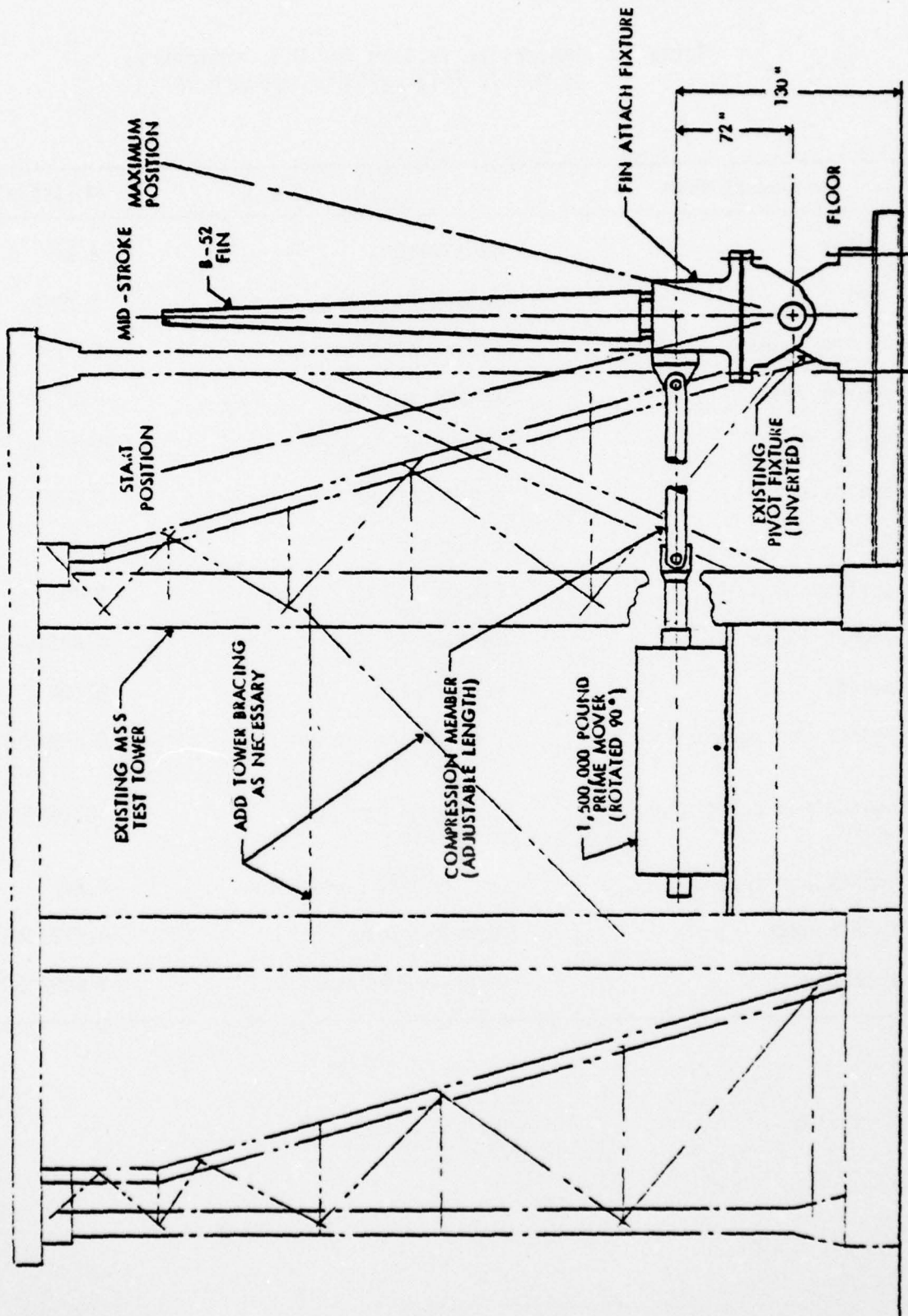


Figure 1-1, Base Shake Test Setup

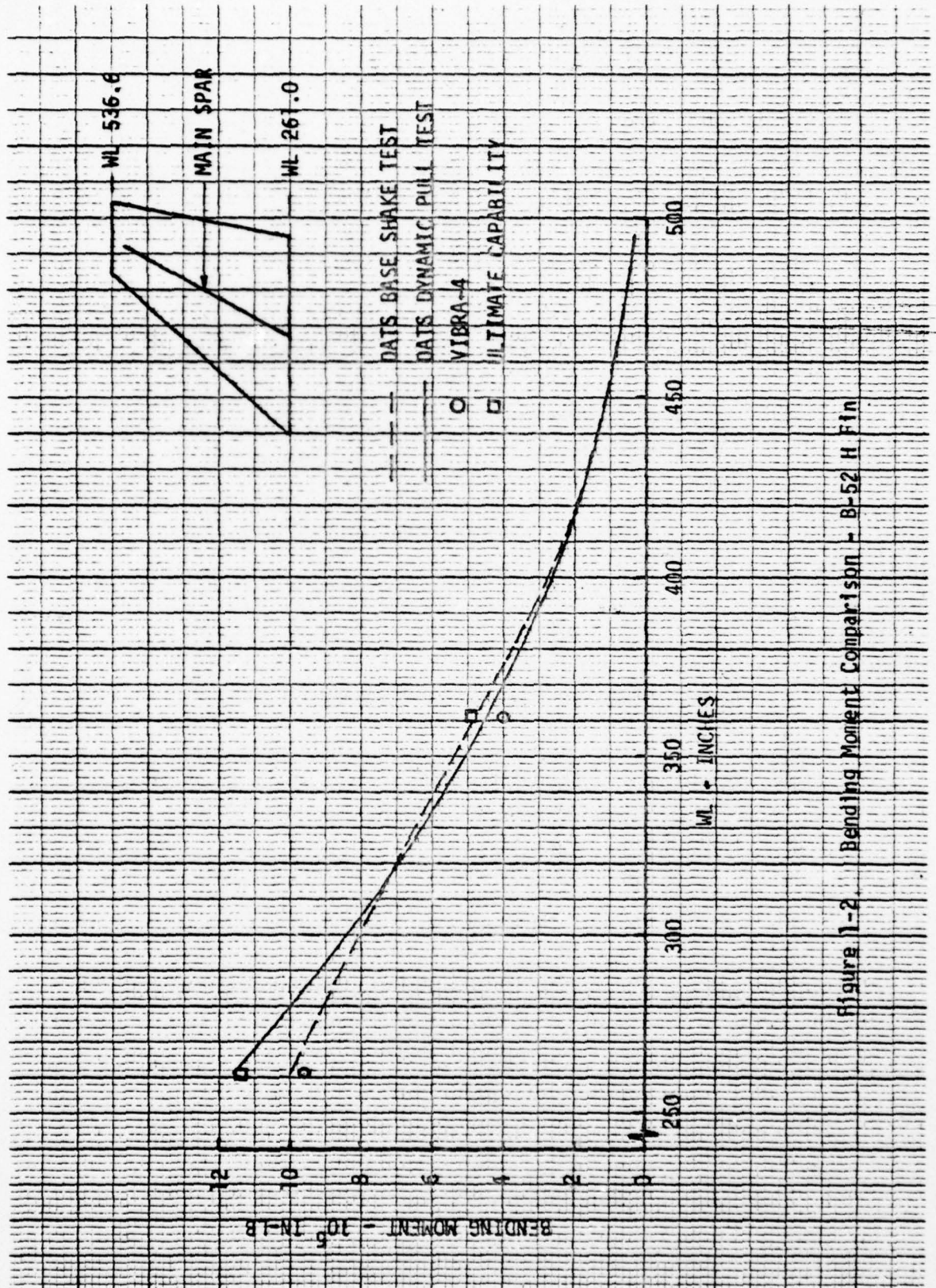


Figure 1-2. Bending Moment Comparison - B-52 H Fin

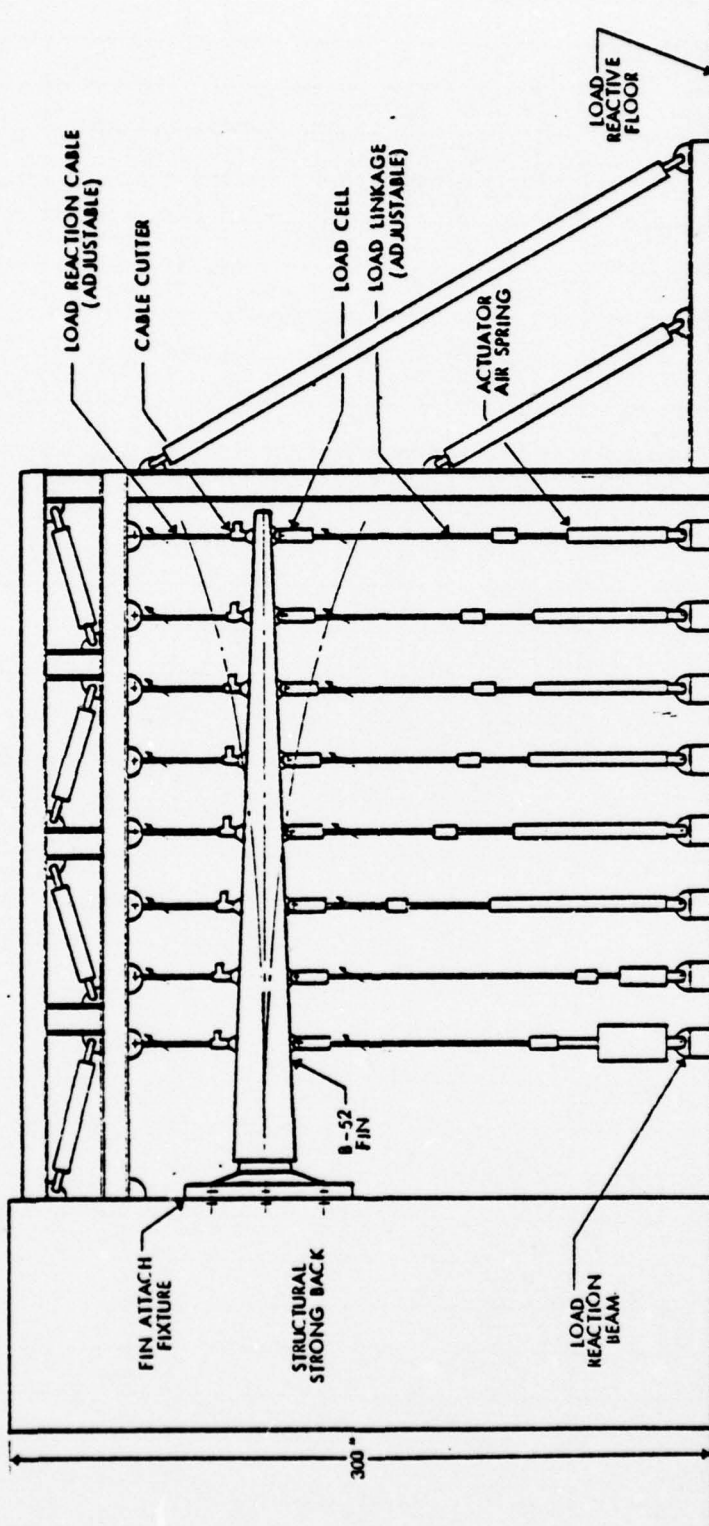


Figure 1-3 Dynamic Pull Test Setup

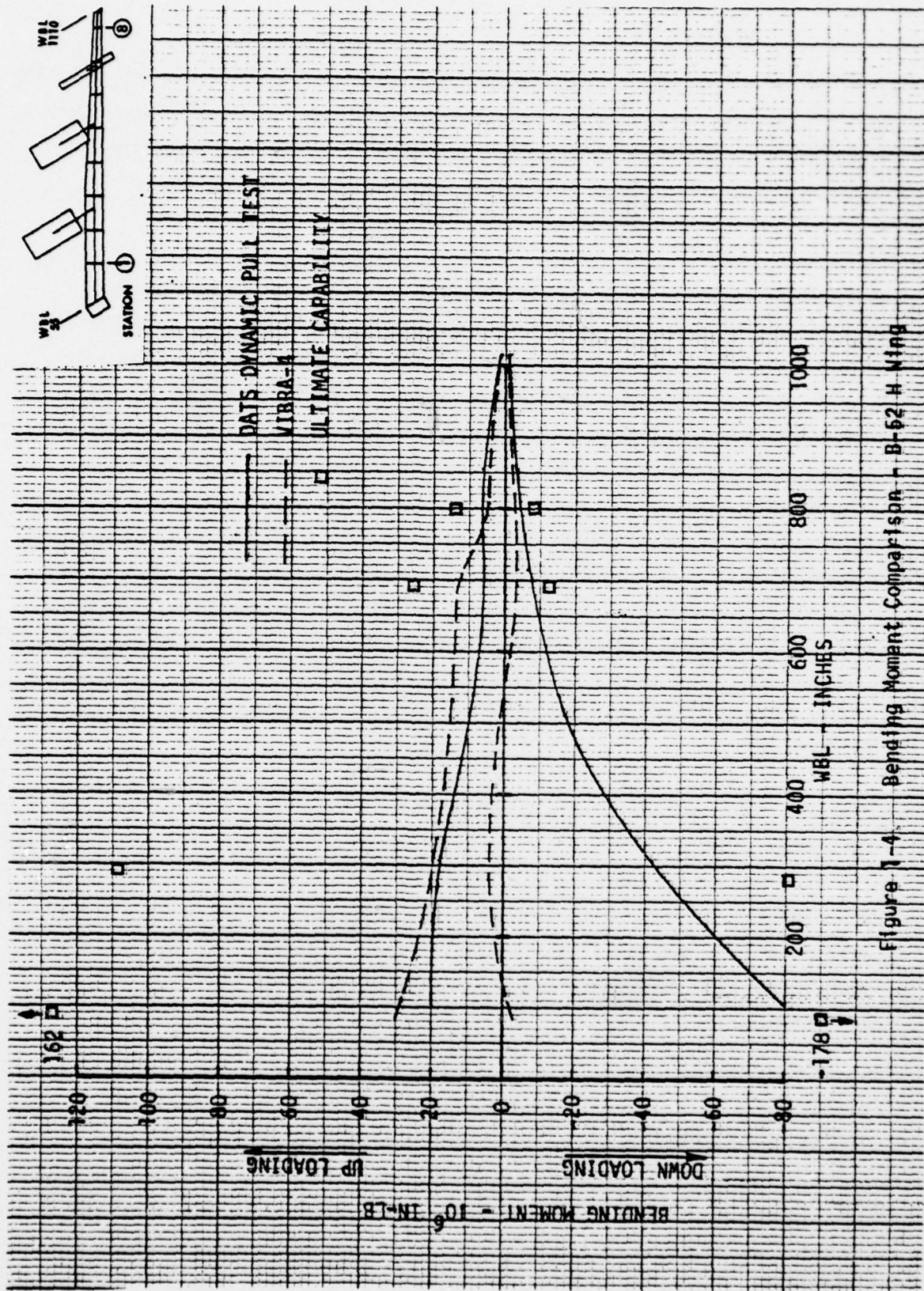


Figure 1-4 Bending Moment Comparison - B-52 H Wing

SECTION II
BLAST LOADING ON B-52H AIRCRAFT

2.0 INTRODUCTION

This section contains an overview of the nuclear blast investigation on the B-52H aircraft. Included are the flight conditions analyzed, the aircraft geometry, the analysis methods and assumptions. The mixed boundary value equations of motion for the test model are derived.

2.1 CONFIGURATION

Two flight conditions were modeled for nuclear blast effects on the B-52H wing and fin. The first is the flush condition in which a heavy gross weight airplane (480,000 lb.) is departing from a basing location and is accelerating away at a medium altitude of 5000 ft. Two blast conditions were checked during flush, an overhead and a side blast. A second condition of low level penetration at a lighter gross weight (230,000 lb.) was investigated for an overhead blast condition. All three of these blast conditions were analyzed, for loads and structural response. Boeing Wichita conducted the VIBRA-4 computer simulation and transmitted the results on magnetic tape to the Boeing Aerospace Company at Seattle. The resultant tapes contained the structural modes and frequencies of the airplane and the time history of blast air loading, as well as 5 moment time histories on the wing and 2 moment time histories on the fin.

Two conditions were selected to be used in the Dynamic Analysis for Test Simulation (DATS). The lateral blast case at 480,000 lb. was used for the DATS simulation of the fin, and the light gross weight (230,000 lb.) was used for the overhead blast investigation of the wing. The light gross weight case is more difficult to test for the wing because of the lower inertia relief. Figures 2-1 and 2-2 itemize the details of the VIBRA-4 conditions.

VIBRA-4 aerodynamic loads are applied at the geometric centroid of panels which are distributed on the aircraft loading surfaces. The VIBRA-4 aerodynamic panels are shown in Figure 2-3 along with the test load application points. VIBRA-4 aerodynamic loads for the fin are beamed to the nearest test load points from the panel centroids. As shown on

2.1 (Continued)

Figure 2-3 the point of resultant test loads are located very close to the main spar. For the math model and test they were considered to act on the main spar. The fin has the rudder attached and is supported at three fuselage attachment points.

The wing geometry and the steady state flight loads are shown in Figures 2-4 through 2-7, and the wing load capabilities are shown in Figures 2-8 and 2-9. The 16 wing aerodynamic panels used for VIBRA-4 are shown in figure 2-4 along with the load points for the blast load simulation. The aerodynamic loads are beamed to the test load points in the same way the fin is loaded. The wing structure for the test simulation includes the wing on one side of the airplane plus the carry through structure through the fuselage. The wing mounting structure is a simple pinned support at the wing/fuselage trunnion. The test configuration has the leading and trailing edge removed and the test loading is applied to the forward and rear spar web with a specially designed fitting to carry local shear.

2.2 VIBRA-4 RESULTS

In order to gain insight on how a component of a dynamic system relates or interfaces with that system, the following equations are presented. The set of equilibrium equations for a component of an aircraft in a dynamic event can be represented by

$$M\ddot{U} + C\dot{U} + KU = F_A \quad (1)$$

where:

- M Mass Matrix of the component
- K Stiffness matrix of the component
- C Damping matrix
- \ddot{U} Absolute acceleration of each point of the body relative to inertial space that is retained for analysis
- F_A Applied aerodynamic forces on aircraft

2.2 (Continued)

At the component interface boundary with the aircraft, the displacement will be considered prescribed in contrast to the remainder of the boundary of the component where the forces are prescribed or considered known.

The absolute motion of the component can be represented as

$$U = L U_I + \phi q \quad (2)$$

where:

- U_I Absolute motion of the component interface which is considered known and for this program is the input from VIBRA-4.
- L Rigid body vector for the component with respect to the interface.
- ϕ Cantilever modes normalized to generalized mass equal to unity.
- q Generalized displacement for cantilever modes.

Substituting equation (2) into the equilibrium equation (1) and making use of modal orthogonality conditions gives

$$\begin{aligned} \ddot{q} + 2\zeta\omega\dot{q} + \omega^2q &= \phi^T F_A - \phi^T ML U_I = \phi^T (F_A - F_I) \\ \text{or} \\ \ddot{q} + 2\zeta\omega\dot{q} + \omega^2q &= \phi^T F_T \end{aligned} \quad (3)$$

where:

- F_I is the inertia loading which must be imposed on the component in addition to the aerodynamic loading in order to simulate the flight conditions.
- $F_T = F_A - F_I$ or the test applied load to simulate the flight dynamic event.
- ζ Factor of critical damping. Five percent of critical was used for this analysis.
- ω^2 Eigenvalue for support modes.

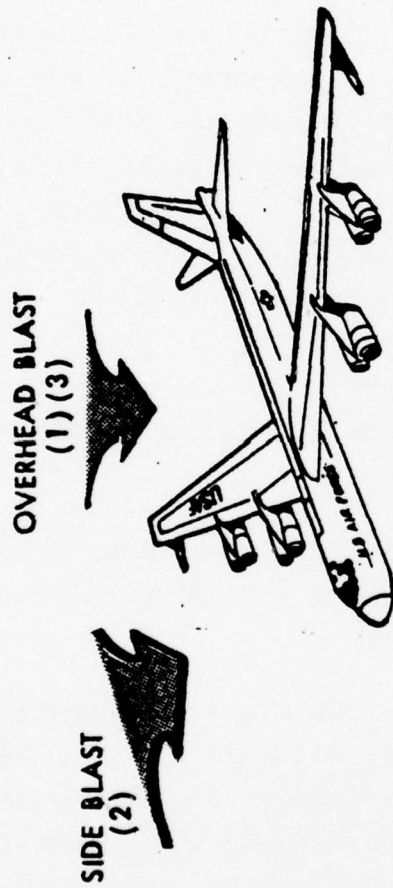
2.2 (Continued)

Equation 3 was used to determine the dynamic response for the test simulation. The quantities, L , U_I , W_n and ϕ came from the VIBRA-4 code. The symmetric VIBRA-4 simulation for the wing response included 30 symmetric structural mode and the Fin analysis included 5 symmetric and 25 antisymmetric modes.

The VIBRA-4 output was input into a load distribution program which calculated the aerodynamic and inertia loads at the test points. Aerodynamic loads and the test loads are shown in Figures 2-10 through 2-37. The inertia load term F_I accounts for the difference in the air load and test load shown on these figures. Figures 2-10 to 2-19 display the wing loads using all 30 modes. Figures 2-20 to 2-29 display the wing loads using only the first 8 wing modes. As can be seen, the 8 mode model suppresses the dominate 25 cps structural mode present in the 30 mode model, and produces slightly lower peak loads. Nacelle loads shown on Figures 2-18, 2-19, 2-28 and 2-29 contain only inertia loads since VIBRA-4 does not calculate aerodynamic loading for the nacelles.

Figures 2-30 - 2-37 depict the Fin aerodynamic and test loads. Comparison of the air load and test loads shows that the inertia load is not as dominate on the fin as on the wing.

VIBRA-4 bending moment for five stations on the wing is presented on Figures 2-38 thru 2-42 and for two stations on the fin on Figure 2-43. Bending moments are directly calculated in VIBRA-4. Fin bending moments directly calculated in VIBRA-4 were checked using the aerodynamic and distributed inertia loading from VIBRA-4 response data. Wing bending moment data includes the steady state lift correction factors shown on Figure 2-7.



CONDITION	GROSS WEIGHT (KIPS)	BLAST DIRECTION	YIELD (KT)	ALTITUDE (FT)	TRUE AIR SPEED (FPS)
(1) FLUSH	480	OVERHEAD	1000	5000	659
(2) FLUSH	480	SIDE	1000	5000	659
(3) PENETRATION	230	OVERHEAD	100	500	619

Figure 2-1 Test Loading Conditions

PARAMETER	WING 480K	WING 230K	FIN 480K
ALTITUDE ~ FT	5000	500	5000
AIRSPEED ~ F/S TRUE	659.18	619.80	659.18
BLAST ORIENTATION	OVERHEAD	OVERHEAD	SIDE
YIELD ~ KT	1000	100	1000
THRUST ~ LBS/POD	7630	6930	7630
SECONDS OF DATA	2.0	2.0	0.5
Δt	.001	.001	.001
# SYM MODES	30	30	5
# ASM MODES	0	0	25

Figure 2-2 VIBRA-4 Conditions

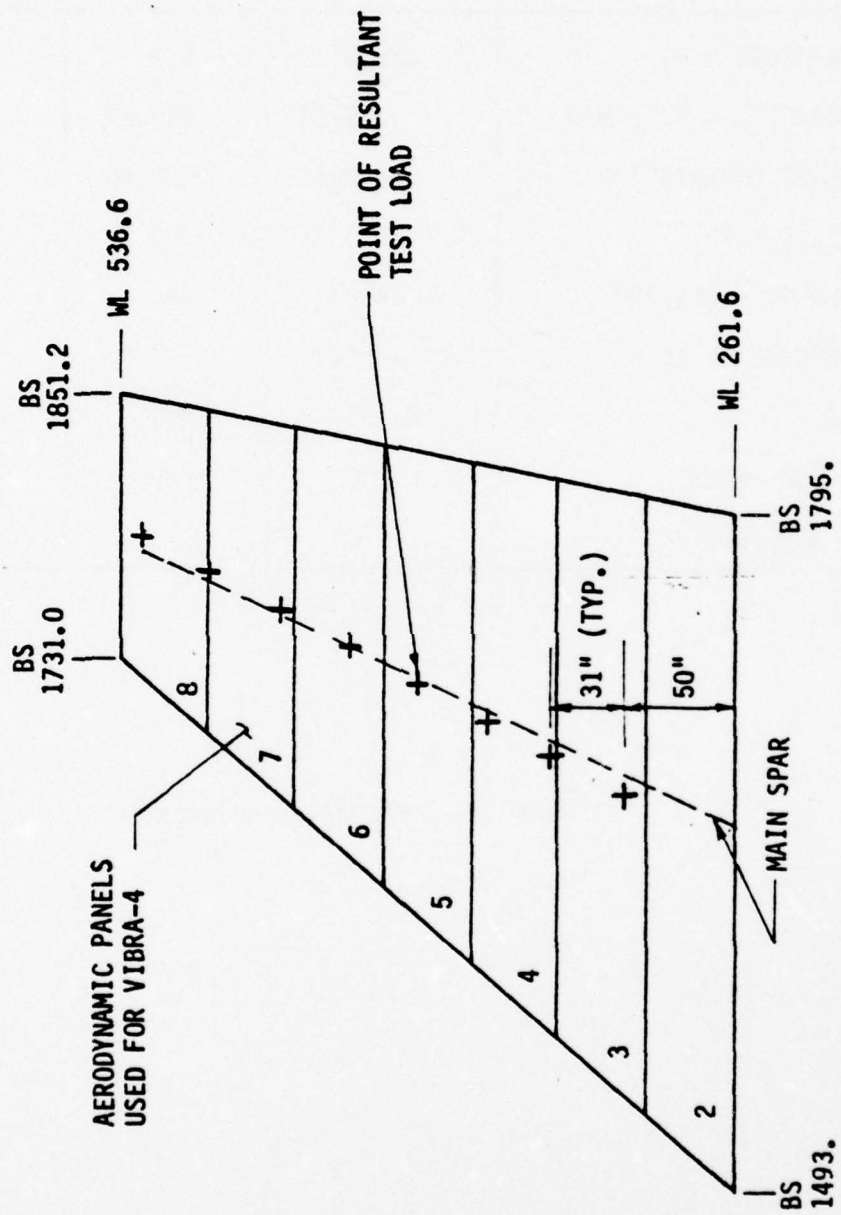


Figure 2-3 B-52H Fin Aerodynamic Loading Distribution For Test

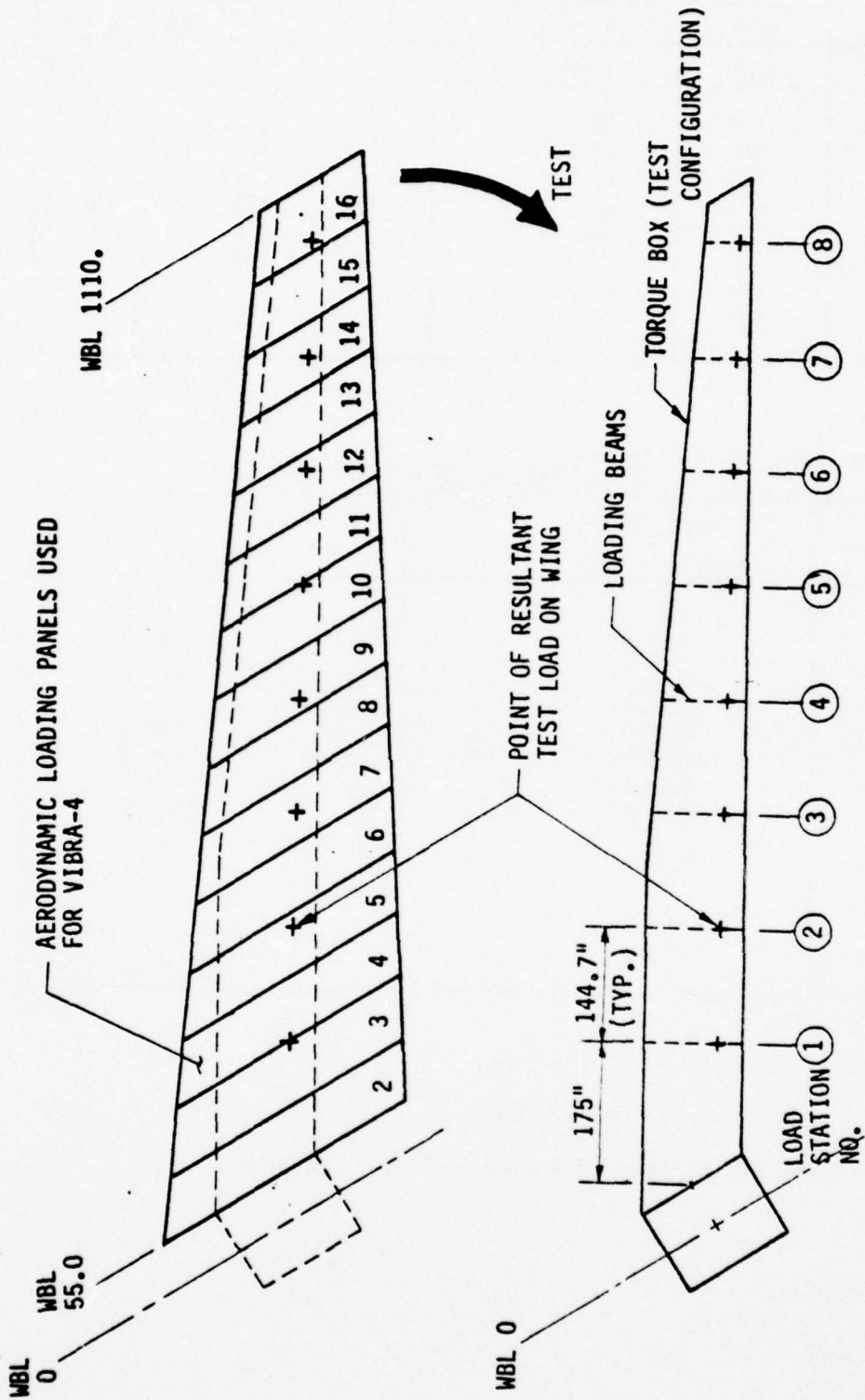


Figure 2-4 B-52H Wing Aerodynamic Loading Distribution For Test

MOMENT LOCATIONS

STA	WING LOCATION (WBL)		FIN LOCATION (WL)	
	DATS	VIBRA-4	DATS	VIBRA-4
1	103	84.6	261.6	261.6
2	308	280	312	
3	719	693	342	
4	856	801	373	361
5	1016	999	404	
6	55		434	
7	788		465	
8	*55		495	

*Wing Shear at WBL 55
LOAD STATION LOCATION

STA	WING DATS LOCATION (WBL)	FIN DATS LOCATION (WL)
1	187.5	311.6
2	310.5	342.3
3	433.4	373.0
4	556.4	404.0
5	679.4	434.4
6	802.3	465.3
7	925.0	496.0
8	1048.0	529.6
Inboard Nacelle	319.0	
Outboard Nacelle	648.8	
Tip Tank	921.1	

Figure 2-5

Location of Bending Moment and Load Stations

PANEL CENTER WBL	480 KIP		230 KIP	
	LBS/IN	LBS/PANEL	LBS/IN	LBS/PANEL
55	263	28930.	143	15730.
165	284	31240.	156	17160.
275	277	30470.	160	17600.
385	270	29700.	165	18150.
495	253	27830.	152	16720.
605	219	24090.	125	13750.
715	183	20130.	101	11110.
825	161	17710.	88	9680.
935	116	12760.	59	6490.
1045	73	8030.	31	3410.

TOTAL = 230890.

TOTAL = 129800.

- NOTES: (1) Panel Width = 110".
- (2) Tail load and nacelle load must be combined with above to balance airplane.

Figure 2-6 Wing Pre-Blast Steady State Lift Distribution (Wichita Loads Program)

WBL	BENDING MOMENTS (IN-LB x 10 ⁻⁶)			
	480 KIP		230 KIP	
	V-4	WICHITA STEADY LOADS PROGRAM	V-4	WICHITA STEADY LOADS PROGRAM
84.6	35.7	49.7	16.7	22.1
280.	20.7	32.1	9.32	15.3
693.	5.06	8.0	3.28	5.6
801.	2.30	3.6	1.39	2.1
999.	0.286	0.10	0.155	0.40

Note: Above based on 30 SYMMETRIC MODES (V-4).

Figure 2-7 Wing Pre-Blast Bending Moments

ULTIMATE BENDING MOMENTS (0 MARGIN)

(~ IN-LB X 10⁻⁶)

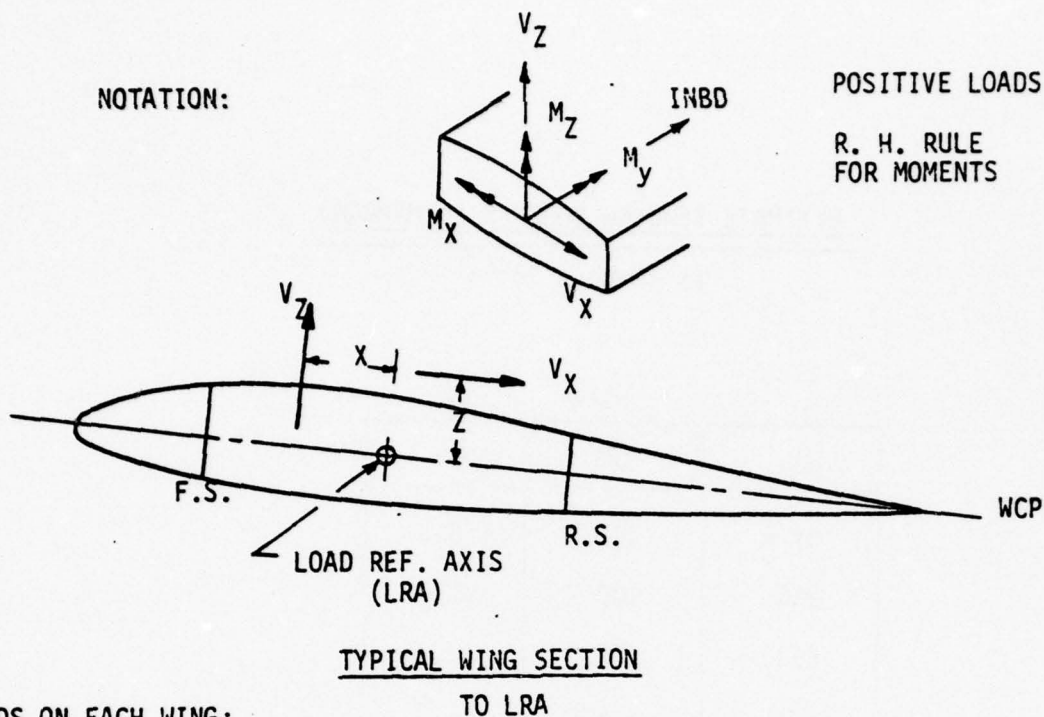
WING

WBL	UP	DOWN
84.6	161.7	178.3
280.	108.7	80.7
693.	26.0	12.2
801.	14.2	7.7
999.	1.79	0.9

FIN

BWL	SIDE
261.6	11.4
361.	4.91

Figure 2-8 B-52H Wing and Fin Ultimate Bending Moment Capability



LOADS ON EACH WING:

WBL	WING STA.	POSITIVE VERT. BENDING				NEGATIVE VERT. BENDING			
		V_Z -KIP	X-IN	V_X -KIP	Z-IN	V_Z -KIP	X-IN	V_X -KIP	Z-IN
248.6	402	32.0	53.4	①		③ -29.89	29.26		
371	547	8.0	60.4	-10.0	-13.1	-25.95	29.08		NO
472	665	23.0	29.7			-21.84	28.85		CHORD
574	785	26.0	30.5	①		-14.02	25.43		LOADS
698	931	14.0	43.3	-8.0	-10.1	-1.36	-26.84		
795.7	1046	26.0	19.5	①		-1.82	-21.24		
950.4	1228	21.0	②	-6.0	-7.5	-2.23	-18.25		
1032.8	1325	16.0	-1.5			-1.64	-23.17		

- ① LOADS APPLIED THROUGH REAR SPAR JACK PAD
- ② C3.44 IN. FWD OF L.R.A. MEASURED ALONG WBL 964.4 (C FORMER)
- ③ INCLUDES CALCULATED FORMER WEIGHT

Figure 2-9 Wing Tested Limit Load Capability

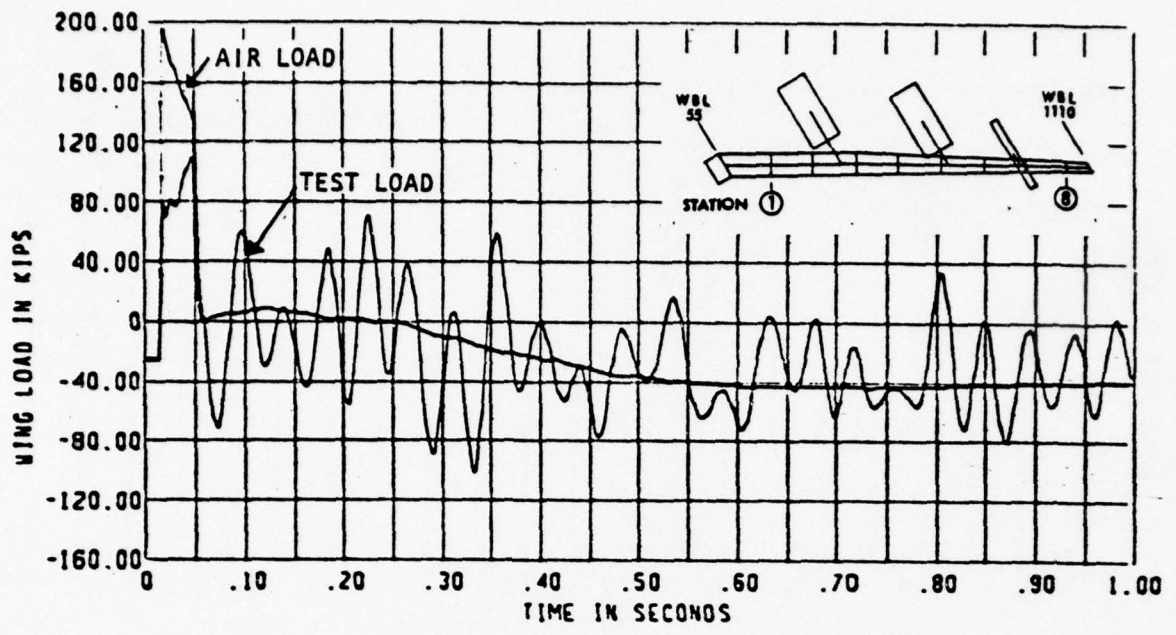


Figure 2-10 Wing Air & Test Load at Station 1

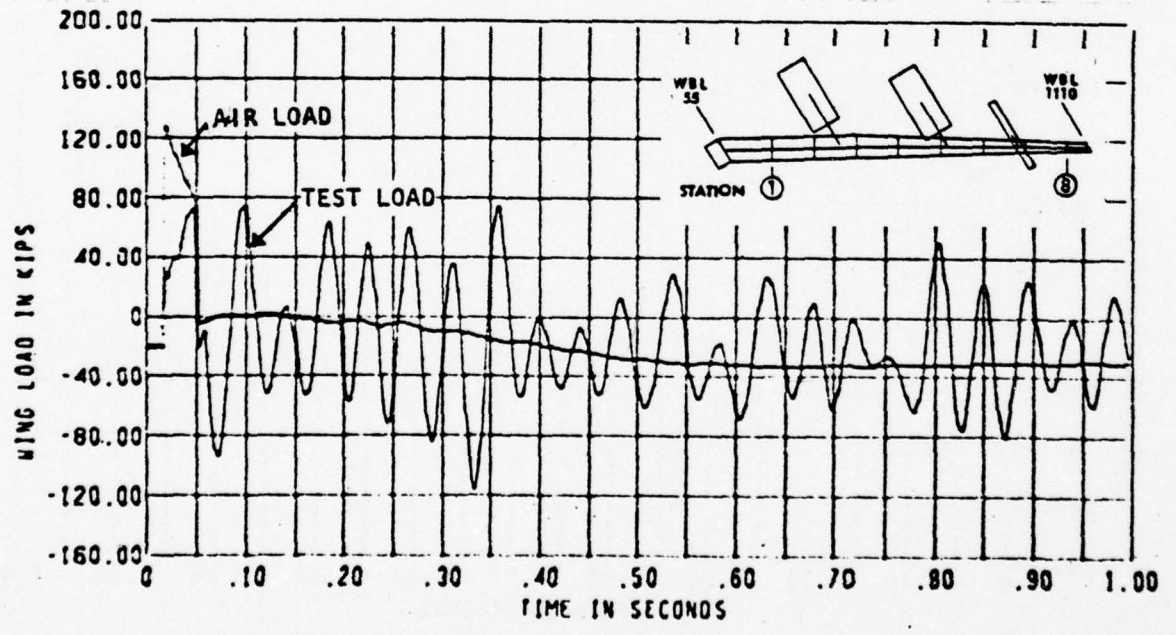


Figure 2-11 Wing Air & Test Load at Station 2

VIBRA 4 (30 Modes) Test Load and Aerodynamic Load B-52H Wing

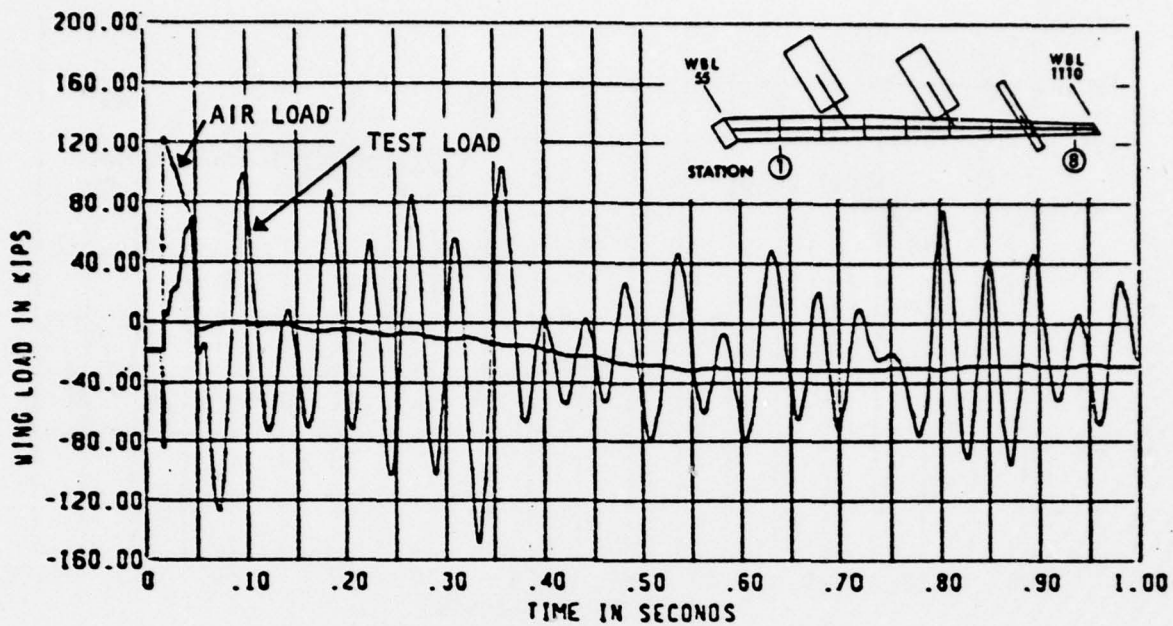


Figure 2-12 Wing Air & Test Load at Station 3

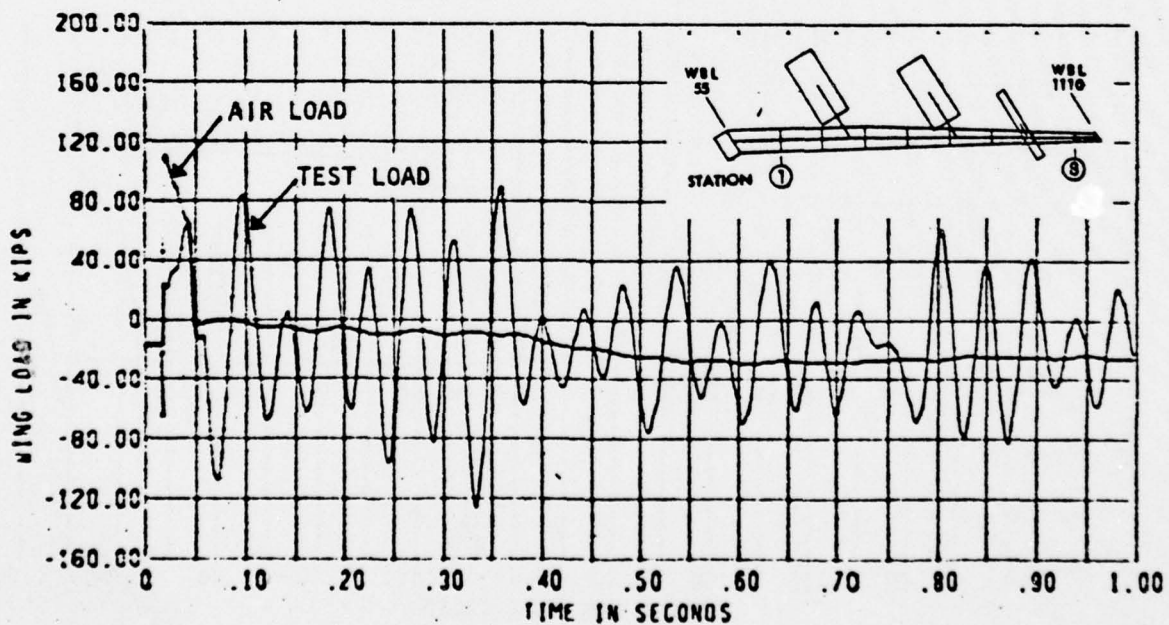


Figure 2-13 Wing Air & Test Load at Station 4

VIBRA 4 (30 Modes) Test Load and Aerodynamic Load B-52H Wing

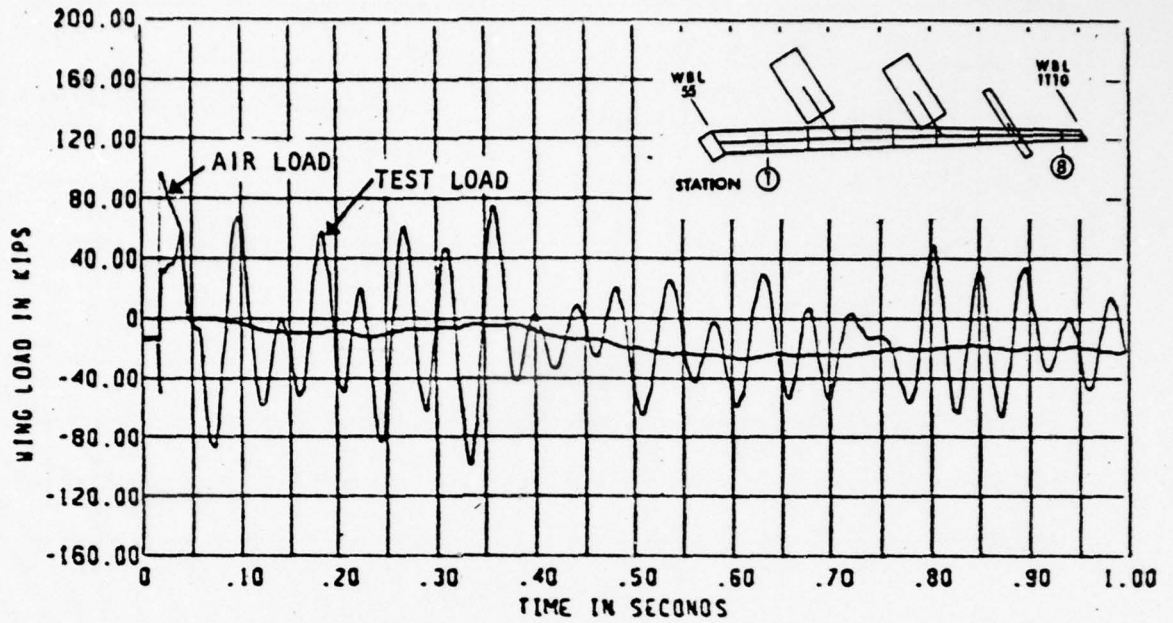


Figure 2-14 Wing Air & Test Load at Station 5

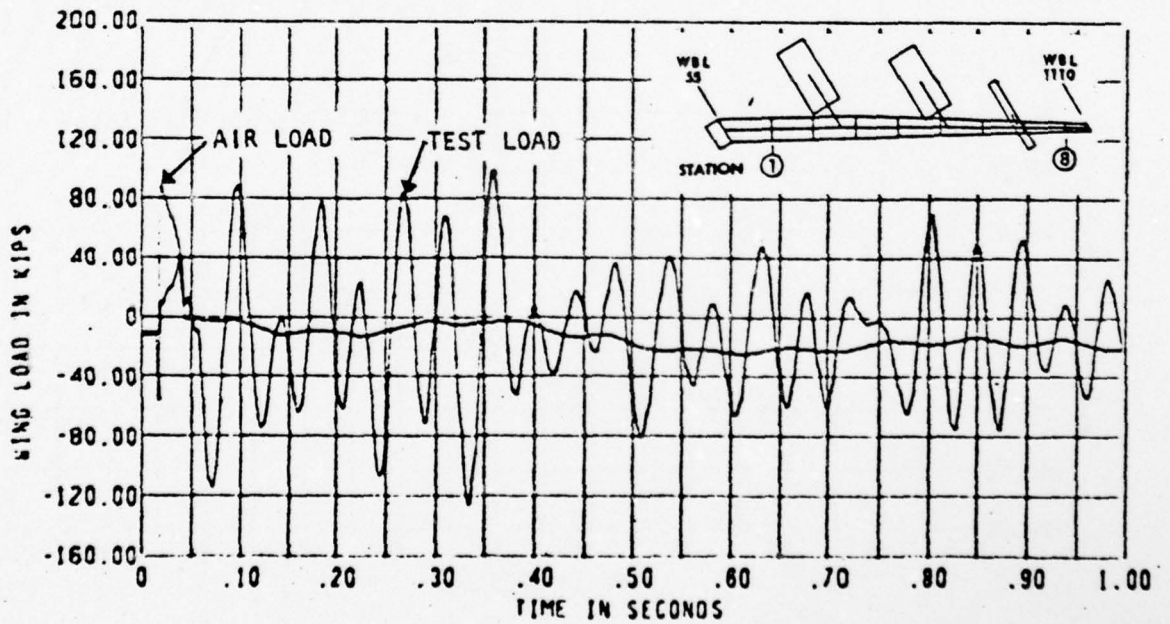


Figure 2-15 Wing Air & Test Load at Station 6

VIBRA 4 (30 Modes) Test Load and Aerodynamic Load B-52H Wing

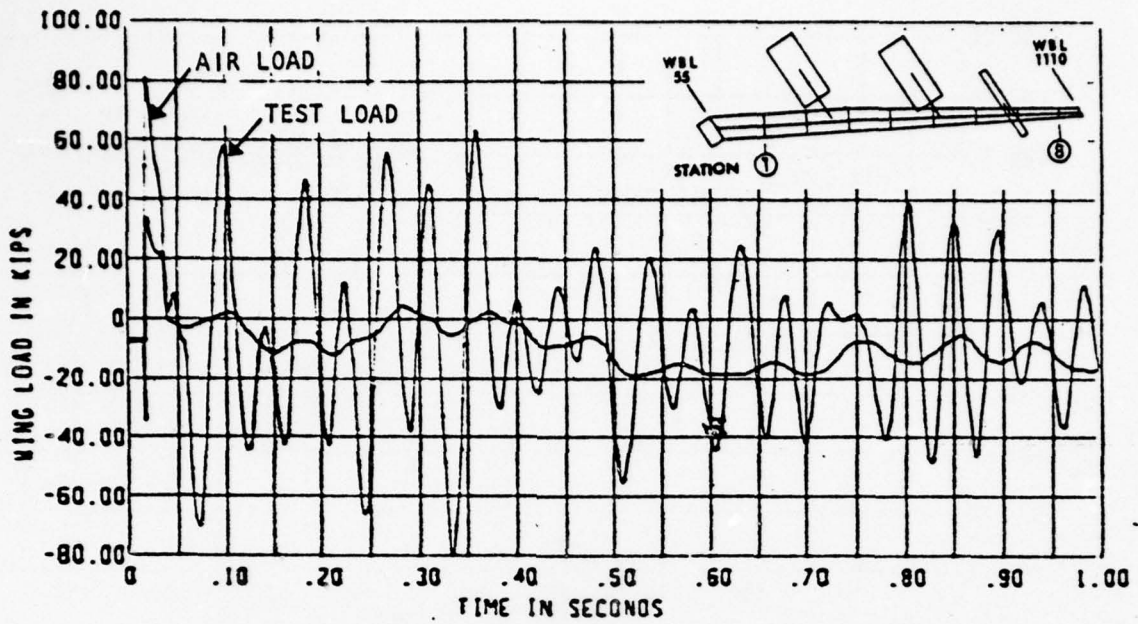


Figure 2-16 Wing Air & Test Load at Station 7

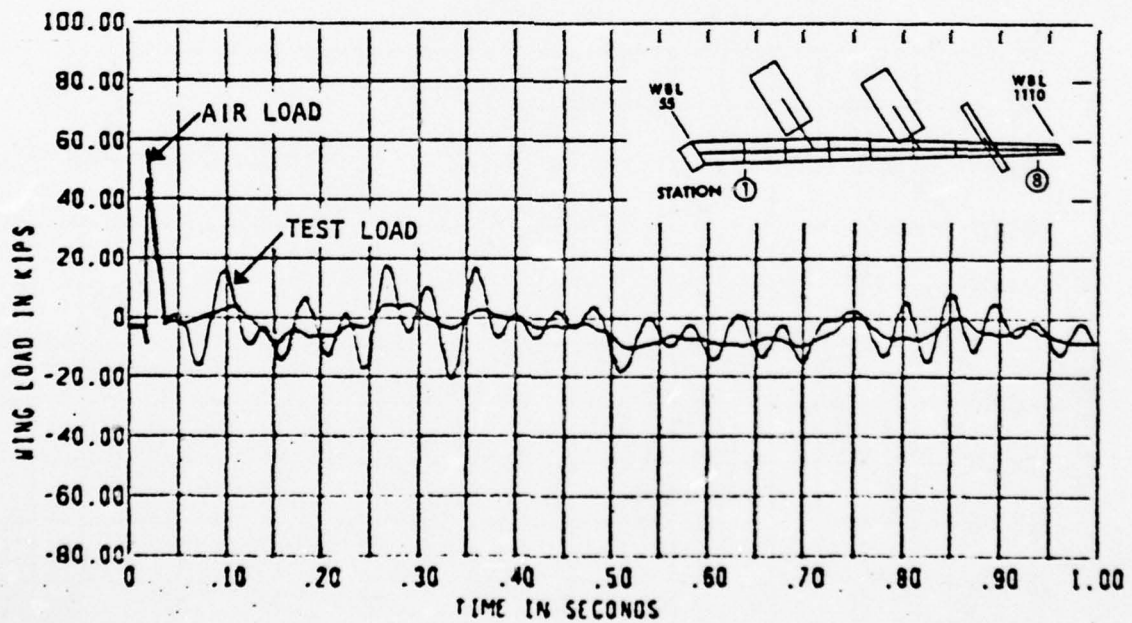


Figure 2-17 Wing Air & Test Load at Station 8

VIBRA 4 (30 Modes) Test Load and Aerodynamic Load B-52H Wing

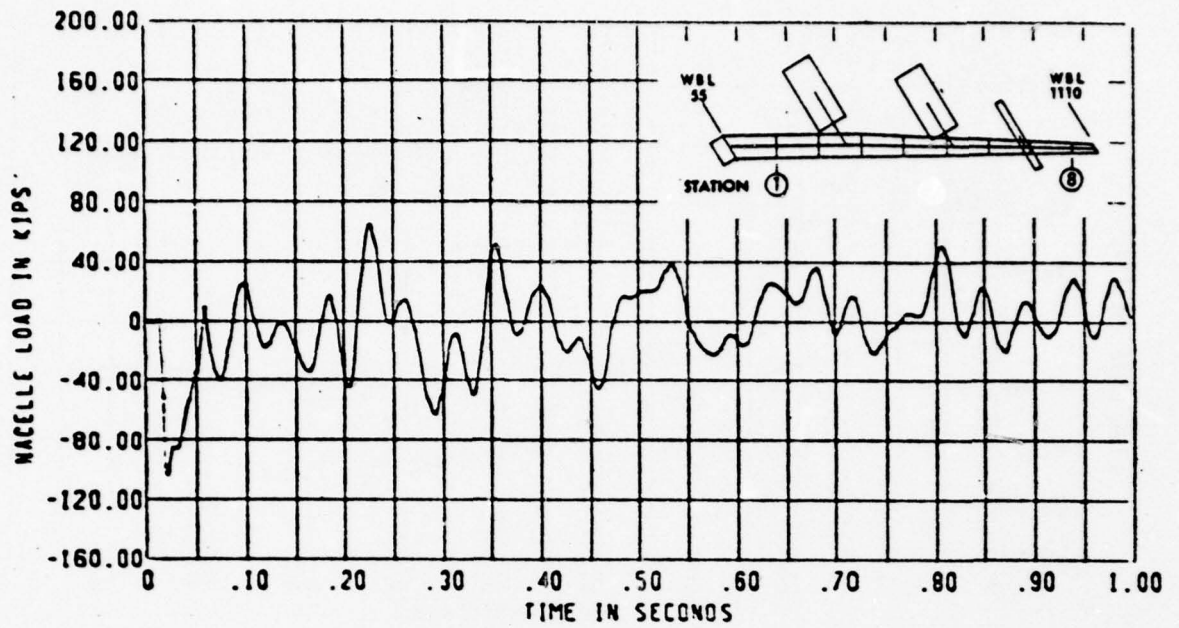


Figure 2-18 Inboard Nacelle Test Load

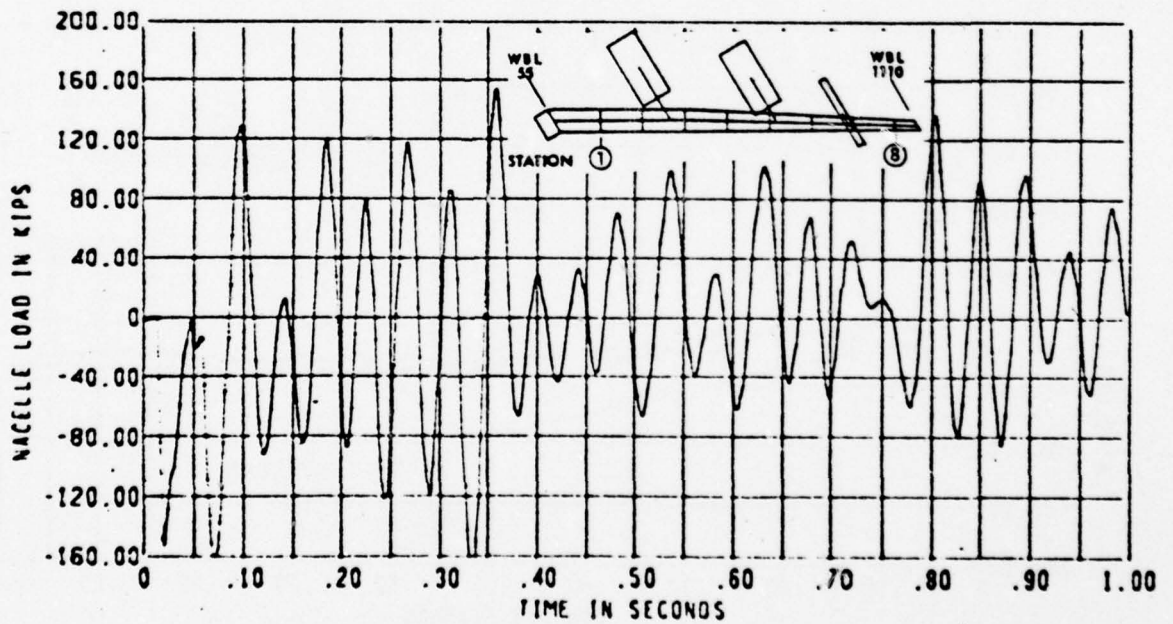


Figure 2-19 Outboard Nacelle Test Load

VIBRA 4 (30 Modes) Test Load and Aerodynamic Load B-52H Wing

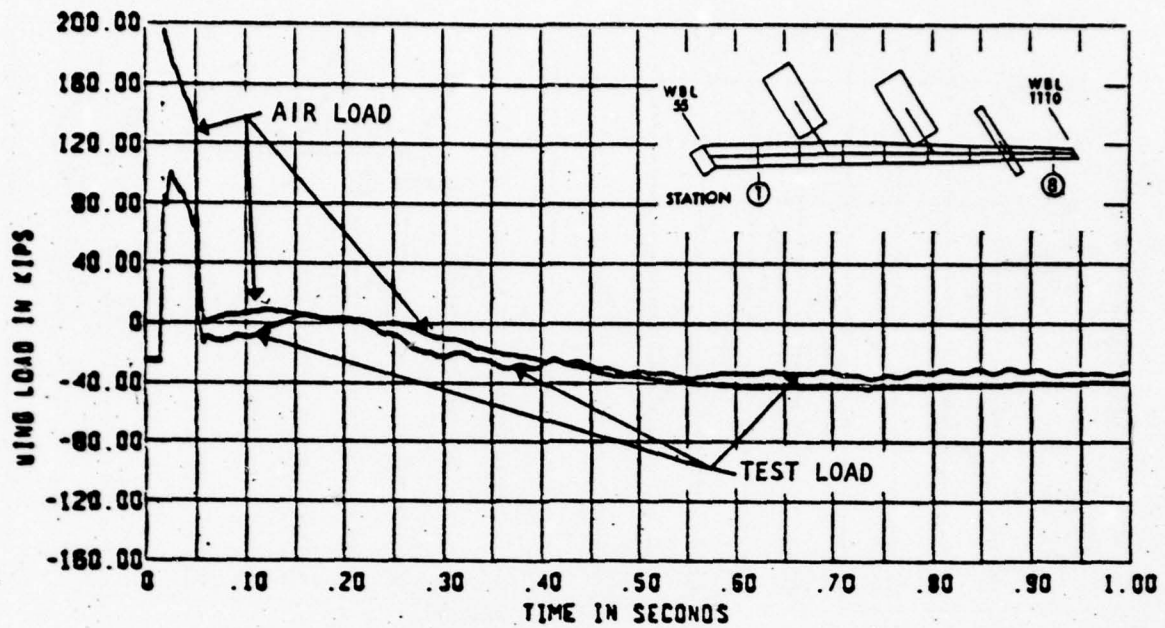


Figure 2-20 Wing Air & Test Load at Station 1

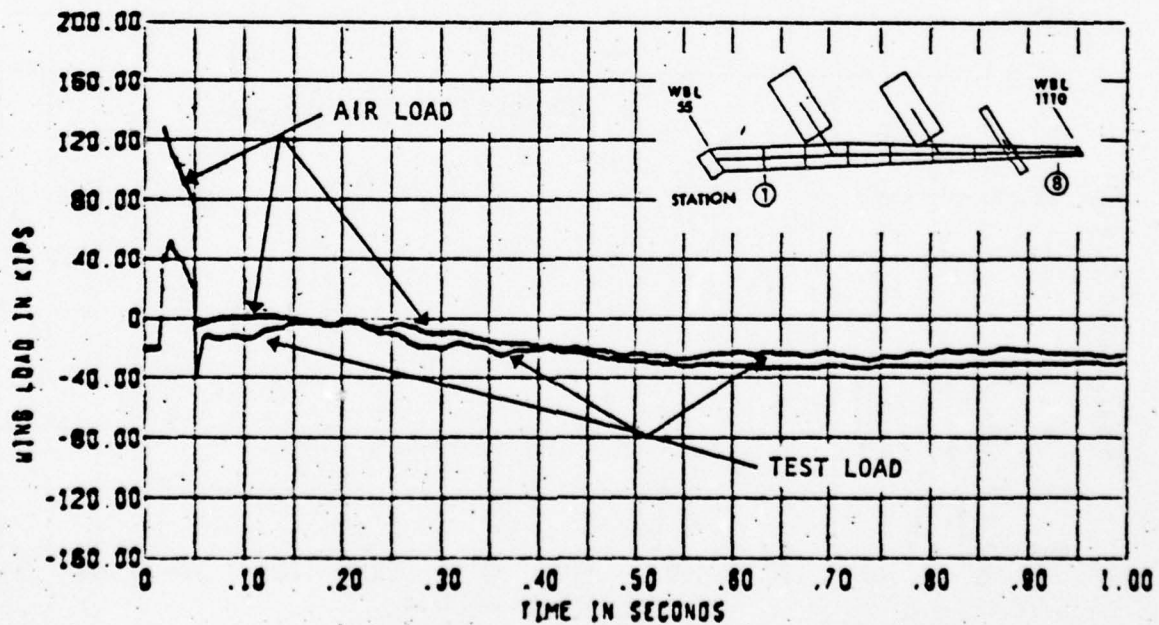


Figure 2-21 Wing Air & Test Load at Station 2

VIBRA 4 (8 Modes) Test Load and Aerodynamic Load B-52H Wing

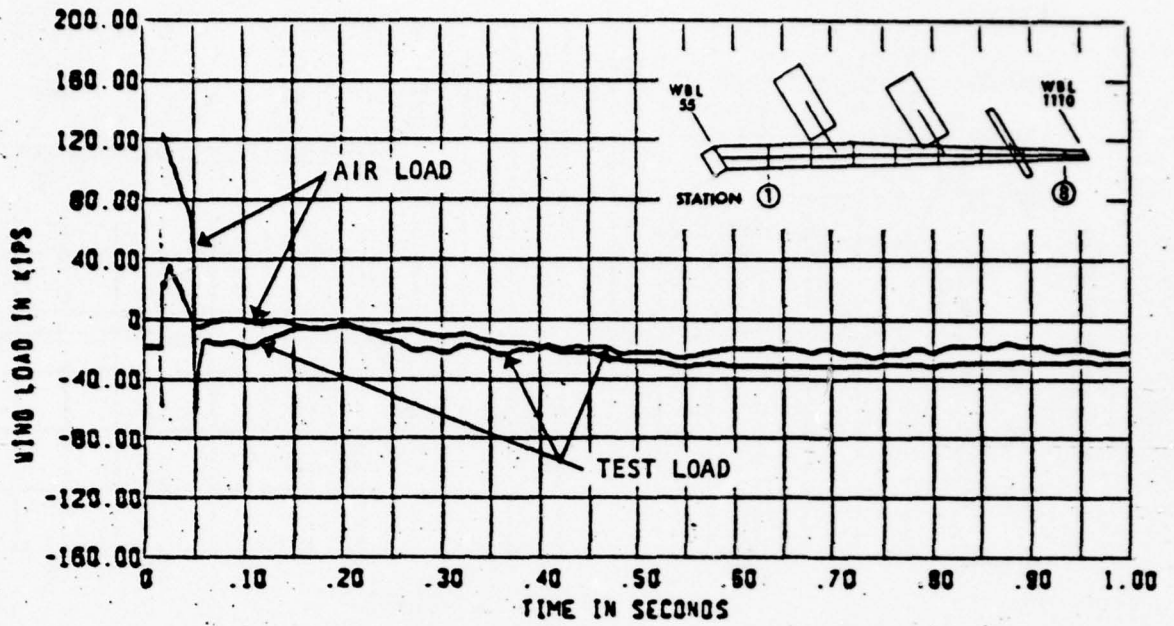


Figure 2-22 Wing Air & Test Load at Station 3

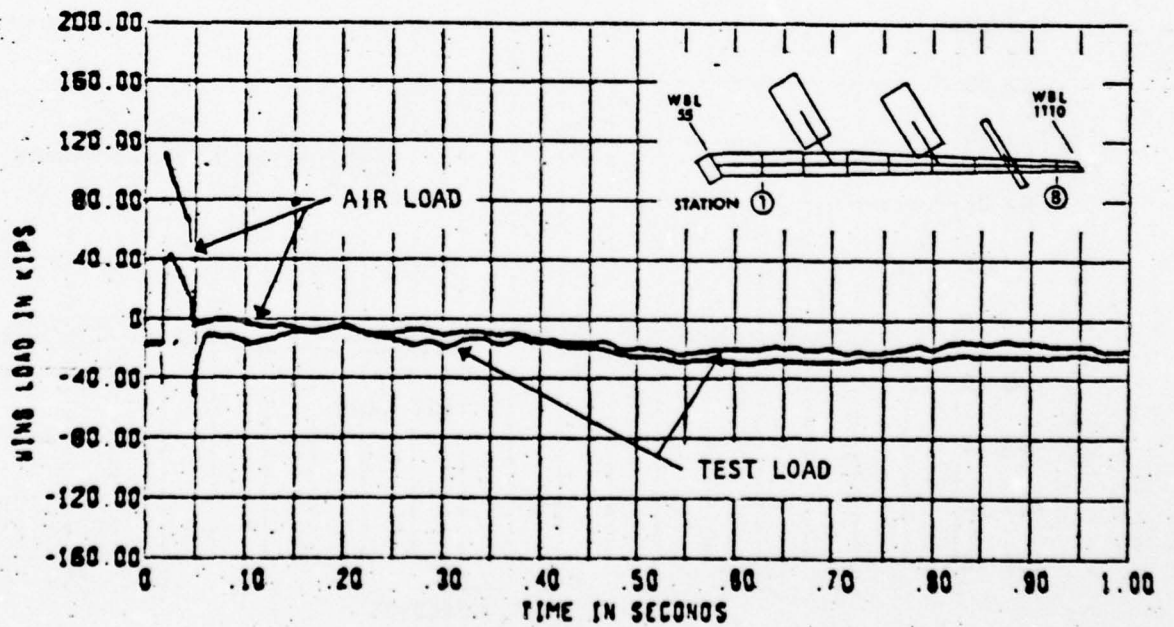


Figure 2-23 Wing Air & Test Load at Station 4

VIBRA 4 (8 Modes) Test Load and Aerodynamic Load B-52H Wing

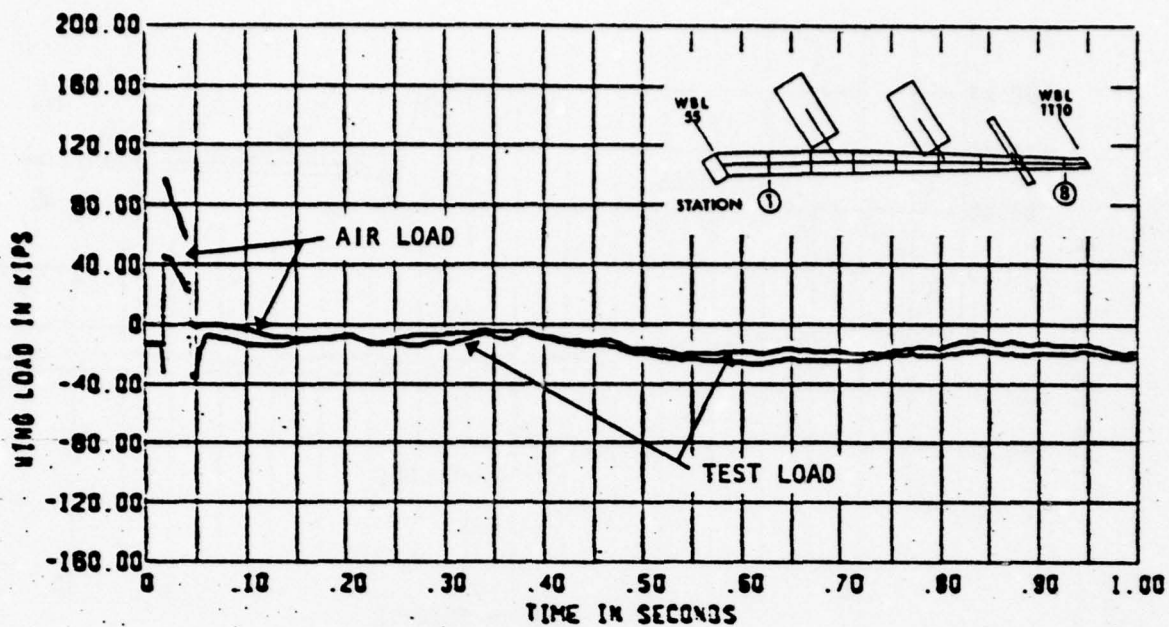


Figure 2-24 Wing Air & Test Load at Station 5

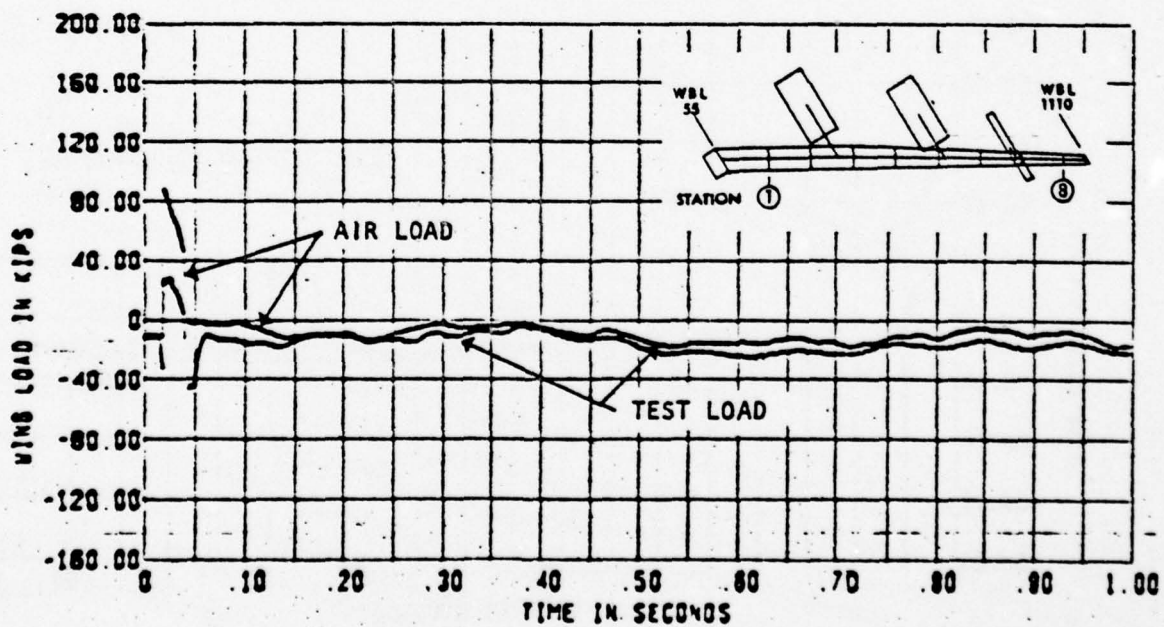


Figure 2-25 Wing Air & Test load at Station 6

VIBRA 4-(8 Modes) Test Load and Aerodynamic Load B-52H Wing

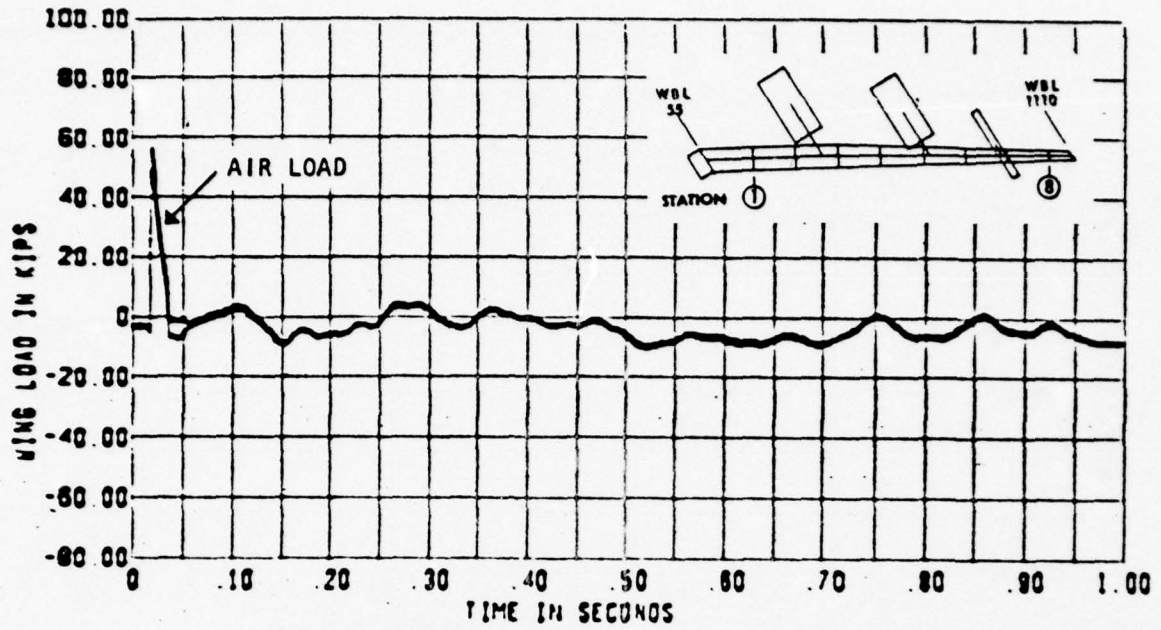


Figure 2-26 Wing Air & Test Load at Station 7

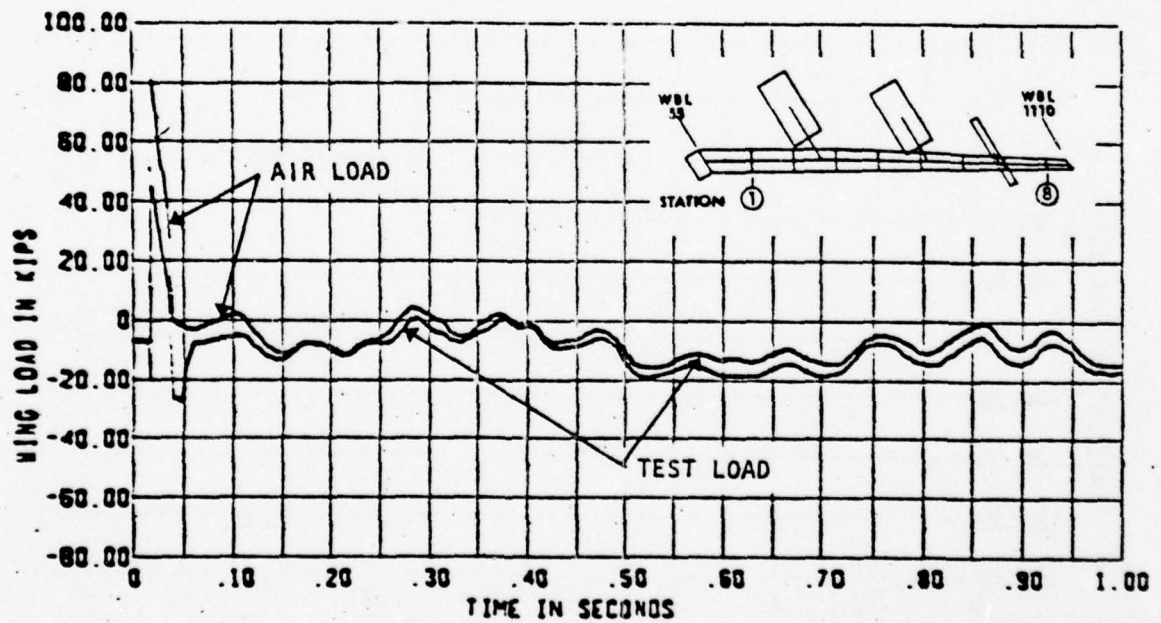


Figure 2-27 Wing Air & Test Load at Station 8

VIBRA 4 (8 Modes) Test Load and Aerodynamic Load B-52H Wing

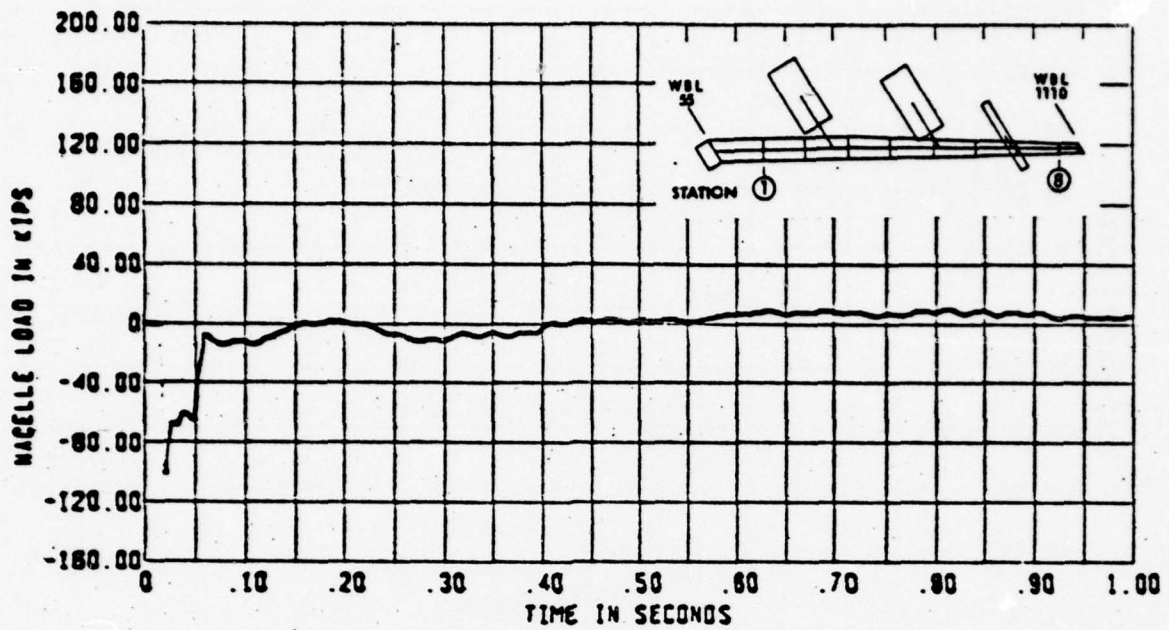


Figure 2-28 Inboard Nacelle Test Load

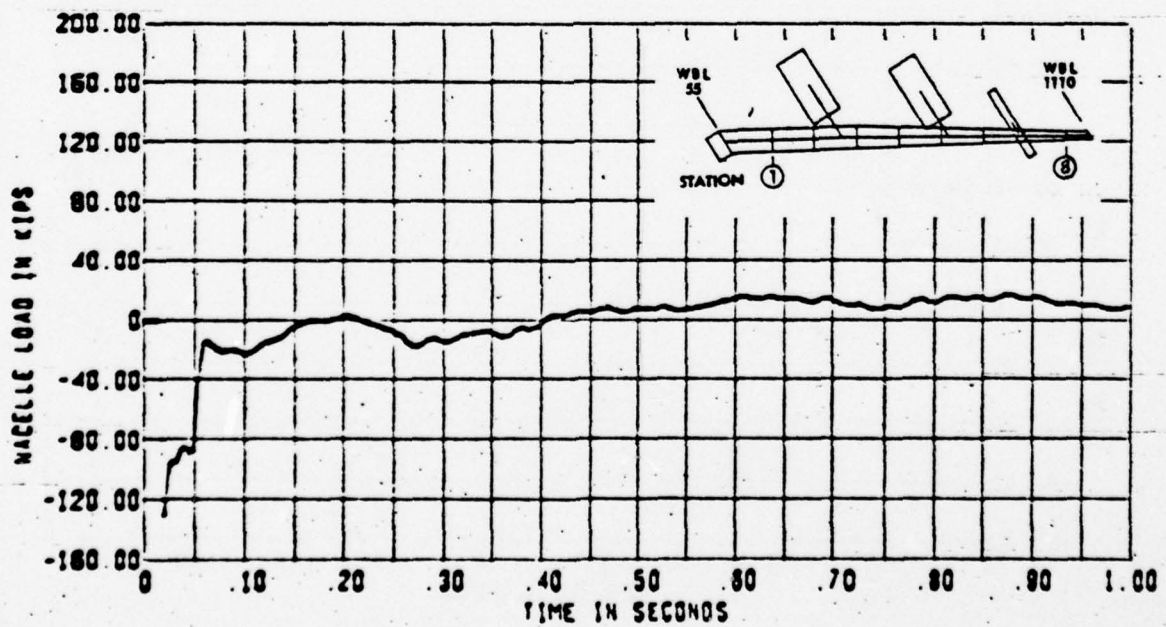


Figure 2-29 Outboard Nacelle Test Load

VIBRA 4 (8 Modes) Test Load and Aerodynamic Load B-52H Wing

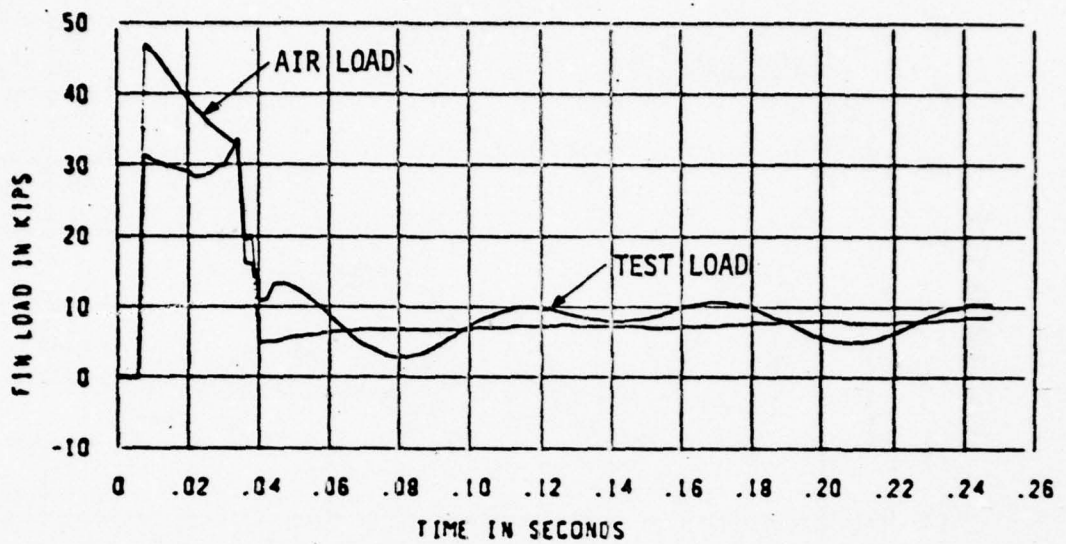


Figure 2-30 VIBRA-4 Test Load and Aerodynamic Load B-52H Fin, Station 1

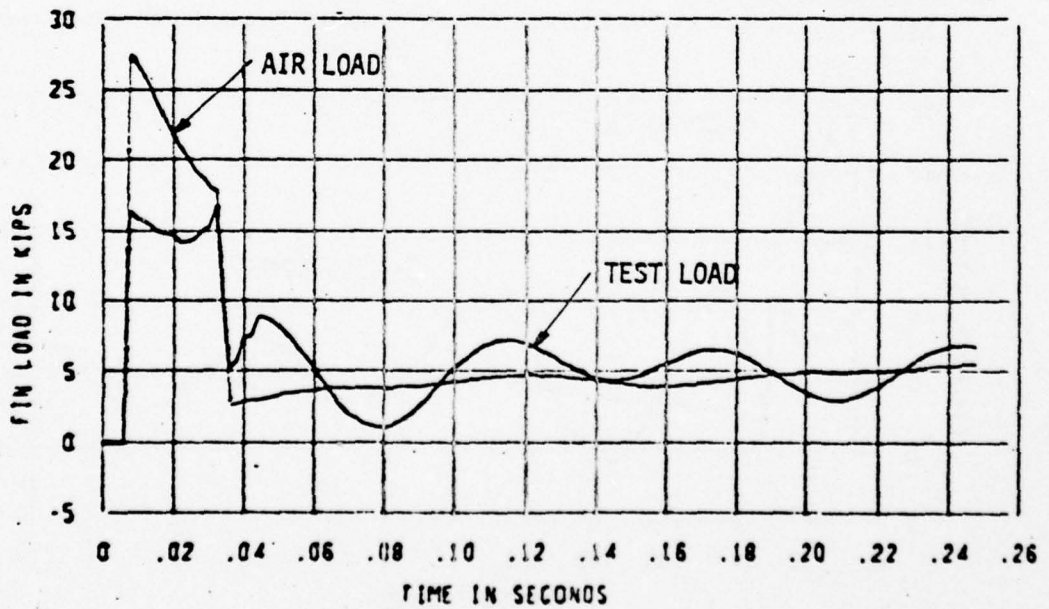
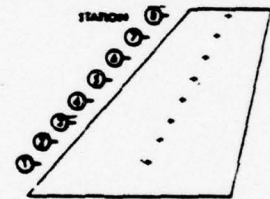


Figure 2-31 VIBRA-4 Test Load and Aerodynamic Load B-52H Fin, Station 2

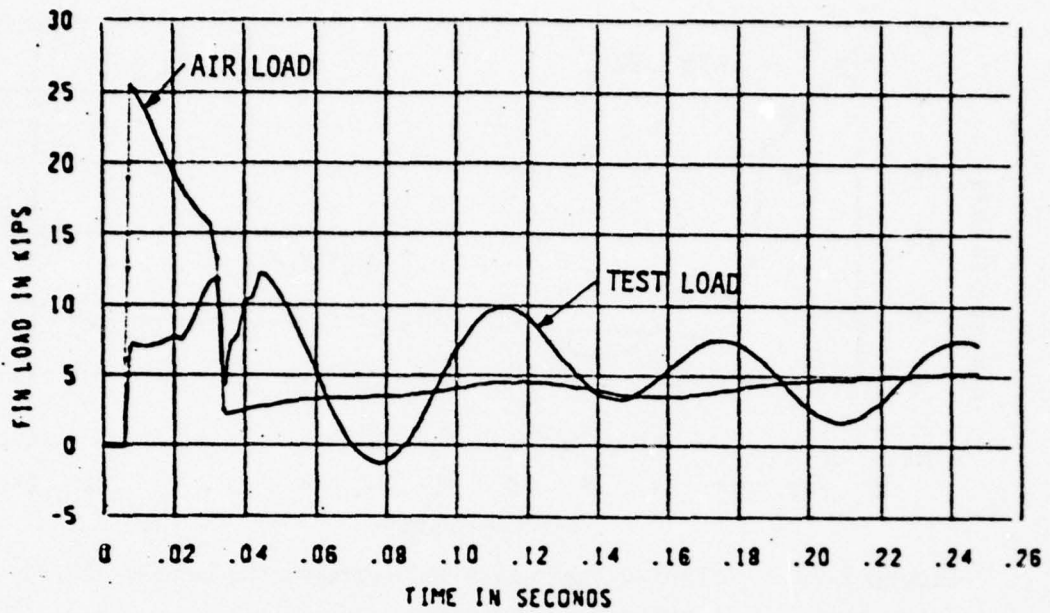


Figure 2-32 VIBRA-4 Test Load and Aerodynamic Load B-52H Fin, Station 3

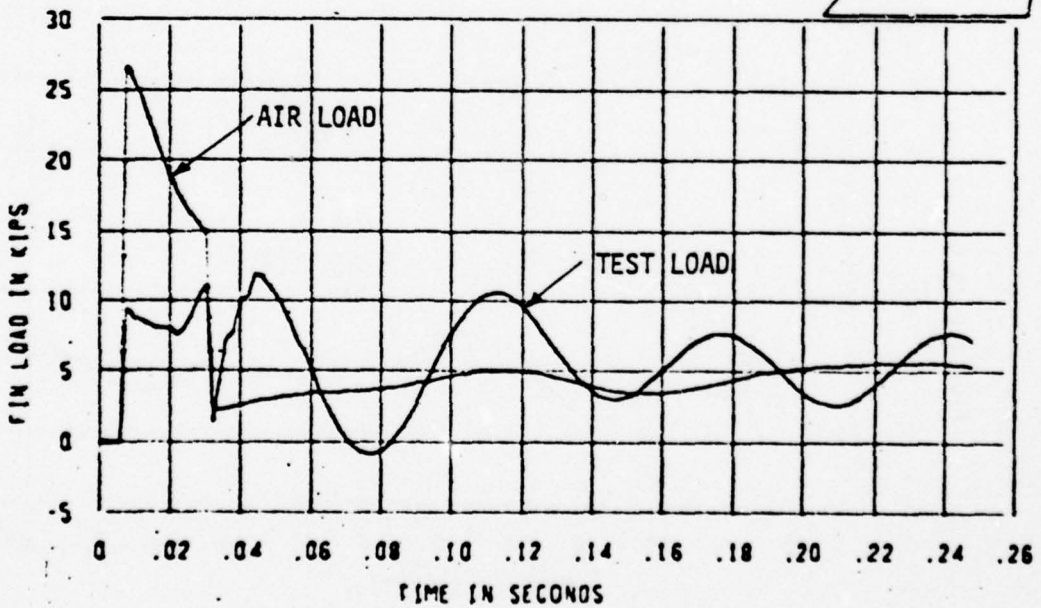


Figure 2-33 VIBRA-4 Test Load and Aerodynamic Load B-52H Fin, Station 4

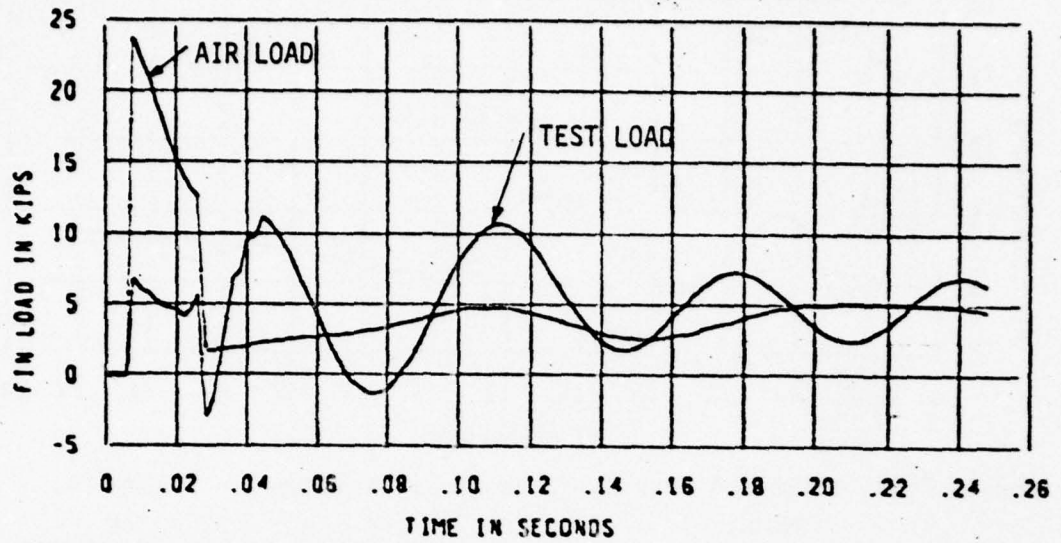


Figure 2-34 VIBRA-4 Test Load and Aerodynamic Load B-52H Fin, Station 5

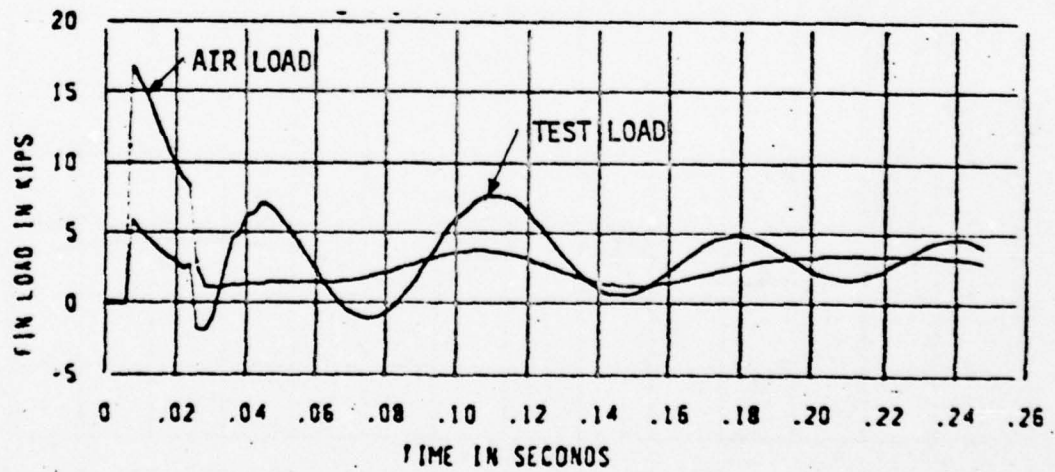
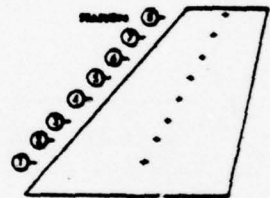


Figure 2-35 VIBRA-4 Test Load and Aerodynamic Load B-52H Fin, Station 6

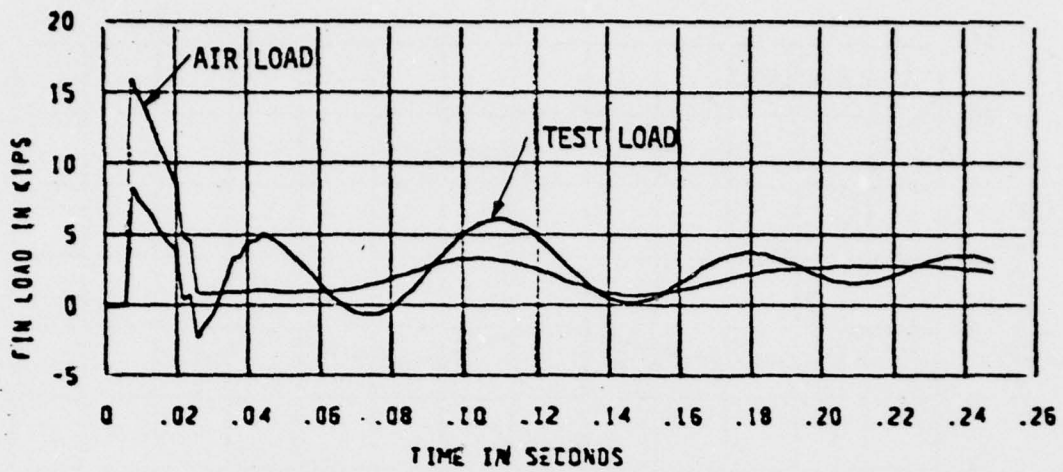


Figure 2-36 VIBRA-4 Test Load and Aerodynamic Load - B-52H Fin, Station 7

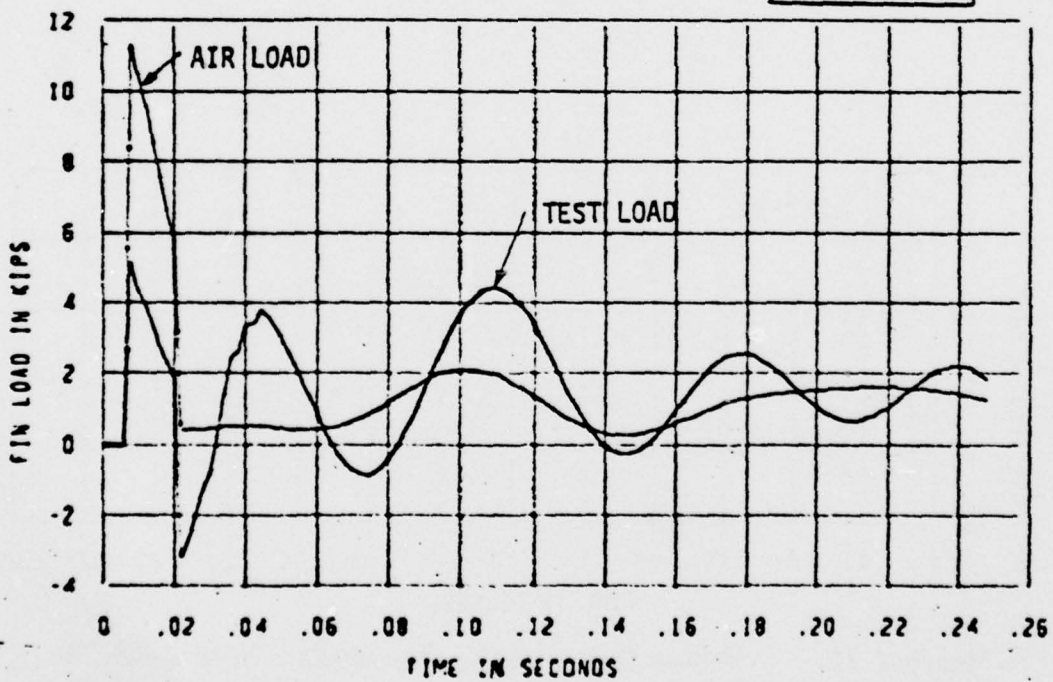
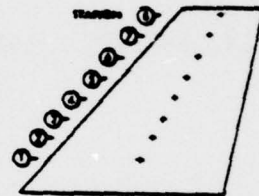


Figure 2-37 VIBRA-4 Test Load and Aerodynamic Load B-52H Fin, Station 8

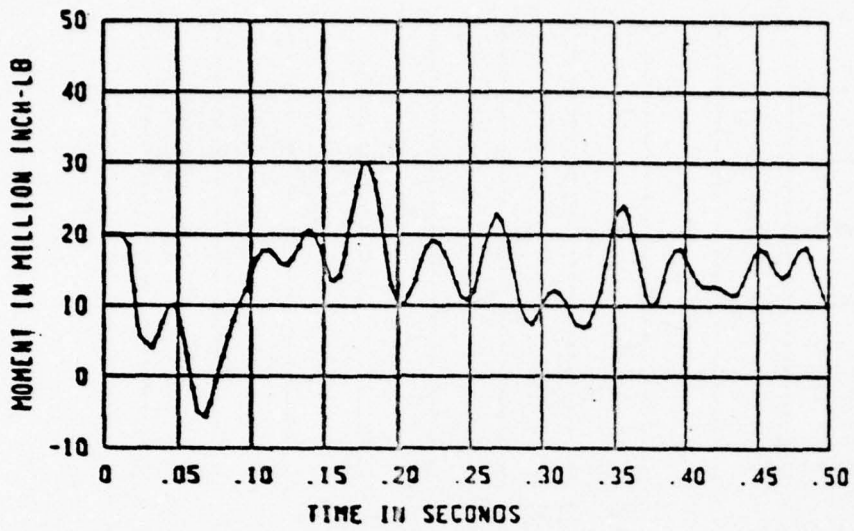


Figure 2-38 VIBRA-4 Bending Moment - B-52H Wing, Sta 1

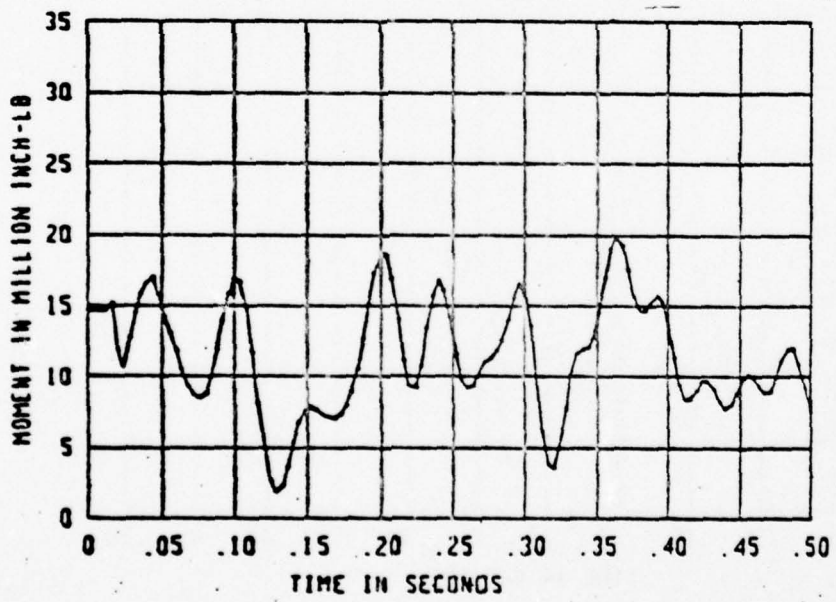
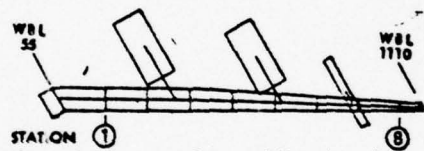


Figure 2-39 VIBRA-4 Bending Moment - B-52H Wing, Sta 2

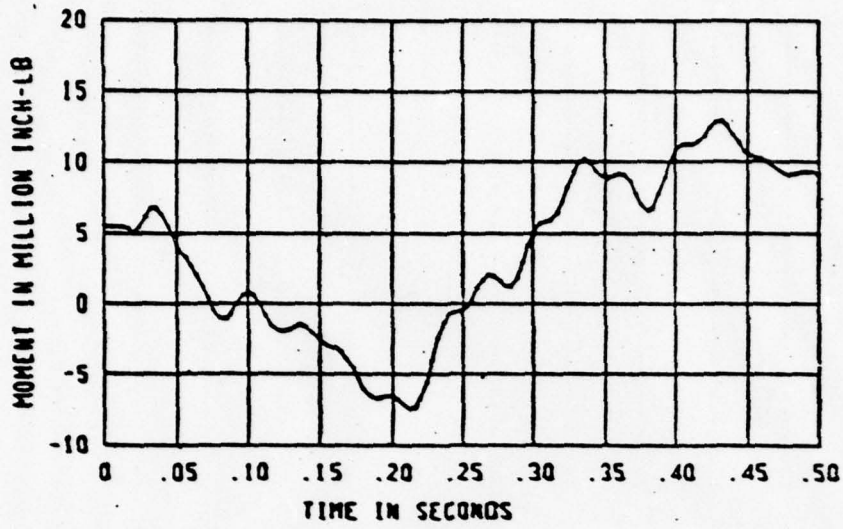


Figure 2-40 VIBRA-4 Bending Moment - B-52H Wing, Sta 3

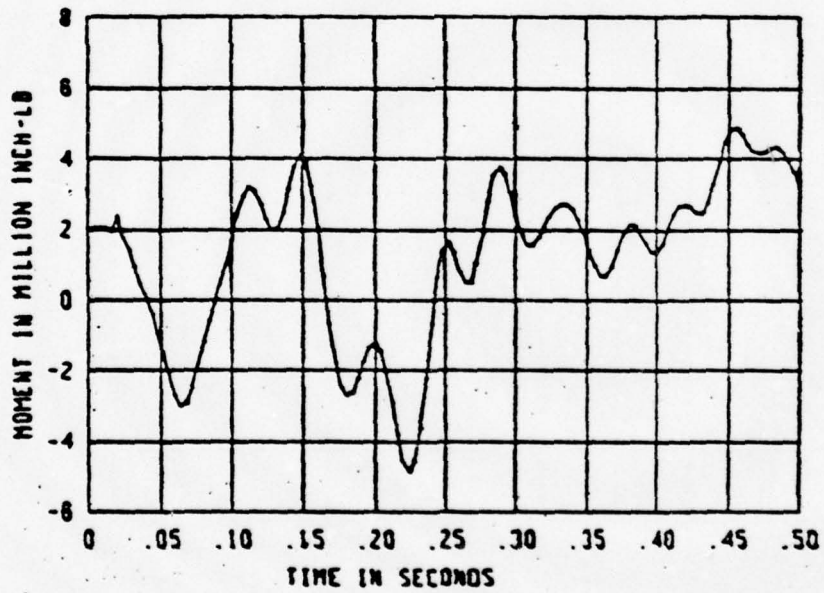
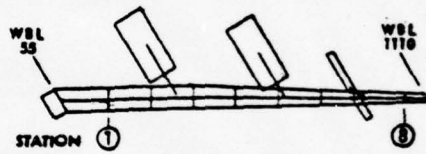


Figure 2-41 VIBRA-4 Bending Moment - B-52H Wing, Sta 4

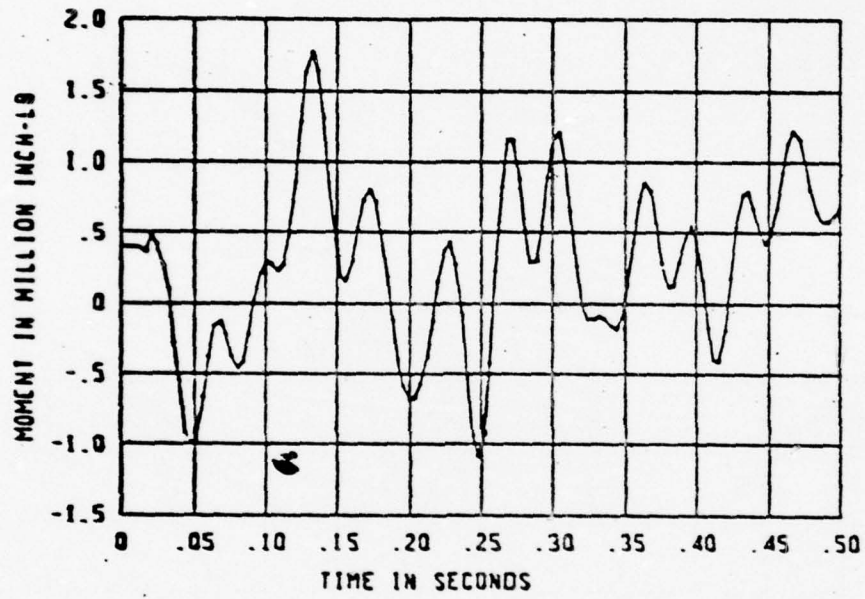
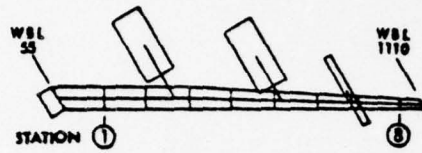


Figure 2-42 VIBRA-4 Bending Moment - B-52H Wing, Sta 5

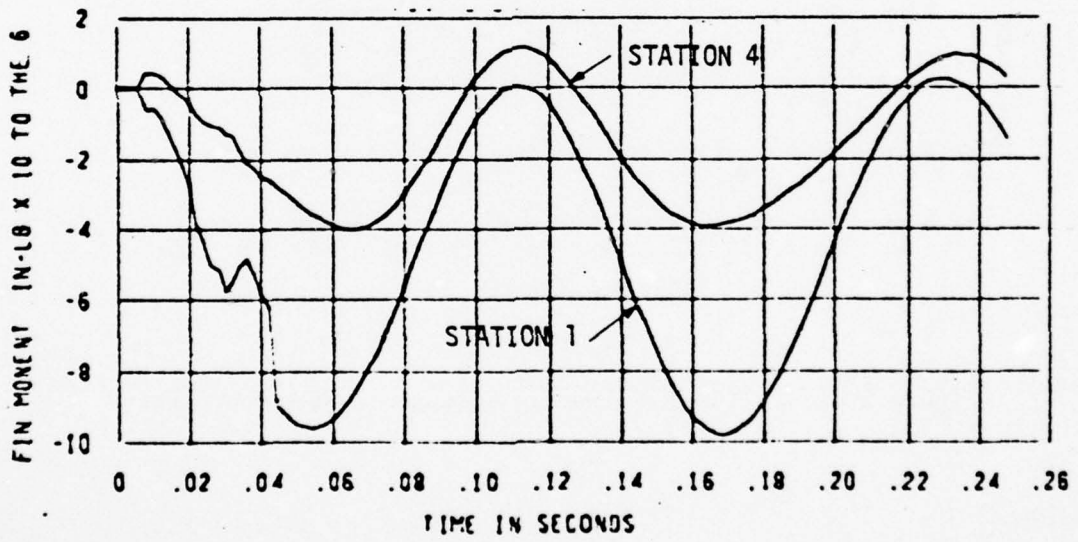
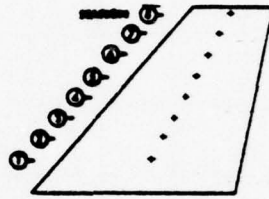


Figure 2-43 VIBRA-4 Bending Moment B-52H Fin.

SECTION III DYNAMIC MODEL OF TEST SIMULATION

3.0 INTRODUCTION

Section III contains the physical description of both the fin and wing models. The results of the test simulation is presented and compared to the response of the model driven by nuclear blast loading. Selected bending moment comparisons are also made with results from the B-52H VIBRA-4 flight loads blast simulation.

3.1 DYNAMIC MODELS

The dynamic models developed for this study are outlined in this section. They include the cantilever models of the B-52H wing and fin described in Reference 1 in addition to the integrated models of the test hardware and test article.

3.1.1 Fin Dynamic Model

The fin dynamic model is described by the data on Figures 3-1 to 3-4. Coordinates, stiffness and mass data were taken directly from Reference 2.

Cantilever modes and frequencies were developed from these properties using the NASTRAN computer code. The comparison of the cantilever frequencies for the fin between NASTRAN calculations and those previous developed by Boeing Wichita Division for loads calculations are given on Figure 3-5. As shown on Figure 3-5 the agreement between the two models is quite good. Discrepancies could be attributed to the constant stiffness element used by NASTRAN verses the linear varying stiffness element used for the Wichita analysis. Other differences are that NASTRAN used the rotatory inertia terms as opposed to the use of separated masses to describe the rotatory terms for the Wichita analysis.

3.1.2 Wing Dynamic Model

The wing dynamic model is described by the data on Figures 3-6 to 3-10. This data was taken directly from Reference 2. Cantilever modes and frequencies were developed from these properties using the NASTRAN computer

3.1.2 (Continued)

code. The wing was considered fixed with respect to bending at the centerline (WBL=0) and restrained from translation at the fuselage (WBL=54.9). Torsion of the wing at the fuselage was assumed to be carried by fuselage. The comparison of the wing supported frequencies developed using the NASTRAN model and the wing symmetric frequencies developed by Wichita for loads calculation for a 230 Kip gross weight configuration are presented on Figure 3-11. In general the agreement is quite good except for the additional frequencies from the NASTRAN model. These are attributed to the extra cantilever freedoms of the nacelles which were merged in the NASTRAN model whereas the Wichita model considered the nacelles to be rigidly mounted to the wing for their symmetric wing model (Wichita added the cantilever nacelle modes when merging the solution for the entire airplane together). Other differences are that NASTRAN used the rotary inertia terms as opposed to separated masses to describe the rotatory terms for the Wichita analysis.

3.1.3 Fin Pull Test Dynamic Model

The fin dynamic model for the pull test is shown schematically on Figure 3-12. This model is mathematically described by equation (3). Because the base of the fin is fixed in inertial space for the test configuration, the absolute motion of the fin is described by

$$U_F = \phi q \quad (4)$$

where:

U_F = Fin absolute motion in the test.

Loading applied to the fin is shown in Figure 3-13. Before quick release (time = 0) the release cable load and the loading spring cable load are equal and the net force to the fin is zero. After quick release (<1 millisecond), the release cable load is zero and the loading spring

3.1.3 (Continued)

cable load is the net load applied to the fin. As the fin deforms towards the loading spring the force applied to the fin decreases. By knowing the deformation characteristics of the fin as a function of time the desired load decay can be achieved. The set of preloads and spring rates which gave the best fit to the VIBRA-4 test loads at the eight fin loading stations is also shown on Figure 3-13.

Moment and shear coefficients were derived for each pin structural member in the NASTRAN model as a function of the generalized acceleration q and applied force F at the eight loading stations. Runge Kutta integration was utilized for the solution of q as a function of time. From generalized displacements the absolute displacements U were determined, and from U , the resulting loading spring forces F were determined. Generalized acceleration q and F , were then used to get the fin bending moment and shears.

A total of ten fin modes (frequencies up to 102.6 Hz) were used in the dynamic analysis. Moments, accelerations and relative displacements were calculated at eight locations as a function of time.

3.1.4 Fin Base Shake Dynamic Model

The fin dynamic model for the base shake test is shown in Figure 3-14. This model is described mathematically by

$$\ddot{q} + 2\zeta\omega\dot{q} + \omega^2q = -\phi^T ML\theta \quad (5)$$

$$V_F = \phi q$$

$$U_F = V_F + L\theta$$

where:

- q, \dot{q}, \ddot{q} Response freedoms of the fin cantilever modes
- ω Natural frequencies of the cantilever fin
- ϕ^T Transpose of the modal values at the mass freedoms of the fin. All modes are normalized to have a generalized mass equal to unity.

3.1.4 (Continued)

M	Mass matrix for fin.
ζ	Factor of critical damping. Five percent of critical was used for this study.
U_F	Fin absolute displacement
V_F	Fin displacement relative to rigid motion of base.
L	Rigid body vector with respect to fixture pivot.
θ	Rotation about fixture pivot.

Loading is applied to the fin by the MSS actuator. The actuator is programmed to the prescribed velocity curve shown also on Figure 3-14. The initial velocity build up accelerates the fin to the right and loads the fin inertially to the left. By varying the distance from the pivot to the base of the fin, the ratio of the inertia loading at the top of the fin with respect to the bottom of the fin can be varied; e.g., increasing the distance decreases this ratio. The choice of pivot height is dependent on the required test loading distribution with respect to W.L., and fin mass distribution. The height shown on Figure 3-14 gave the best fit to VIBRA-4 test loads at the eight fin loading locations.

Once the product $(-\phi^T ML)$ is formed, this base shake analysis proceeds identical to that presented for the dynamics pull test in Section 3.1.3.

3.1.5 Wing Pull Test Dynamic Model

The wing dynamic model for the pull test is shown schematically on Figure 3-15. This model is described mathematically the same as the fin pull test dynamic model in Section 3-15, except for the addition of the gravitational forces. Loading applied to the wing for the pull test is illustrated on Figure 3-16. Before quick release (time = 0) the loading spring load is set to the desired peak diffraction test loading and the release cable load on the wing is adjusted until it exceeds the loading spring cable load by the value of aerodynamic lift at that loading station. This results in a net load applied to the wing equal to the steady state lift and deforms the wing the same as in 1G

3.1.5 (Continued)

flight. After quick release the net load applied to the wing is equal to the load in the loading spring. As the wing deforms toward the loading spring the force applied to the wing decreases. By knowing the deformation characteristics as a function of time the desired load decay can be achieved. In order to better match the loading on the wing for the overhead blast condition it is necessary to release the load spring cables after the diffractive load phase is over. The set of preloads, spring rates, and time of release of the loading springs which gave the best fit to the VIBRA-4 test loads are also given on Figure 3-16. Outside of the requirement of calculations for the initial deformation due to gravity and steady state lift, the wing pull test computer program is identical to that for the fin pull test.

3.2 COMPARISON OF THE VIBRA-4 AND DATS

In order to verify the DATS a comparison was made using the VIBRA-4 test loading as an input to DATS and then comparing bending moment calculated by DATS to the bending moment calculated by VIBRA-4. As shown in Section 2.2 the responses and hence the bending moments should be identical if both VIBRA-4 and DATS equations of motion are formulated exactly the same. A number of differences exists between the sets of equilibrium equations. The first item is modal truncation. In order to fit in the VIBRA-4 code the total number modes is reduced to a maximum system frequency of less than 20 Hz such that only one or two flexible fin modes are contained in the coupled system. In contrast the DATS analysis uses ten fin modes with a cutoff frequency of 102 Hz. Another point of difference is that DATS test loading is applied only at the eight loading station on the fin and at 10 loading stations on the wing whereas VIBRA-4 effectively applies its loading at the mass points and aerodynamic panel centers. Different modeling techniques for the wing and fin for DATS and VIBRA-4 which were discussed in Section 3.1 will also contribute to differences in the results.

3.2 (Continued)

VIBRA-4 and DATS peak bending moments are plotted on Figure 3-17 for the B-52H fin as a function fin WL. DATS moments were evaluated using the same VIBRA-4 input but with ten (10) and one (1) cantilever fin modes. The DATS solution with one (1) fin modes gives the best fit to VIBRA-4 which also effectively has one fin mode. Both DATS solutions compare quite well with the VIBRA-4 solution indicating that one fin mode is probably adequate for fin bending moment evaluation. Except for the check case all DATS analysis for the fin used ten (10) modes. Ultimate fin bending moment capability is also shown on Figure 3-17 and demonstrates that the check case is at levels high enough to qualify the calculation. Time histories of DATS fin bending moments using ten (10) fin modes are compared to VIBRA-4 on Figures 3-18 and 3-19 for the two WL stations where VIBRA-4 moments were computed and for the closest corresponding locations from DATS. Both solutions have good agreement in phasing and peak values. DATS time histories of bending moment for ten (10) fin modes and one (1) fin modes are shown on Figure 3-20 thru 3-27 for eight fin locations.

VIBRA-4 and DATS peak bending moments are plotted on Figure 3-28 for the overhead blast on the B-52H wing as a function WBL. The VIBRA-4 bending moments were calculated using 30 VIBRA-4 flexible modes for five Wing stations. The DATS solution was evaluated using the VIBRA-4 test load which was calculated using eight (8) and thirty (30) VIBRA-4 modes. In both cases the DATS solution used twenty-five (25) cantilever modes. Bending moment due to up loading gave good correlation with VIBRA-4 Outboard of WBL 800. The DATS and VIBRA-4 bending moments due to down load fit well, but DATS appeared to be smaller than VIBRA-4 for the stations inboard of WBL 800. Since the down bending moment in board of WBL 800 is reduced by the inertia of the wing and nacelles it suggests that the DATS inertia resistance to the diffractive loading phase was more effective than VIBRA-4. It is also interesting to note that the highly oscillatory 25 Hz test loading for the thirty (30) modes VIBRA-4 test load shown on Figures 2-10 thru 2-19 gave essentially the same peak

3.2 (Continued)

moments as the eight (8) mode VIBRA-4 test load shown on Figures 2-20 thru 2-29. This suggests that it will not be necessary to simulate these oscillations for test input on the wing for bending moment considerations. Ultimate bending moment capability is shown on the plot to emphasize that the portion of the wing which is important in the test is outboard of WBL 700. Time histories of bending moments for the VIBRA-4 calculation and DATS using VIBRA-4 input loads (30 modes) are shown on Figure 3-29 thru 3-33. During the initial down loading and first rebound the phasing and peak values agree quite well which encompasses the time to reach the critical down bending moment. After that the modal frequencies differences between the two models causes shifts in the response time histories.

3.3 SIMULATION OF FIN TEST

The results of the fin test dynamic analysis for the base shake test and dynamic pull test are reported in this section. All results of the DATS analysis for the test are compared against the DATS analysis using the VIBRA-4 test load input. This technique was used because the main goal was to demonstrate that the test technique was satisfied rather than demonstrate differences in the analysis between DATS and VIBRA-4. Peak moments, lateral acceleration, and relative deflections are compared for the DATS analysis for

- a) VIBRA-4 input (10 fin modes)
- b) VIBRA-4 input (1 fin mode)
- c) Base shake
- d) Dynamic pull test

on Figures 3-34 thru 3-36. For bending moment, the most significant parameter, there is good agreement. Base shake moments have the largest deviation on the high side, but could be made to match the VIBRA-4 input results by lowering the input pulse. Peak lateral acceleration comparison is not quite as good as the bending moment results. It is interesting to note that larger deviations occur between DATS using ten (10) modes and one (1) mode with VIBRA-4 input than does for the DATS base shake and dynamic pull test. This is due to the fact that the larger accelerations occur in the higher modes which are truncated in the one (1) mode solution. However, the higher modes do not significantly contribute to the deflections or bending. Peak relative deflection for the base shake is larger than DATS with VIBRA-4 input as shown on Figure 6-36. Again this is due to a slightly too large base input pulse.

3.3.1 Base Shake Test

A number of base shake test inputs were analyzed by varying the type of input pulse. The pulse was varied by changing the initial and final slope and peak velocity of the curve shown on Figure 3-14 within the constraints of 100 G's acceleration, 1200 inches per second velocity and 36 inches displacement. Of the pulses studied, the one which gave the best fit to the peak bending moment is shown on Figure 3-14. The peak

3.3.1 (Continued)

acceleration of 8.3 g's, velocity of 160 inches per second, and displacement of 18 inches is well within the capability of the MSS actuator. See section 4.2 for a prediction the actual response of the prime mover.

Test loading from the base shake is input at the base. The equivalent station loading to compare with VIBRA-4 and dynamic pull test is the inertia load term ($ML\theta$) which was discussed in section 3.1.4. This value is compared on Figure 3-37 thru 3-44 to the VIBRA-4 input. Only the general form of the VIBRA-4 loading is matched by the base shake test, namely the diffractive loading duration and average magnitude. It appears that the success of this test approach in achieving the correct peak bending moments both in magnitude and spatial distribution is dependent on exciting the primary loading modes. Time histories of bending moments and relative displacement for the base shake are compared to the DATS analysis on Figures 3-45 and 3-52. No attempt was made to assure that fin response match the VIBRA-4 input results after the peak bending moment was reached (~.090 seconds).

3.3.2 Dynamic Pull Test

The fin pull test was designed to match the bending moment results from VIBRA-4. This was done first by running DATS using the VIBRA-4 test load. By comparing the test load at each station to the calculated deformation it was possible to come up with a spring rate which in the mean sense gave the best overall fit to the desired load time history input. The initial preload was chosen to fit the maximum diffractive load at each station. Preloads values and spring rates which gave the best fit to the bending moment data are shown on Figure 3-13.

Test load time histories for the dynamic pull test and DATS using the VIBRA-4 input are shown on figures 3-61 thru 3-68. The correlation of the test loading is better for the dynamic pull test than for the base shake. Comparison of DATS bending moments and relative deflections using VIBRA-4 load input to the dynamic pull test are shown on Figures 3-73 thru 3-84. The match of the bending moment and relative deflection

3.3.2 (Continued)

data is about the same, at least until the time maximum bending moment is reached. After maximum bending moment is achieved from the diffractive loading the fin accelerates in the opposite direction and is restrained by the loading springs which tends to simulate the lift build up loads. However the base shake does not provide this restraint and the fin rebounds to maximum deflection in the opposite direction. Since simulation of the dynamic condition up to maximum bending moment is the goal, the deviations after the time of maximum bending moments are not of concern unless they result in a more severe test environment.

3.4 ANALYSIS OF WING TEST

The results of the wing test dynamic analysis for the wing dynamic pull test are reported in this section. All results of the DATS analysis of the test are compared against the DATS analysis using the VIBRA-4 test load input. This technique was used because the main goal was to demonstrate that the test technique was satisfied rather than demonstrate differences in the analysis between DATS and VIBRA-4.

3.4.1 Dynamic Pull Test

The dynamic pull test for the wing was designed to simulate the dynamic loading on the critical loaded portion of the wing up to the time of the peak moment. The critical portion of the wing for the down blast is the down loading bending moment on that portion of the wing outboard of the outboard nacelle (WBL 719) as shown on Figure 3-85. The time to reach the maximum down bending moment is roughly .20 seconds. The release and loading spring cables were sized using the same technique as used for the fin dynamic pull test described in section 3.3.2. Additional adjustment was required in cable loading to match the initial steady state flight aerodynamic loads for conditions prior to the test. A further technique was added to quick release the loading spring cables from the wing after the diffractive phase loading since the lift build up forces required loading in the opposite direction of the loading spring forces. Spring loading cables on the nacelles which loaded in a direction opposite to

3.4.1 (Continued)

the loading springs on the wing were required because of the large inertial loading on the nacelles. Values of release cable preload, and spring loading cable preloads, spring rates, and time required to quick release which gave the best fit to the outboard wing bending moment are presented on Figure 3-16.

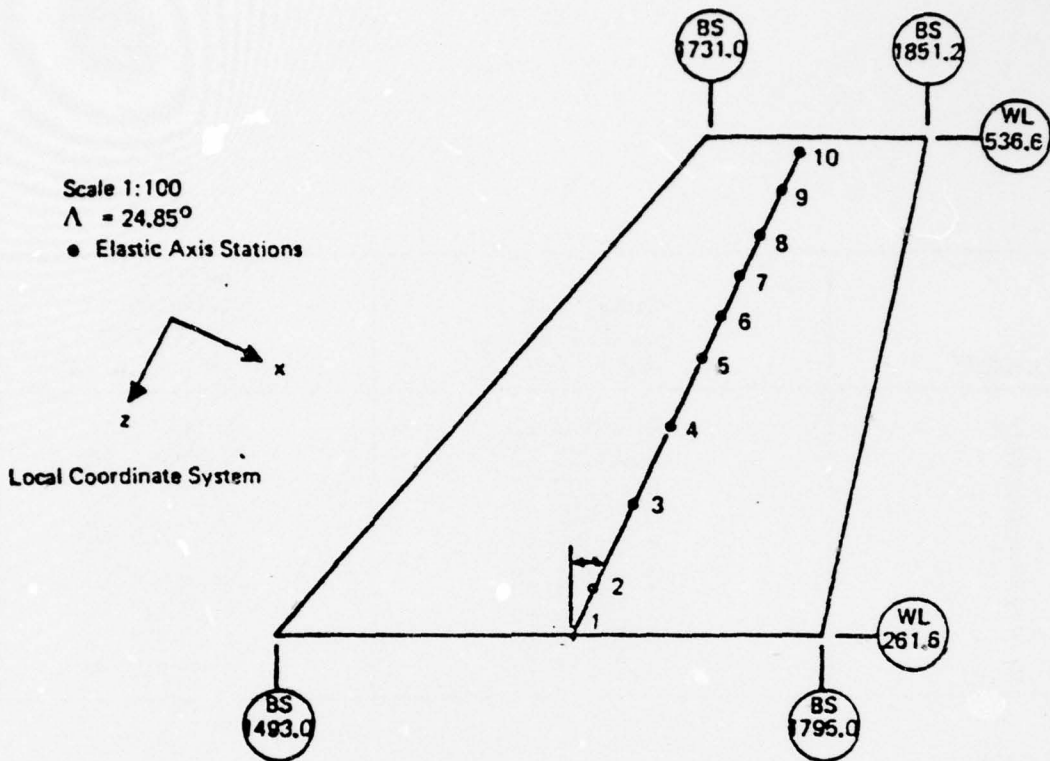
Peak bending moments and accelerations are compared for the DATS analysis for a) VIBRA-4 input using 30 modes, b) VIBRA-4 input using 8 modes and c) dynamic pull test on figures 3-85 and 3-86. The dynamic pull test gave a good fit to the peak moment outboard of the outboard nacelle (Station 719). For the down loading condition inboard of this point the dynamic pull test moments exceeded the VIBRA-4 results because the steady state build up lift component was not present in the test. In order to simulate this another set of loading springs would have to engage and provide the lift build up loads. Because an additional set of loading springs would have made a more complex test to simulate bending moments on a non-critical portion of the wing, this modification to the load system was not pursued. It is interesting to note that for a blast loading underneath the aircraft that the character of the test loading would be similar to that for the fin and hence much more adaptable to the dynamic pull test technique used for the fin.

The effect of the 25 hz oscillatory test load on the wing bending moment for the 30 mode VIBRA-4 solution was evaluated by comparing it to the 8 mode VIBRA-4 solution. As shown on Figure 3-87 bending moment data there is not a significant difference between the two solutions. This indicated that it was not necessary to duplicate the oscillatory load in order to get a good structural dynamic test for the blast loading. There was good agreement between the dynamic pull test and DATS using VIBRA-4 test load peak acceleration results as shown on Figure 3.-35.

Time histories of test loading at the ten loading stations are compared to VIBRA-4 test loads on Figure 3-87 to 3-96. The dynamic pull test load goes to zero when the loading spring is released from the wing.

3.4.1 (Continued)

Bending moment and relative deflection time histories are compared for eight WBL locations on the wing on Figures 3-97 thru 3-101. Moments due to down loading inboard of the outboard nacelle get considerably larger in the dynamic pull test because of the absence of the lift build up loads. This effect is also present in the relative deflection time history results on Figures 3-102 thru 3-111.



Ea Station No.	BS	WL
1	1656.8	261.6
2	1667.1	284.0
3	1688.6	330.3
4	1710.0	376.5
5	1728.1	411.2
6	1736.8	434.4
7	1747.5	457.5
8	1758.2	480.7
9	1769.0	503.8
10	1779.7	526.9

Figure 3-1 B-52H Fin Dynamic Model Node Numbers and Coordinates

SEGMENT	TORSIONAL STIFFNESS (GJ ~ LB- IN^2)	LATERAL BENDING STIFFNESS (EI ~ LB- IN^2)
1*	0.2753E 11	0.5460E 11
2	0.2220E 11	0.2966E 11
3	0.1550E 11	0.1208E 11
4	0.1042E 11	0.5670E 10
5	0.7250E 10	0.3150E 10
6	0.5330E 10	0.1630E 10
7	0.3840E 10	0.9300E 09
8	0.2830E 10	0.6400E 09
9	0.1800E 10	0.5100E 09

*Segment 1 goes from node 1.

Figure 3-2 B-52H Fin Dynamic Model Stiffness Data

The mass property headings of Figure 3-4 & 3-8 are defined as follows:

W	Weight - Lbs
WX	Unbalance Moments - In.-Lbs
WY	
WZ	
X	Distances (Inches) from Elastic Axis Station to Mass CG
Y	
Z	
IXX	Moments of Inertia - Lb-In. ²
IYY	
IZZ	
IXY	Products of Inertia - Lb-In. ²
IXZ	
IYZ	

Note: The Above Mass Properties are Defined with Respect to the Local Coordinate Systems of Figures

Figure 3-3 Mass Data Terminology

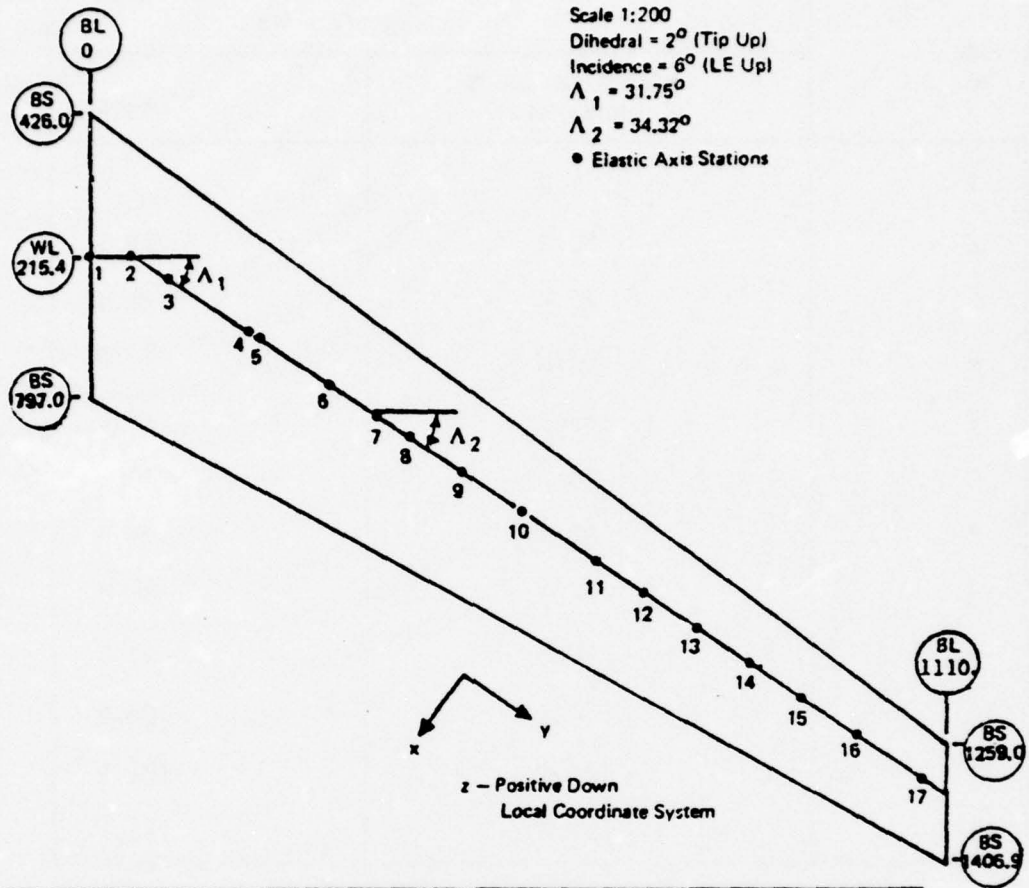
STA.	W	WX	WY	WZ	X	Y	Z
1	2.453E+02	-2.141E+04	0.	6.215E+03	-8.730E+01	0.	2.534E+01
2	7.073E+02	-9.903E+03	0.	3.395E+03	-1.400E+01	0.	4.800E+00
3	4.498E+02	1.439E+03	0.	2.251E+02	3.200E+00	0.	5.005E-01
4	4.176E+02	4.175E+03	0.	-9.604E+02	9.999E+00	0.	-2.300E+00
5	2.643E+02	1.771E+03	0.	8.061E+02	6.699E+00	0.	3.050E+00
6	1.821E+02	1.111E+03	0.	-2.824E+02	6.100E+00	0.	-1.551E+00
7	1.461E+02	1.373E+03	0.	1.826E+02	9.400E+00	0.	1.250E+00
8	8.492E+01	1.129E+03	0.	3.825E+01	1.330E+01	0.	4.505E-01
9	7.154E+01	7.369E+02	0.	2.505E+01	1.030E+01	0.	3.501E-01
10	5.727E+01	1.724E+03	0.	-1.747E+02	3.010E+01	0.	-3.050E+00

STA.	IXX	IXY	IXZ	IYY	IYZ	IZZ
1	2.539E+05	0.	-6.093E+05	2.397E+06	0.	2.190E+06
2	2.906E+05	0.	-4.753E+04	2.173E+06	0.	2.030E+06
3	1.310E+05	0.	7.203E+02	1.637E+06	0.	1.558E+06
4	1.201E+05	0.	-9.603E+03	1.292E+06	0.	1.199E+06
5	2.571E+04	0.	5.400E+03	4.821E+05	0.	4.684E+05
6	1.429E+04	0.	-1.723E+03	3.117E+05	0.	3.036E+05
7	1.214E+04	0.	1.716E+03	2.683E+05	0.	2.623E+05
8	5.722E+03	0.	5.088E+02	1.606E+05	0.	1.575E+05
9	4.271E+03	0.	2.580E+02	9.362E+04	0.	9.073E+04
10	7.976E+03	0.	-1.220E+04	9.850E+04	0.	9.152E+04

Figure 3-4 B-52H Fin Dynamic Model Mass Data

Mode No.	Frequency - Hz	
	Wichita Loads Analysis	NASTRAN
1	7.9	7.8
2	20.3	19.5
3	22.9	21.9
4	42.0	40.0
5	53.8	49.6
6	64.1	60.0
7	82.3	74.8
8	94.0	86.0
9	96.8	92.8
10	114.7	102.6
11	141.5	121.1
12	154.7	141.1

Figure 3-5 Comparison of B-52H Fin Cantilever Frequencies



Ea Station No.	BS	BL
1	616.3	0.0
2	616.3	54.9
3	645.8	102.6
4	709.4	205.1
5	717.7	218.4
6	773.1	307.7
7	819.2	382.7
8	838.1	409.6
9	891.0	487.0
10	944.0	564.5
11	997.0	641.9
12	1049.9	719.3
13	1096.6	787.6
14	1143.3	855.8
15	1188.0	921.1
16	1253.3	1016.5
17	1316.5	1108.9

Figure 3-6 B-52H Wing Dynamic Model Node Numbers and Coordinates

SEGMENT	TORSIONAL STIFFNESS (GJ ~ LB-IN ²)	VERTICAL BENDING STIFFNESS (EI ~ LB-IN ²)	CHORDWISE BENDING STIFFNESS (EI ~ LB-IN ²)
1*	0.0000E 00	0.7354E 12	0.0000E 00
2	0.6300E 12	0.7200E 12	0.3650E 13
3	0.4530E 12	0.6000E 12	0.3460E 13
4	0.3650E 12	0.4850E 12	0.3300E 13
5	0.3090E 12	0.3880E 12	0.3140E 13
6	0.2400E 12	0.2880E 12	0.2870E 13
7	0.2040E 12	0.2420E 12	0.2630E 13
8	0.1670E 12	0.1900E 12	0.2270E 13
9	0.1200E 12	0.1340E 12	0.1780E 13
10	0.8500E 11	0.9400E 11	0.1380E 13
11	0.5900E 11	0.6650E 11	0.1100E 13
12	0.3760E 11	0.4500E 11	0.8850E 12
13	0.2200E 11	0.2930E 11	0.7000E 12
14	0.1350E 11	0.1680E 11	0.5700E 12
15	0.7100E 10	0.9200E 10	0.3670E 12
16	0.3850E 10	0.3700E 10	0.1550E 12

*Segment 1 between node 1 and 2.

Figure 3-7 B-52H Wing Dynamic Model Stiffness Data

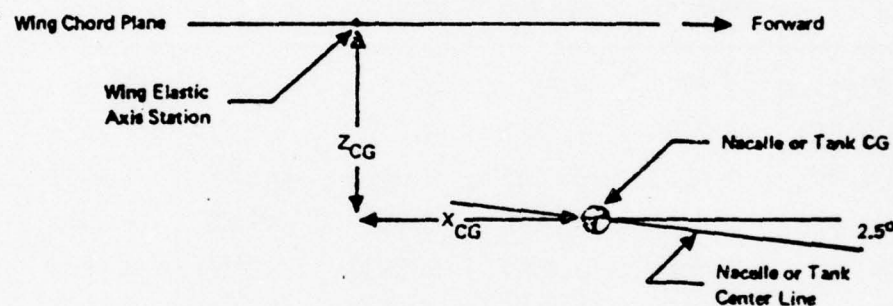
230,000 POUNDS GROSS WEIGHT

STA.	W	WX	WY	WZ	X	Y	Z
1	0.	0.	0.	0.	0.	0.	0.
2	2.890E+03	1.642E+04	-3.007E+04	1.499E+04	5.683E+00	-1.041E+01	5.186E+00
3	6.823E+03	3.026E+04	-4.223E+04	3.132E+04	4.435E+00	-6.189E+00	4.591E+00
4	6.123E+03	1.038E+05	-6.889E+03	3.717E+04	1.695E+01	-1.125E+00	6.071E+00
5	0.	0.	0.	0.	0.	0.	0.
6	5.277E+03	1.185E+05	1.314E+04	2.218E+04	2.246E+01	2.499E+00	4.204E+00
7	0.	0.	0.	0.	0.	0.	0.
8	8.029E+03	4.329E+04	-1.079E+05	4.245E+04	5.392E+00	-1.343E+01	5.288E+00
9	4.775E+03	1.048E+05	2.046E+03	1.419E+04	2.194E+01	4.284E-01	2.971E+00
10	3.351E+03	8.431E+04	-3.027E+03	8.390E+03	2.516E+01	-9.033E-01	2.504E+00
11	2.075E+03	5.466E+04	-1.514E+03	3.167E+03	2.634E+01	-7.299E-01	1.526E+00
12	2.348E+03	-1.317E+04	-4.198E+04	1.248E+04	-5.611E+00	-1.788E+01	5.316E+00
13	1.995E+03	2.408E+04	2.363E+04	-1.782E+03	1.207E+01	1.184E+01	-8.932E-01
14	2.398E+03	3.361E+04	-6.761E+03	2.010E+03	1.402E+01	-2.819E+00	8.382E-01
15	1.445E+03	-3.950E+03	-1.921E+04	1.358E+04	-2.734E+00	-1.330E+01	9.401E+00
16	4.590E+02	5.049E+03	-9.380E+02	0.	1.100E+01	-2.044E+00	0.
17	2.030E+02	4.060E+03	-5.230E+03	0.	2.000E+01	-2.575E+01	0.

STA.	IXA	IXY	IXZ	IYY	IYZ	IZZ
1	0.	0.	0.	0.	0.	0.
2	3.083E+06	-4.679E+05	-2.379E+05	7.601E+06	1.649E+05	8.033E+06
3	1.077E+07	6.537E+05	1.623E+05	1.779E+07	5.907E+05	2.382E+07
4	8.538E+06	1.455E+04	4.032E+05	1.867E+07	-1.985E+05	2.438E+07
5	0.	0.	0.	0.	0.	0.
6	7.987E+06	1.464E+05	3.383E+05	1.667E+07	-1.652E+05	2.301E+07
7	0.	0.	0.	0.	0.	0.
8	1.288E+07	4.869E+06	-2.417E+06	2.603E+07	-1.917E+06	3.583E+07
9	3.825E+06	3.599E+05	-6.140E+04	1.230E+07	-1.430E+05	1.542E+07
10	2.785E+06	1.109E+05	3.130E+04	8.867E+06	-9.971E+04	1.118E+07
11	4.509E+06	3.673E+04	4.464E+04	2.897E+06	-5.412E+04	7.122E+06
12	4.482E+06	4.038E+06	-1.161E+06	1.127E+07	-8.065E+05	1.471E+07
13	1.335E+06	1.290E+05	-5.062E+04	2.672E+06	-4.894E+04	3.827E+06
14	1.465E+06	8.243E+04	-6.342E+04	2.878E+06	-6.589E+04	4.169E+06
15	2.202E+06	1.342E+06	-6.696E+05	3.817E+06	-4.783E+05	4.978E+06
16	4.999E+05	-1.032E+04	0.	5.485E+05	0.	1.019E+06
17	3.748E+05	-1.046E+05	0.	1.752E+05	0.	5.380E+05

Figure 3-8 B-52H Wing Dynamic Model Mass Data

	Inboard Nacelle	Outboard Nacelle	External Tank	
			Empty	Full
Wing EA Station	8	12	15	15
W - lbs	11004.5	10828.6	408.5	4883.5
X_{CG} - in.	203.47	182.64	59.2	72.0
Z_{CG} - in.	70.93	60.84	24.7	33.7
$I_{XX_{CG}}$ - Lb \cdot in. ²	1.16301E+7	1.14826E+7	1.775E+5	7.529E+5
$I_{YY_{CG}}$ - Lb \cdot in. ²	2.31467E+7	2.26992E+7	1.868E+6	1.797E+7
$I_{ZZ_{CG}}$ - Lb \cdot in. ²	2.98483E+7	2.92630E+7	1.862E+6	1.797E+7



Notes:

1. Nacelle Strut or Tank Pylon is Attached to Wing at the Designated Wing Elastic Axis Station (Ref. Figure 12)
2. The Distances X_{CG} and Z_{CG} are Positive as Shown and are Parallel and Normal, Respectively, to the Wing Chord Plane
3. The Moments of Inertia $I_{XX_{CG}}$, $I_{YY_{CG}}$, and $I_{ZZ_{CG}}$ are Defined with Respect to the Nacelle or Tank Center Line
4. The Nacelles and External Tank are Pitched 2.5° Nose Down with Respect to the Wing Chord Plane

Figure 3-9 B-52H Dynamic Model Nacelle and External Tank Mass Data

	INBOARD NACELLE			OUTBOARD NACELLE		
	SIDE BENDING	VERTICAL BENDING	TORSION	SIDE BENDING	VERTICAL BENDING	TORSION
FREQ - RAD/SEC	12.57	25.89	32.17	12.94	23.76	32.17
X/b - NON-DIM	-0.0385	0.3425	-0.0176	-0.0182	0.2819	-0.0131
Y/b - NON-DIM	1.0000	-0.0231	0.0136	-0.8719	0.0439	0.0422
Z/b - NON-DIM	0.0044	0.9396	-0.0510	0.0106	0.9381	-0.0765
θ_x - RAD	-0.8432	0.4621	1.0000	1.0000	0.3998	1.0000
θ_y - RAD	0.0188	1.0000	-0.0006	0.0563	1.0000	0.0223
θ_z - RAD	-0.6706	-0.0949	-0.3274	0.6746	-0.2122	-0.3224

NOTES:

1. Nacelle Model Displacements and Rotations are Motions at the Nacelle CG Oriented with Respect to Nacelle Coordinates (x Positive Aft, y Positive Left, and z Positive Down)
2. The Nondimensional Displacements x/b, y/b, and z/b are based on a Reference Length b = 130 Inches

Figure 3-10 B-52H Dynamic Model Nacelle Cantilever Modal Data

Mode No.	Frequency - Hz	
	Wichita* Loads Analysis	Nastran
1	.87	.87
2	--	1.8
3	--	1.9
4	2.0	2.0
5	2.6	2.6
6	--	3.1
7	3.6	3.6
8	--	4.1
9	4.2	4.2
10	6.7	6.6
11	8.7	9.5
12	10.6	10.8
13	13.1	12.3
14	16.8	15.5
15	18.1	19.0
16	22.1	22.1
17	--	23.0
18	--	25.4
19	27.7	26.0
20	31.3	32.7
21	31.8	32.8
22	33.4	36.5
23	40.0	40.0
24	41.0	43.7
25	45.5	44.0

*Wichita Loads Analysis had rigid members for Nacelle support member whereas Seattle test analysis had cantilever modal data.

Figure 3-11 Comparison of B-52H Wing Cantilever Frequencies - 230 Kip Gross Weight

+ = LOADING STATIONS

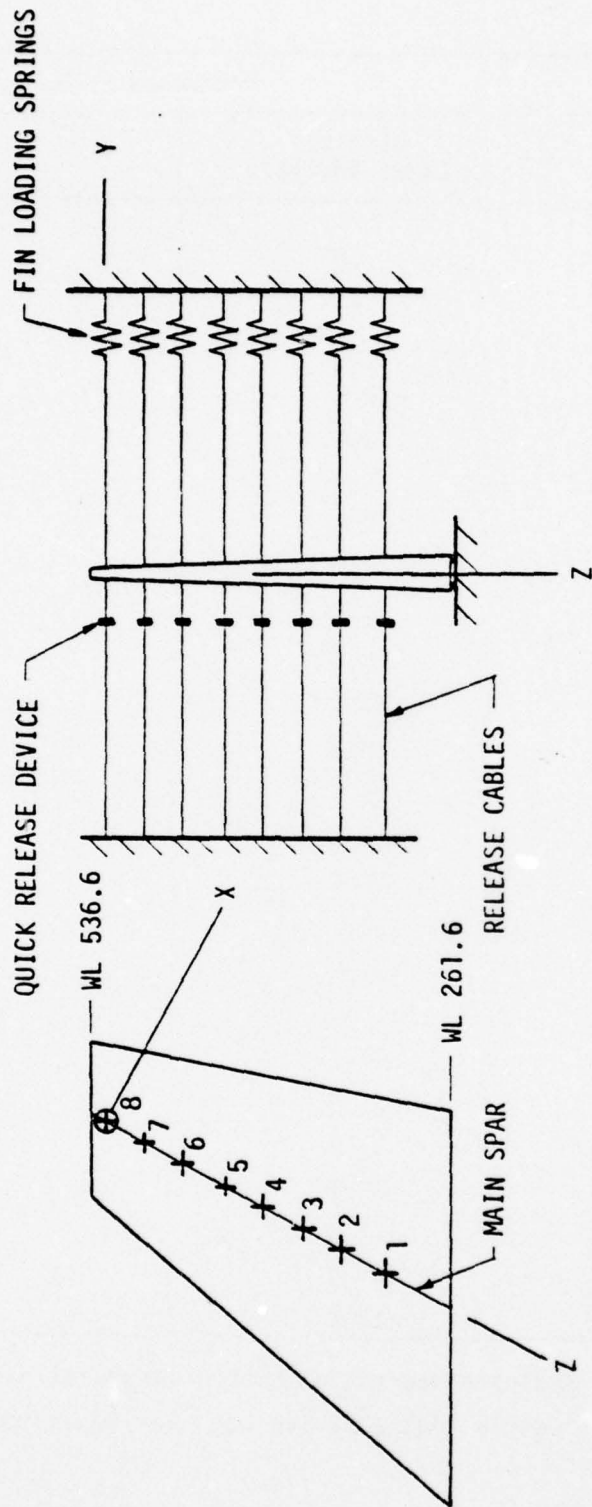
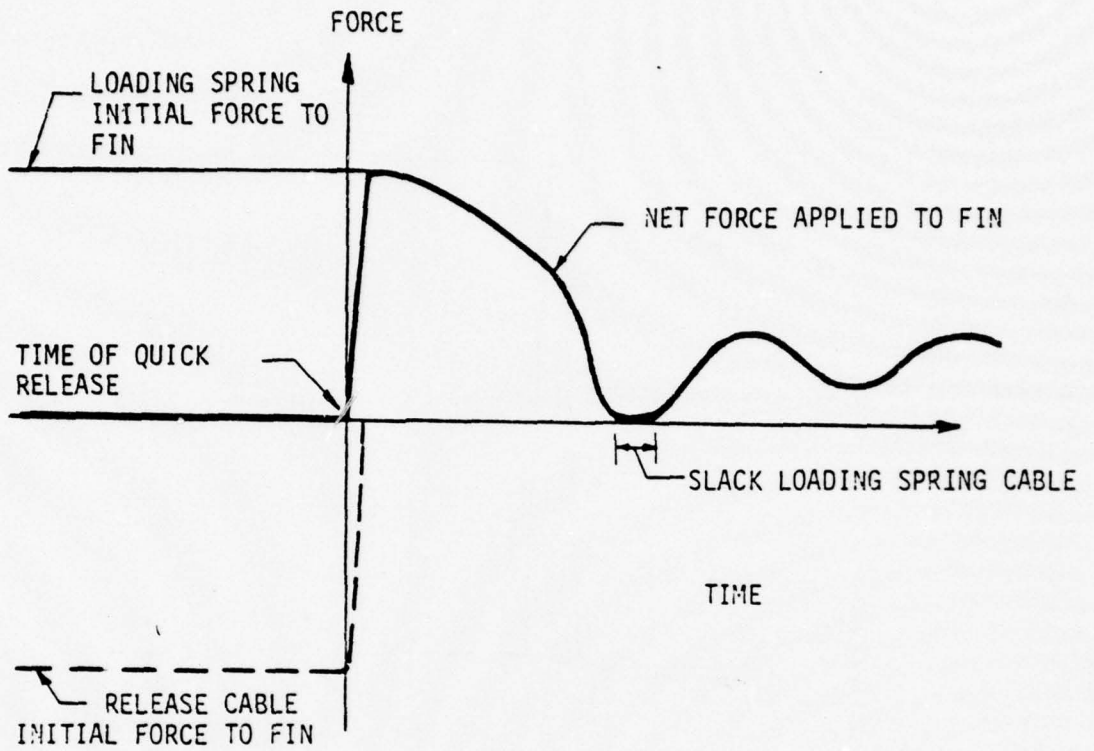


Figure 3-12 Fin Pull Test Dynamic Model



LOADING STATION	LOAD SPRING INITIAL FORCE KIPS	LOADING SPRING SPRING RATE KIPS/IN
1	29.	60.
2	15.	8.
3	7.0	0.7
4	9.0	0.7
5	7.5	0.7
6	7.0	0.6
7	9.0	0.6
8	6.1	0.5

Figure 3-13 Fin Pull Test Loading Characteristics

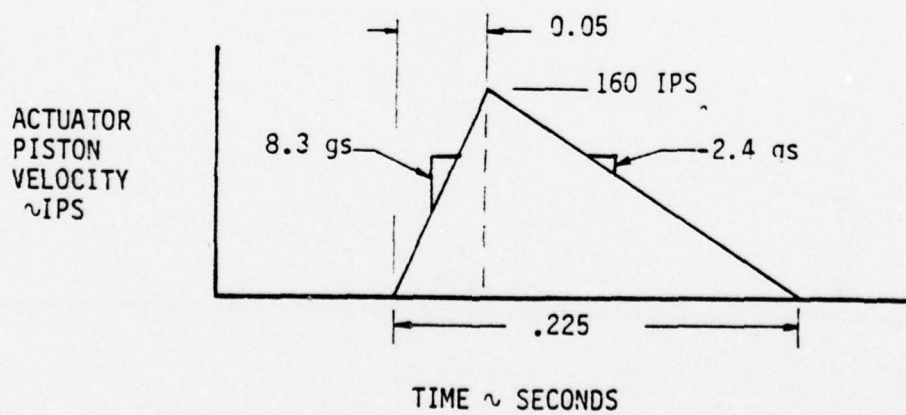
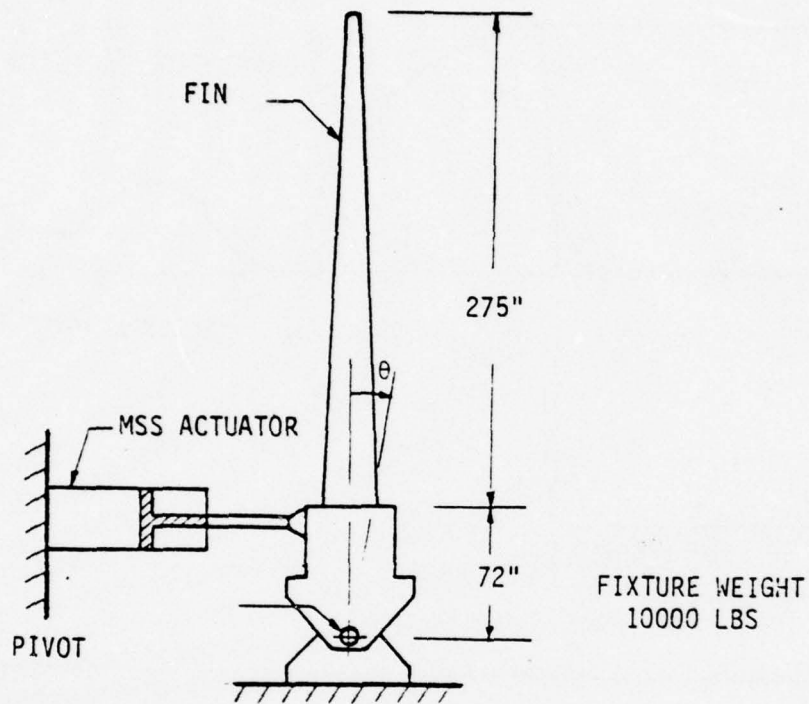


Figure 3-14 Fin-Base Shake Dynamic Model

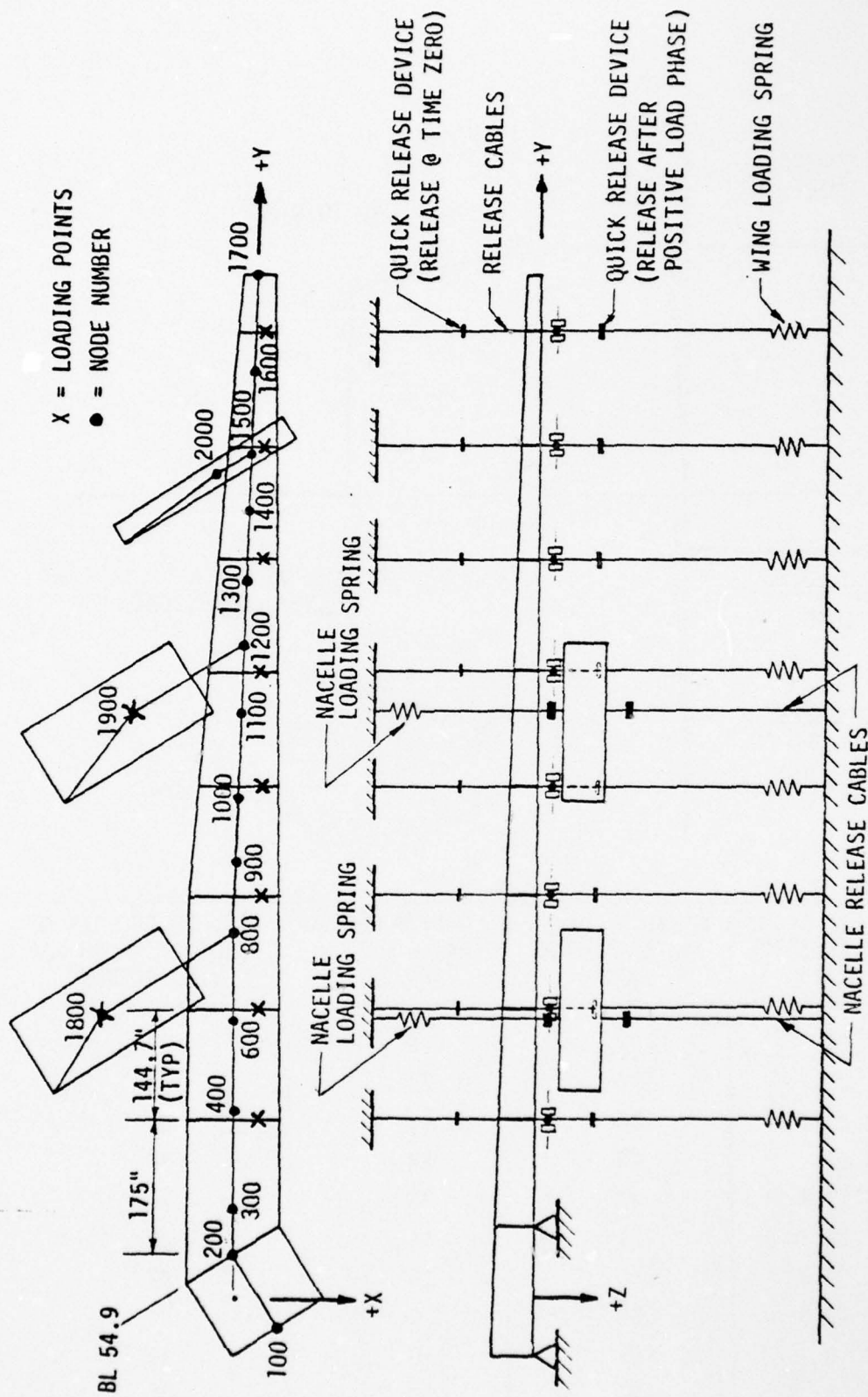
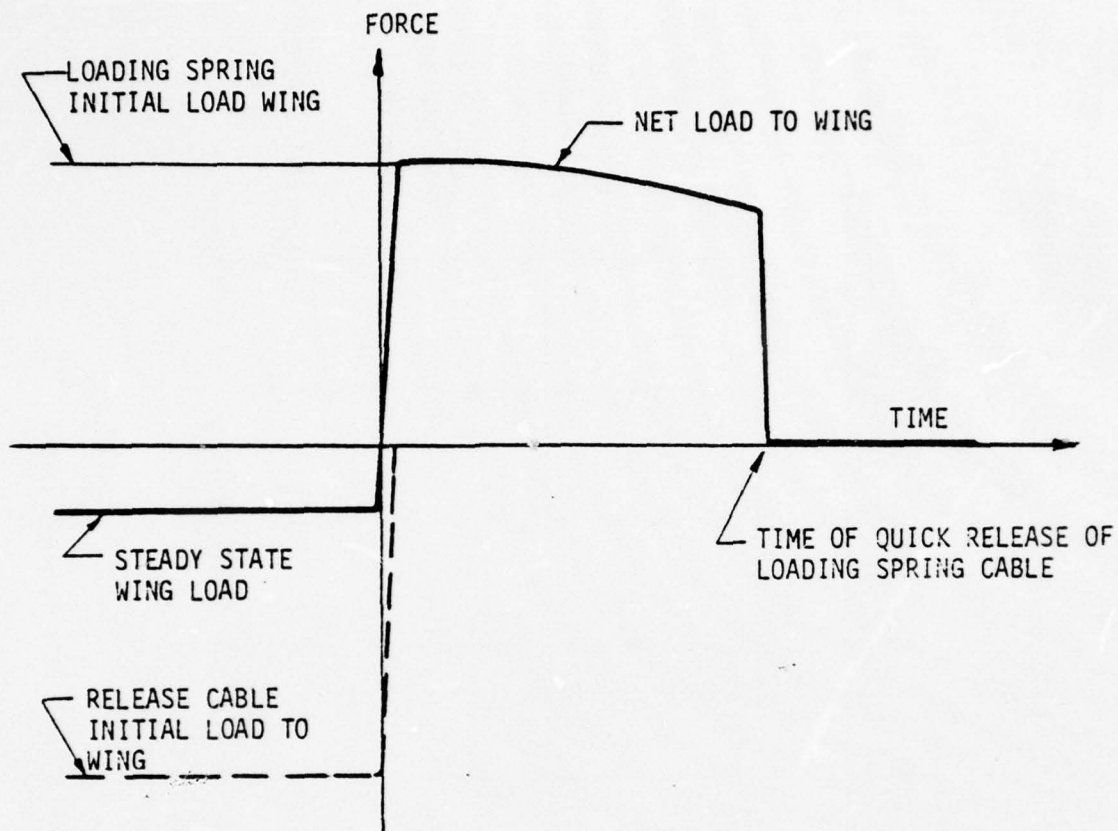


Figure 3-15 Wing Pull Test Dynamic Model



LOADING STATION	RELEASE CABLE INITIAL FORCE KIPS	LOADING SPRING INITIAL FORCE KIPS	LOADING SPRING SPRING RATE KIPS/IN	TIME OF RELEASE OF LOADING SPRING CABLE MILLISECONDS
1	26	90	110	38
2	20	50	28	34
3	20	30	14	31
4	17	40	28	30
5	13.8	47	25	26
6	12.3	29	14	23
7	7.9	50	14	22
8	-3.0	50	6	20
9	0	95	110	39
10	0	130	20	41

Figure 3-16 Wing Pull Test Loading Characteristics

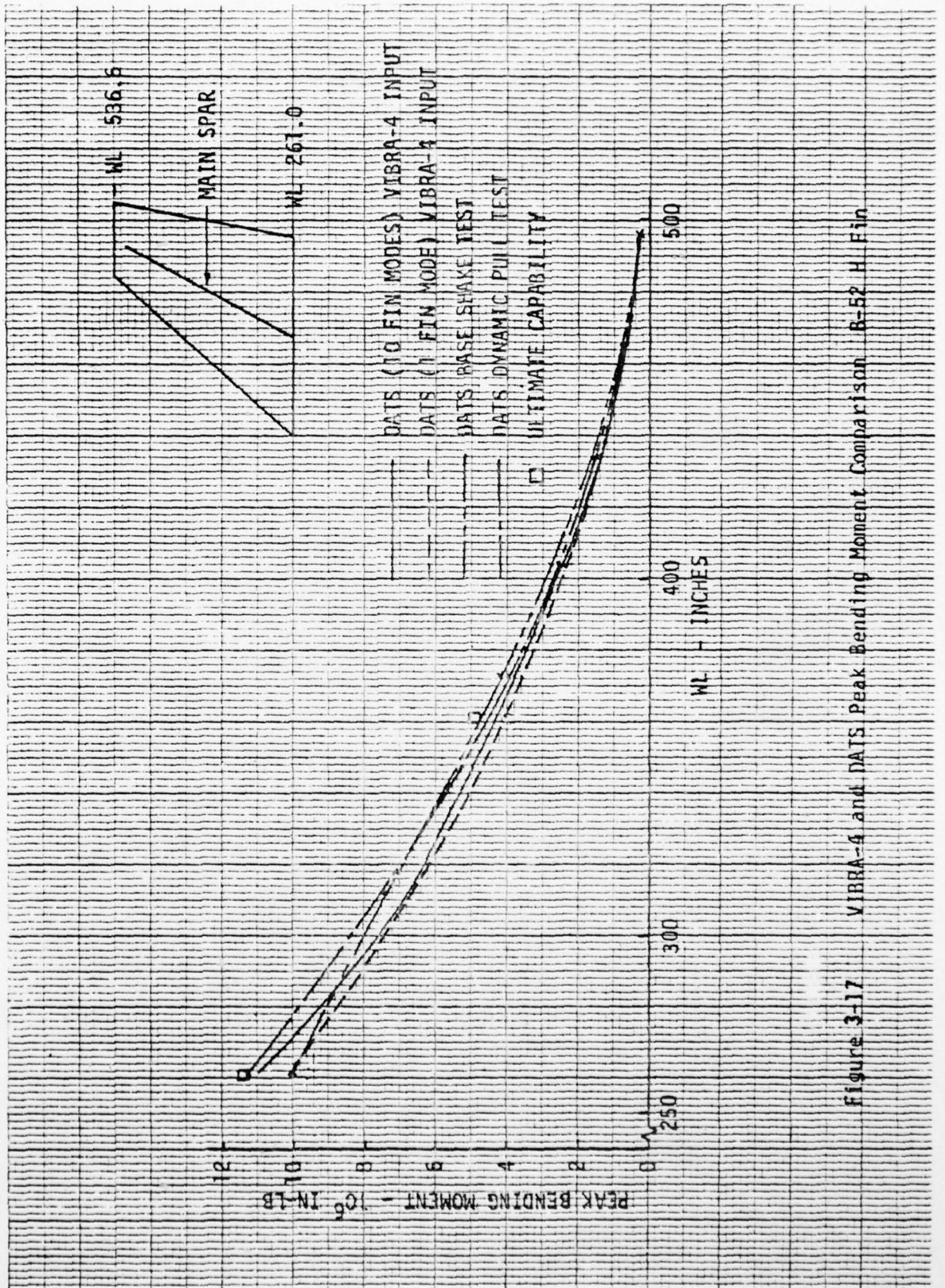


Figure 3-17 VIBRA-4 and DATS Peak Bending Moment Comparison R-52 H Fin

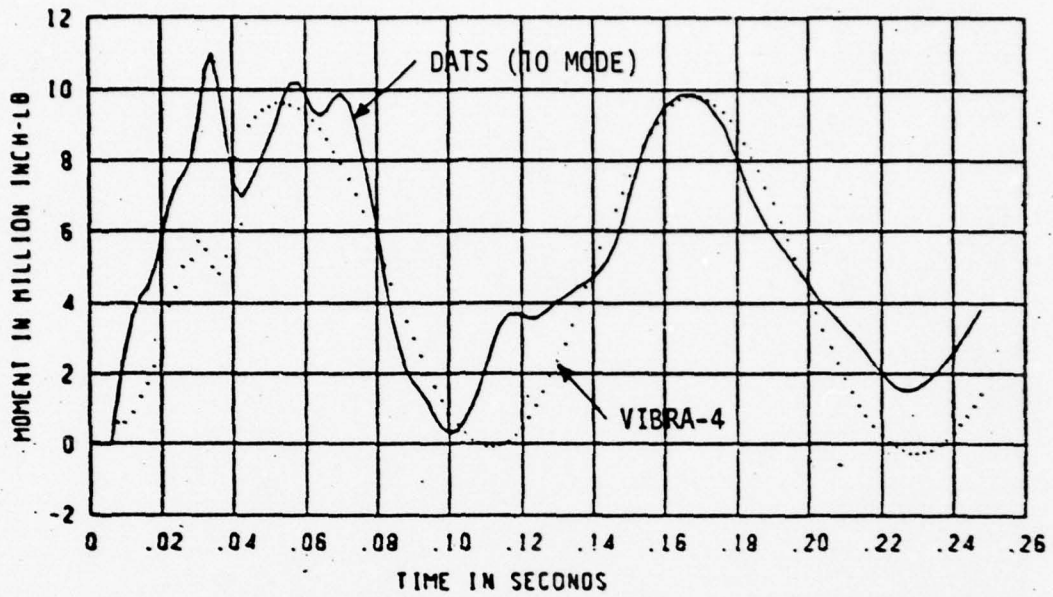


Figure 3-18 VIBRA-4 and DATS Bending Moment Time History - Fin, Sta. 1

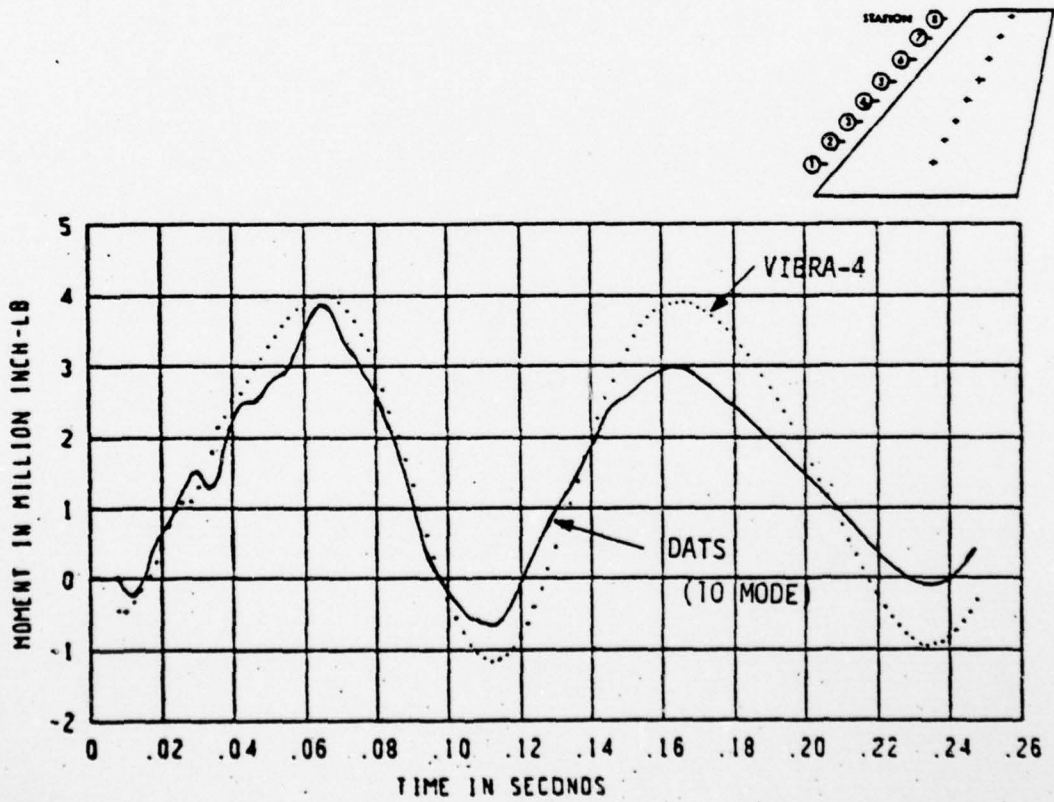


Figure 3-19 VIBRA-4 and DATS Bending Moment Time History - Fin, Sta. 4

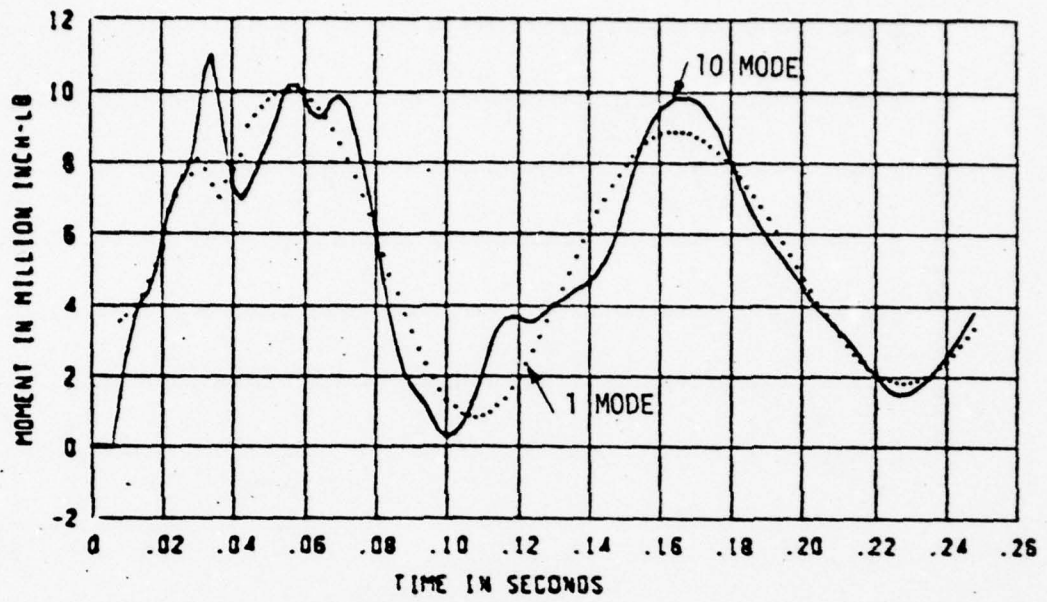


Figure 3-20 DATS Fin Bending Moment for 10 Modes and 1 Mode, VIBRA-4 Input, Sta. 1

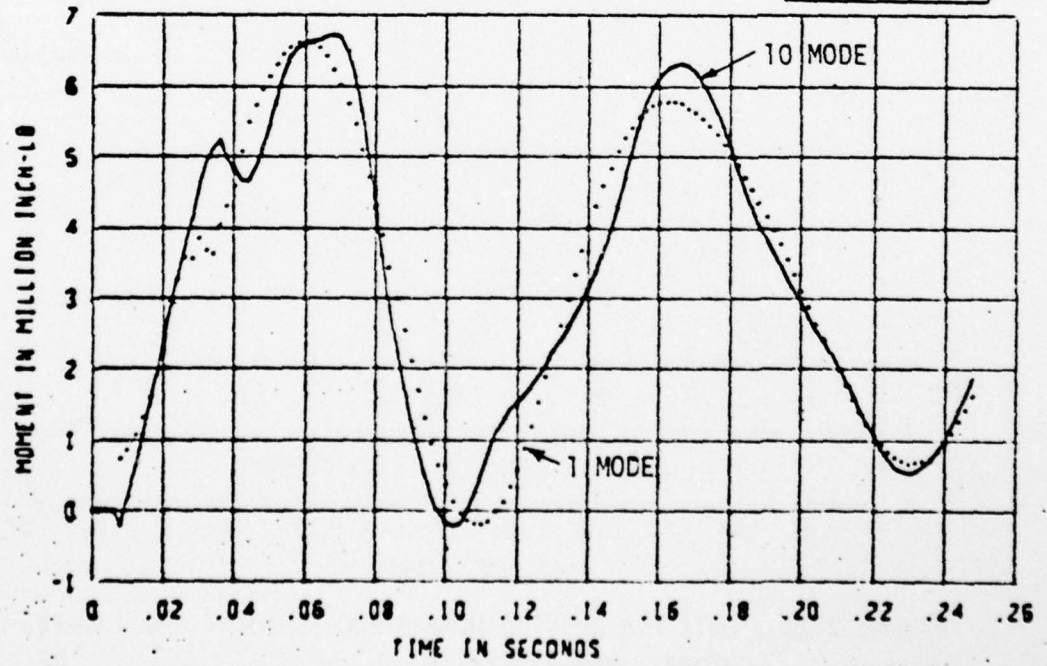
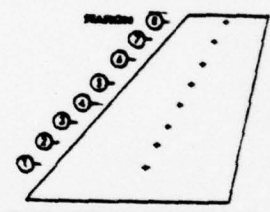


Figure 3-21 DATS Fin Bending Moment for 10 Modes and 1 Mode, VIBRA-4 Input, Sta. 2

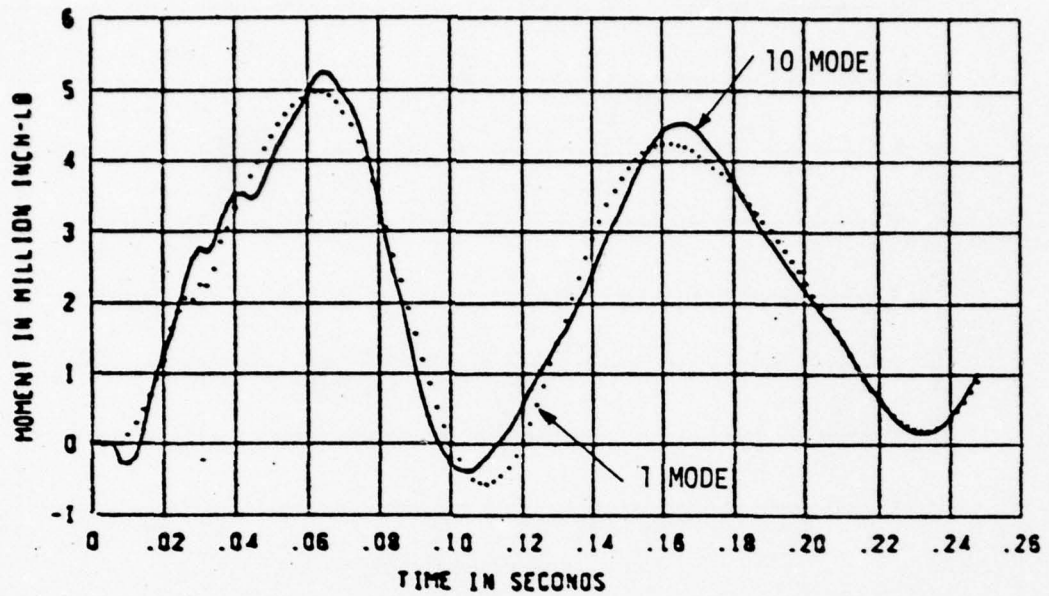


Figure 3-22 DATS Fin Bending Moment for 10 Modes and 1 Mode, VIBRA-4 Input, Sta. 3

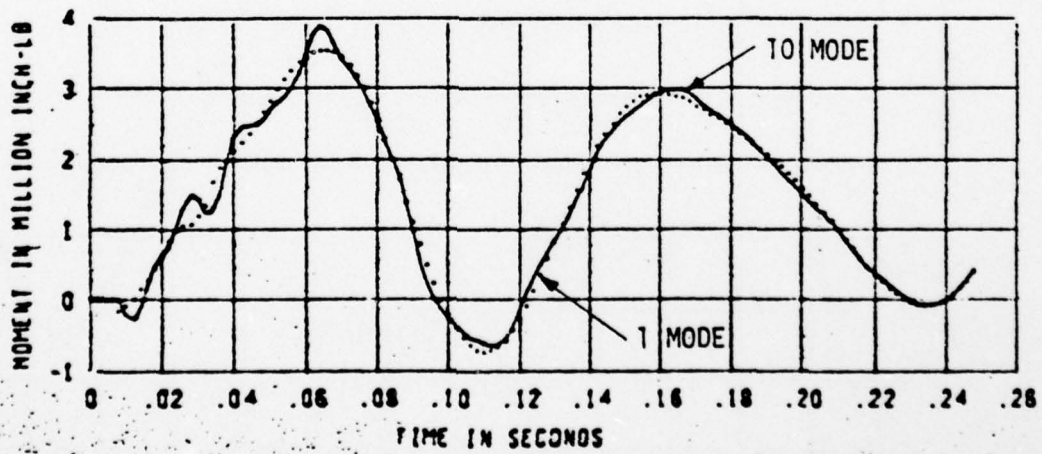
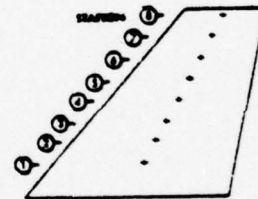


Figure 3-23 DATS Fin Bending Moment for 10 Modes and 1 Mode, VIBRA-4 Input, Sta. 4

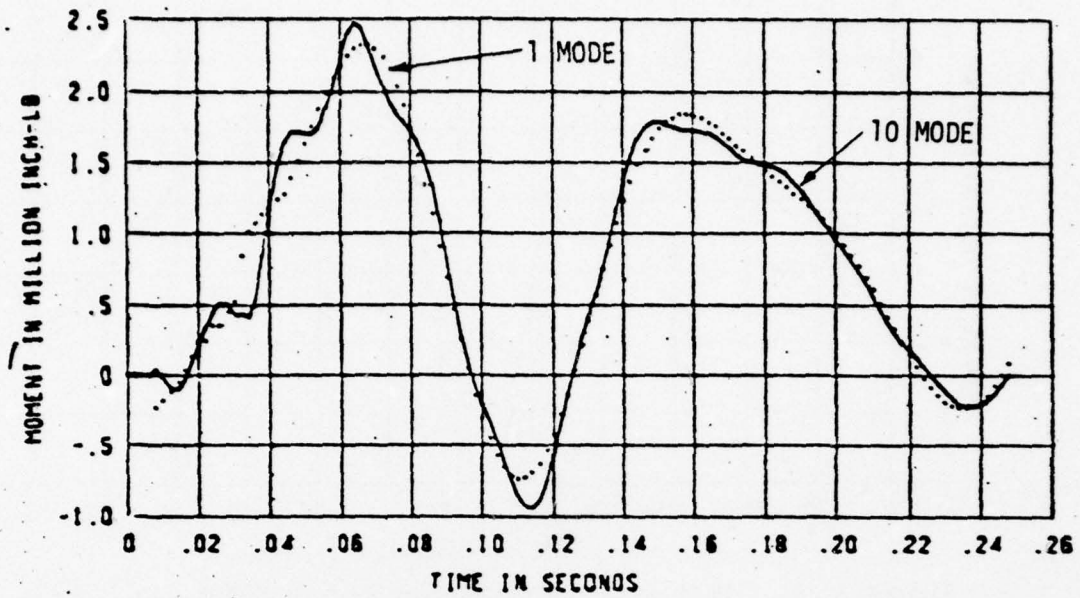


Figure 3-24 DATS Fin Bending Moment for 10 Modes and 1 Mode, VIBRA-4 Input, Sta. 5

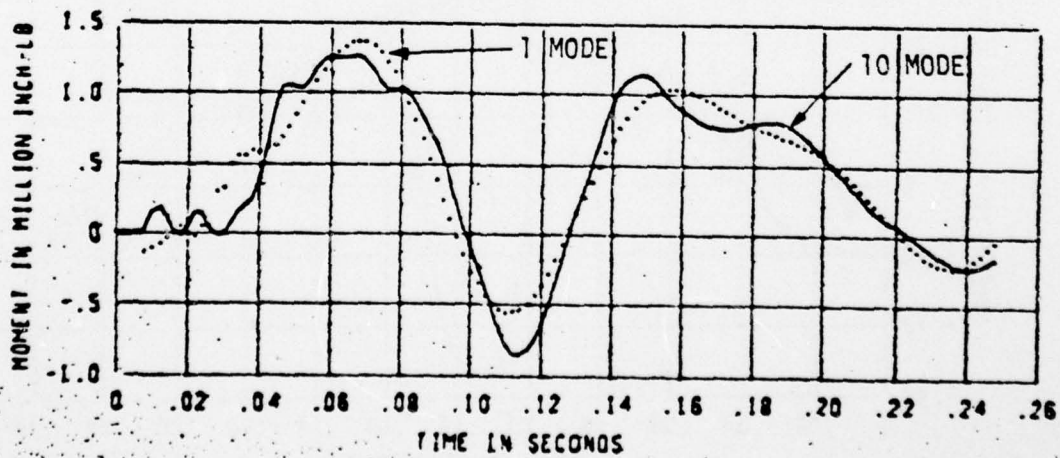
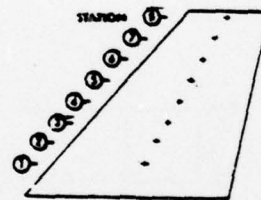


Figure 3-25 DATS Fin Bending Moment for 10 Modes and 1 Mode, VIBRA-4 Input, Sta. 6

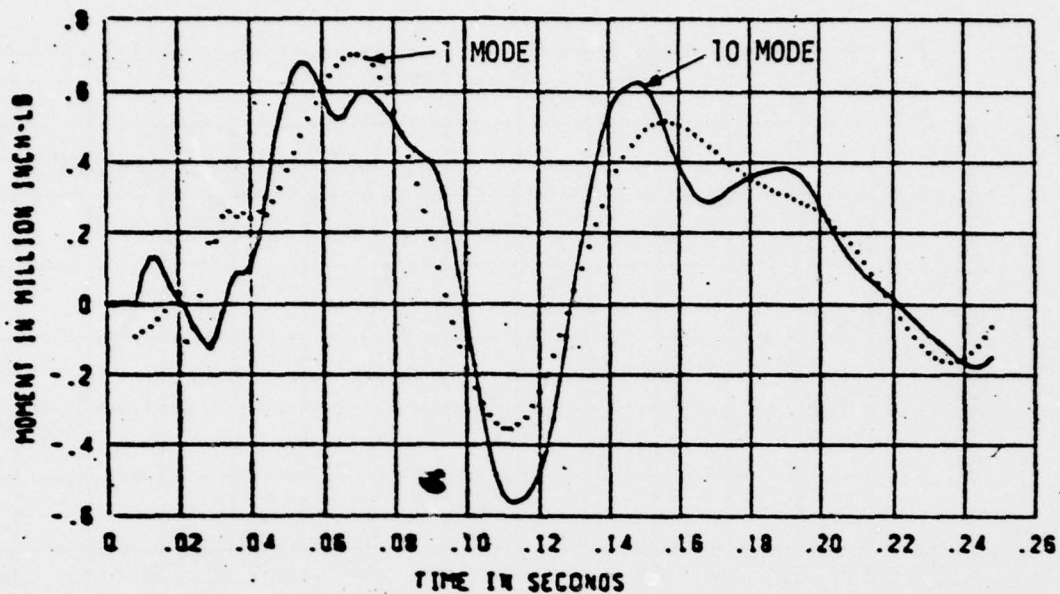


Figure 3-26 DATS Fin Bending Moment for 10 Modes and 1 Mode, VIBRA-4 Input, Sta. 7

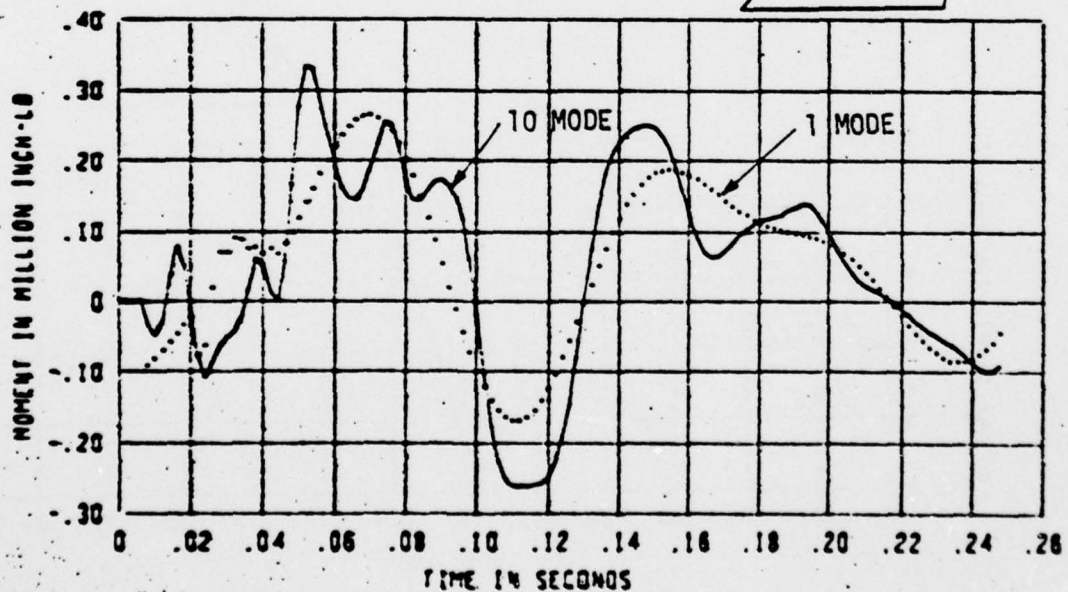
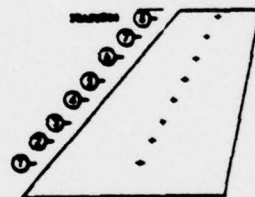


Figure 3-27 DATS Fin Bending Moment for 10 Modes and 1 Mode, VIBRA-4 Input, Sta. 8

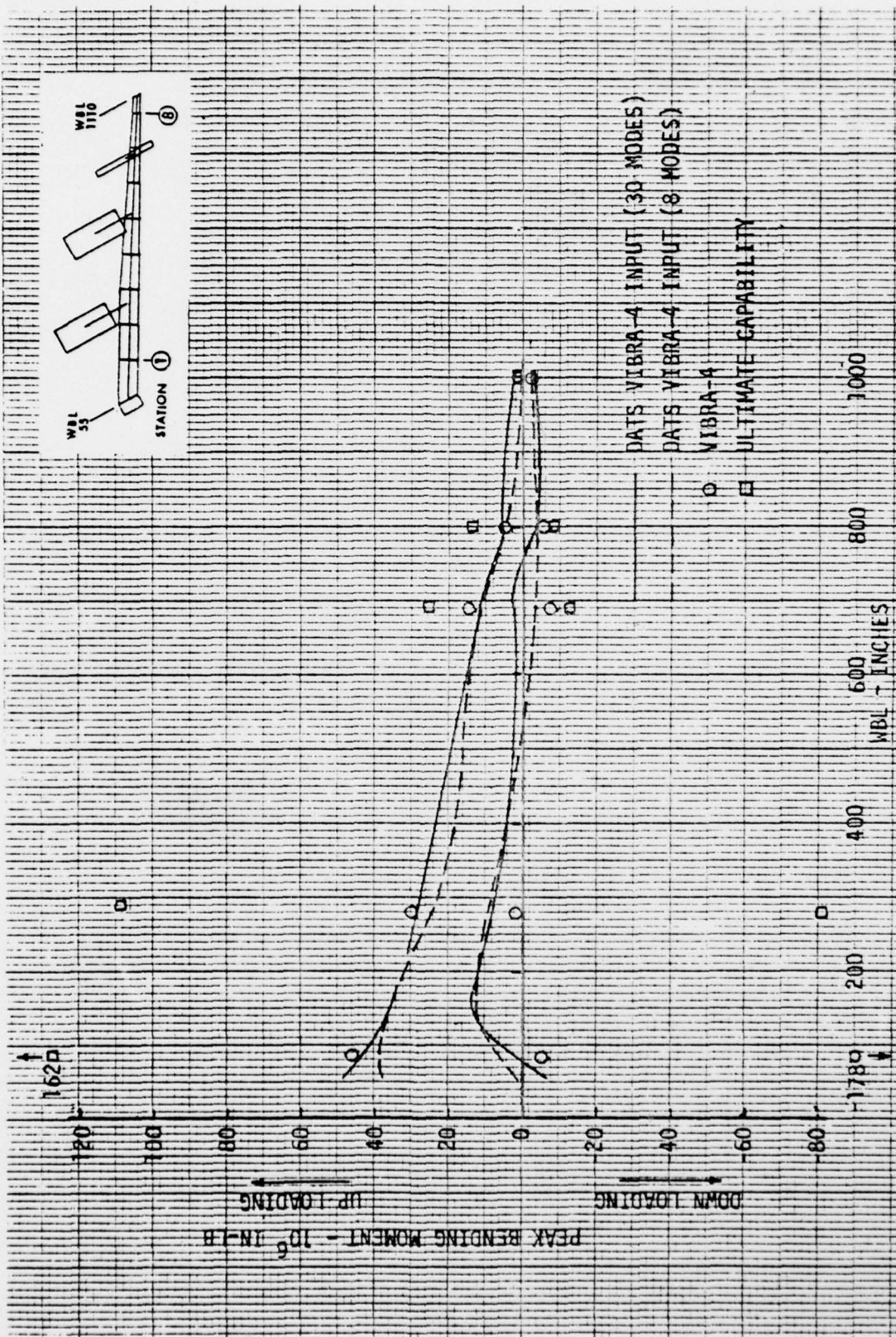


Figure 3-28 VIBRA-4/DATS Peak Bending Moment Comparison - B-52 H Wing

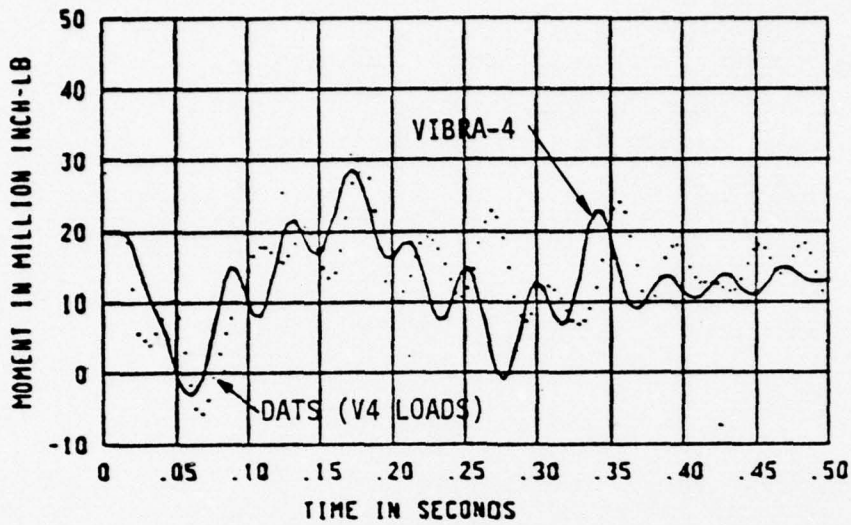


Figure 3-29 VIBRA-4 and DATS Bending Moment Time History - Wing, Sta 1

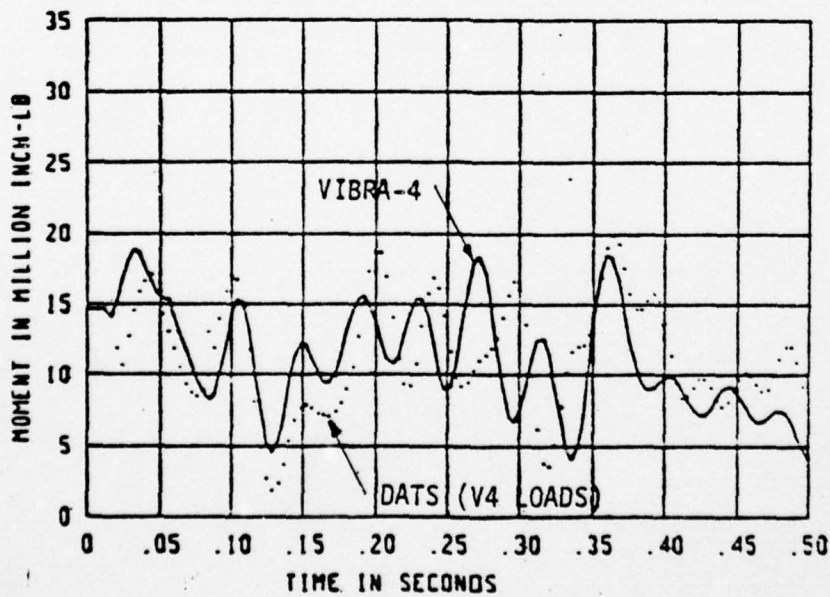
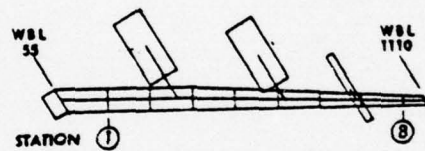


Figure 3-30 VIBRA-4 and DATS Bending Moment Time History - Wing, Sta 2

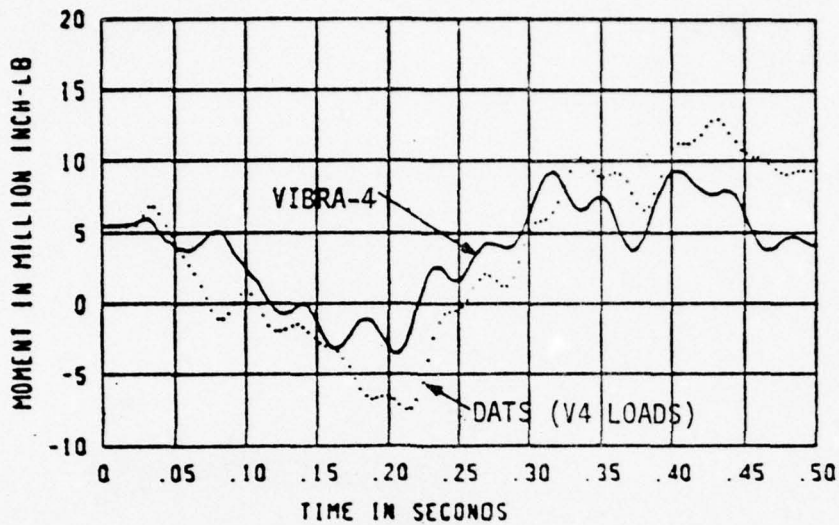


Figure 3-31 VIBRA-4 and DATS Bending Moment Time History - Wing, Sta 3

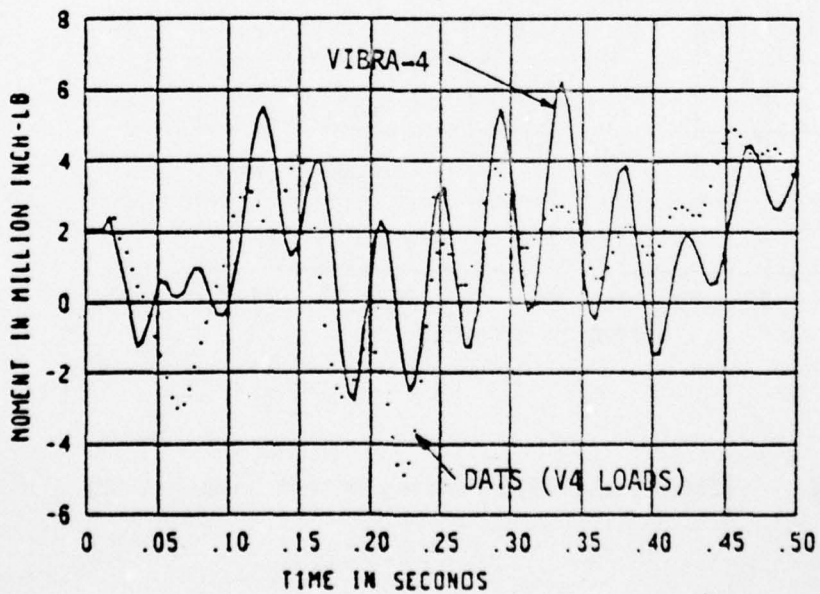
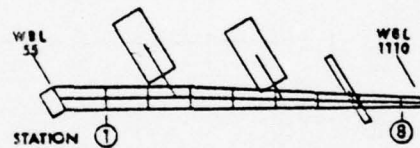


Figure 3-32 VIBRA-4 and DATS Bending Moment Time History - Wing, Sta 4

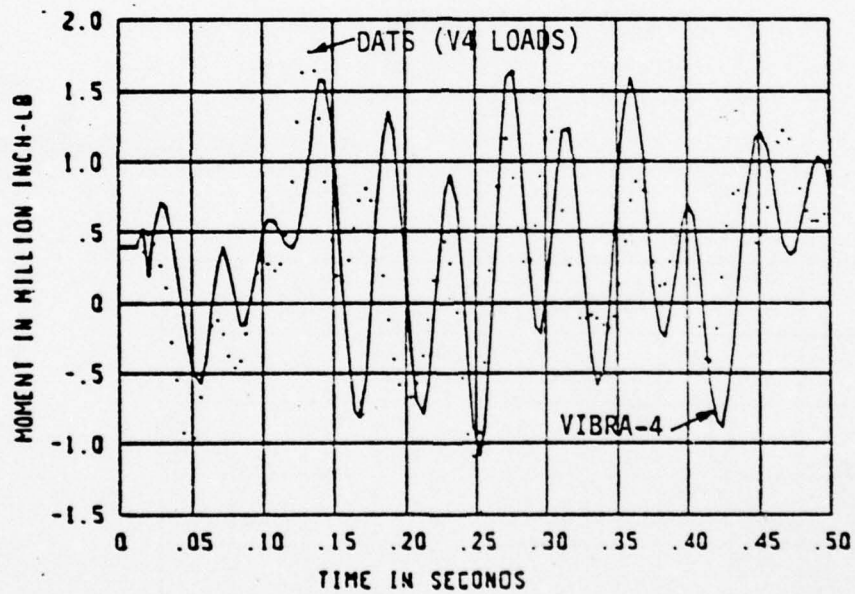
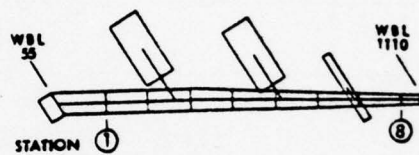


Figure 3-33 VIBRA-4 and DATS Bending Moment Time History - Wing, Sta 5

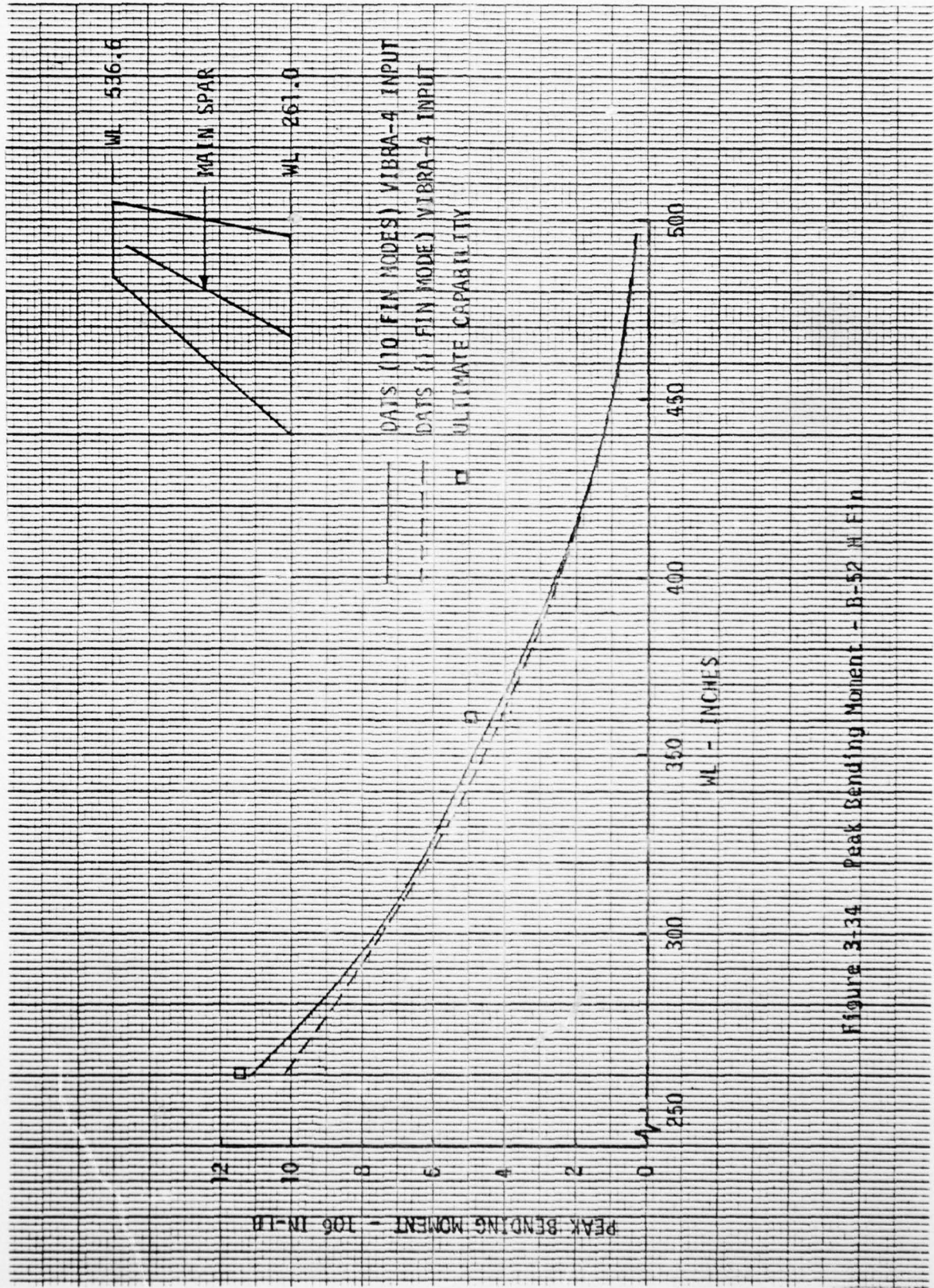


Figure 3-34 Peak Bending Moment - B-52 W Fin

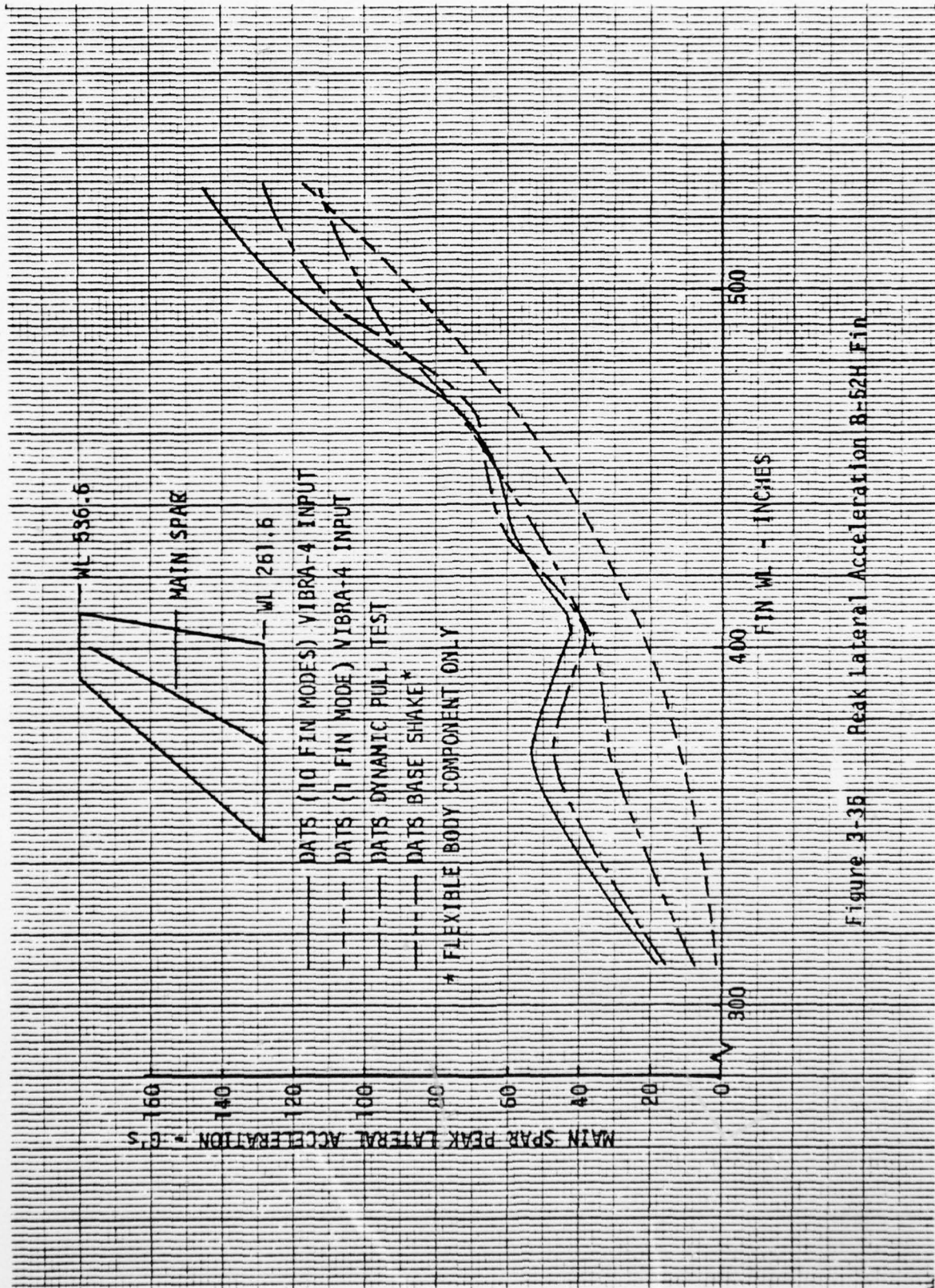


Figure 3-35 Peak Lateral Acceleration B-52H Fin

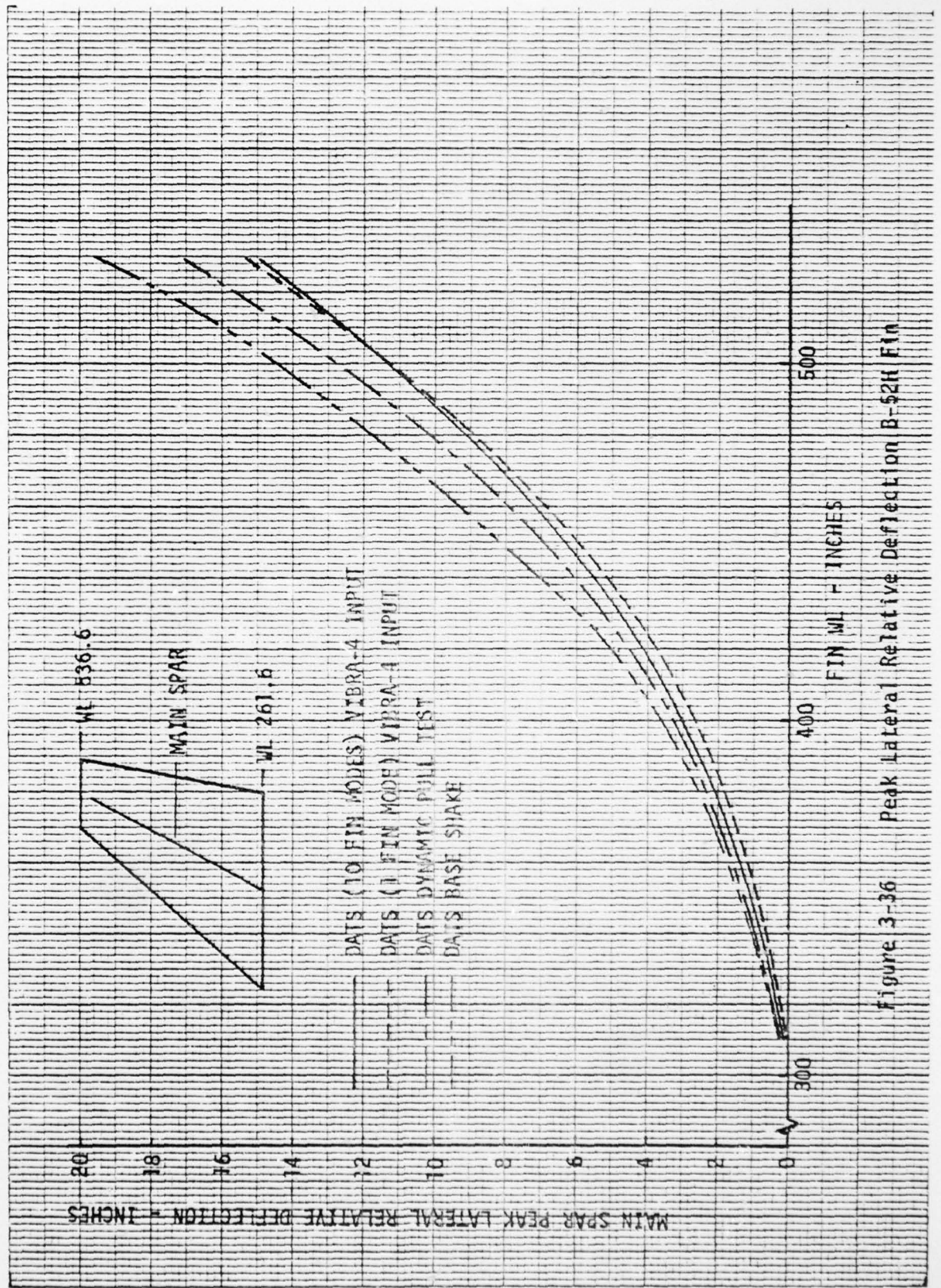


Figure 3-36 Peak Lateral Relative Deflection B-52H Fin

AD-A053 466

BOEING AEROSPACE CO SEATTLE WASH
SIMULATED NUCLEAR GUST TESTING OF MAJOR AIRPLANE STRUCTURAL COM--ETC(U)
JAN 77 D M ECKBLAD, N E FUNSTON

F/G 19/4
DNA001-76-C-0367

UNCLASSIFIED

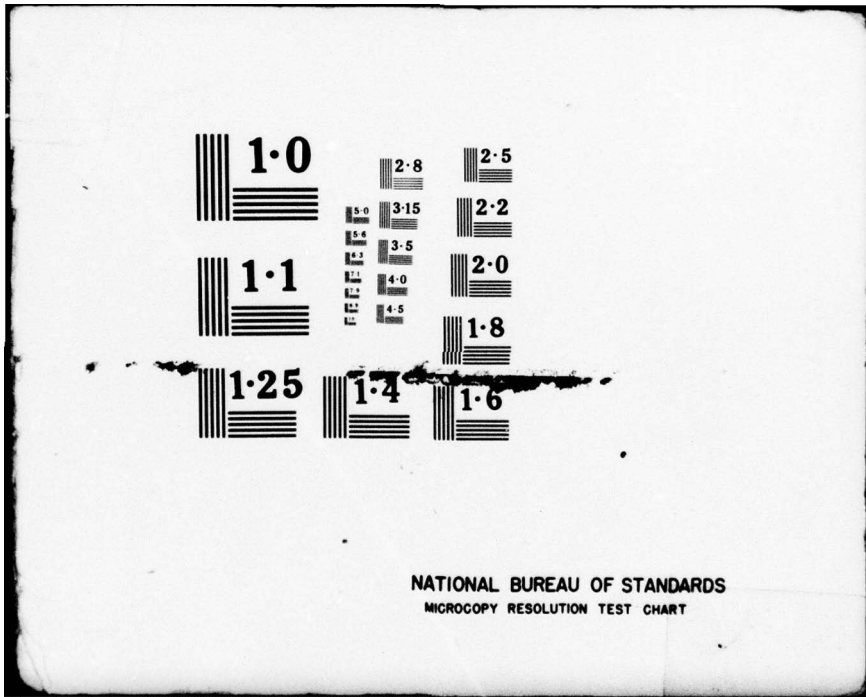
DNA-4243F

NL

2 OF 2
ADA
053466



END
DATE
FILMED
6-78
DDC



1.0

1.1

1.25

1.4

1.6

2.8
3.15
3.5
4.0
4.5

2.5

2.2

2.0

1.8

NATIONAL BUREAU OF STANDARDS
MICROCOPY RESOLUTION TEST CHART

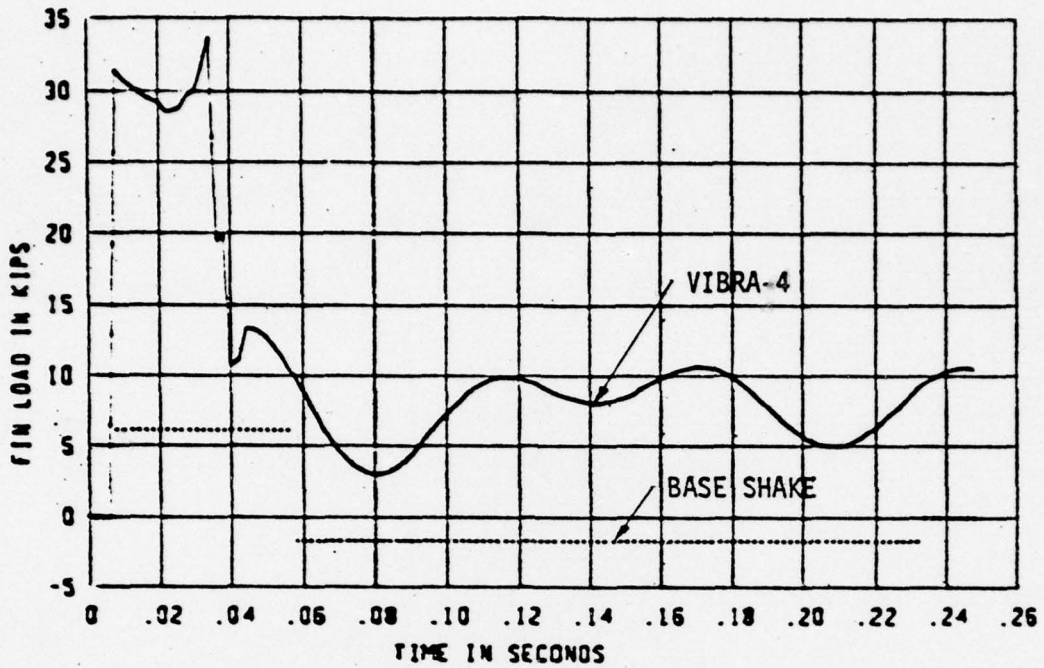


Figure 3-37 Test Loading - Fin Base Shake - Sta. 1

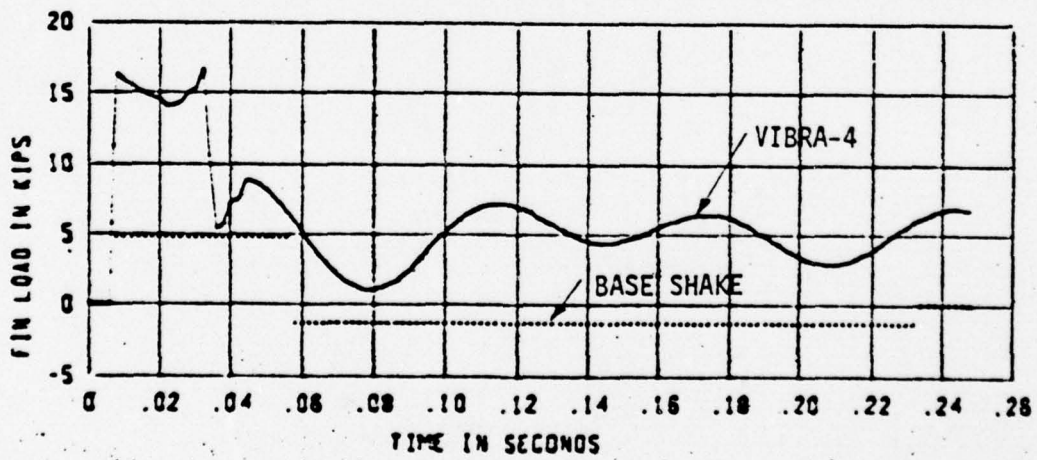
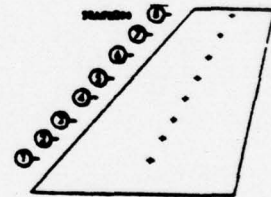


Figure 3-38 Test Loading - Fin Base Shake - Sta. 2

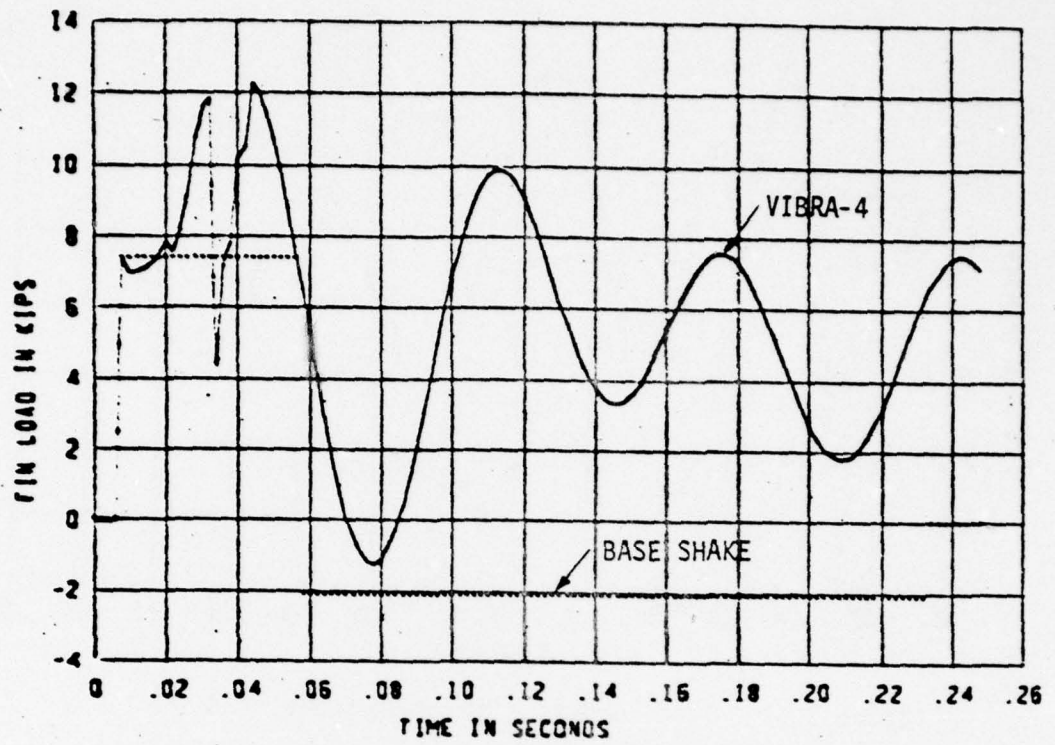


Figure 3-39 Test Loading - Fin Base Shake - Sta. 3

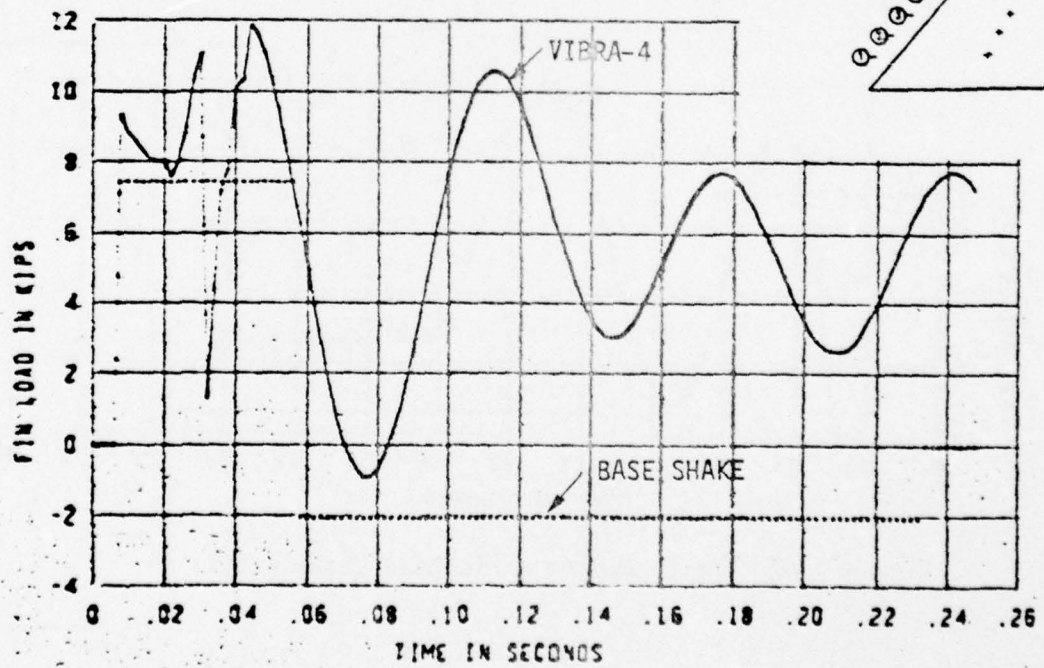


Figure 3-40 Test Loading - Fin Base Shake - Sta. 4

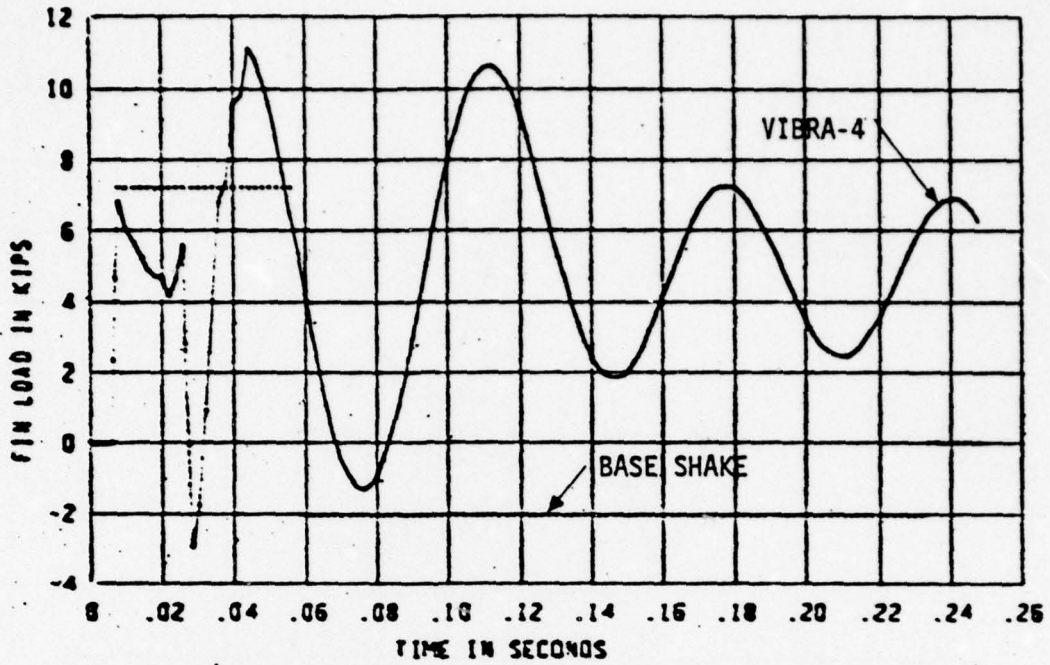


Figure 3-41 Test Loading - Fin Base Shake - Sta. 5

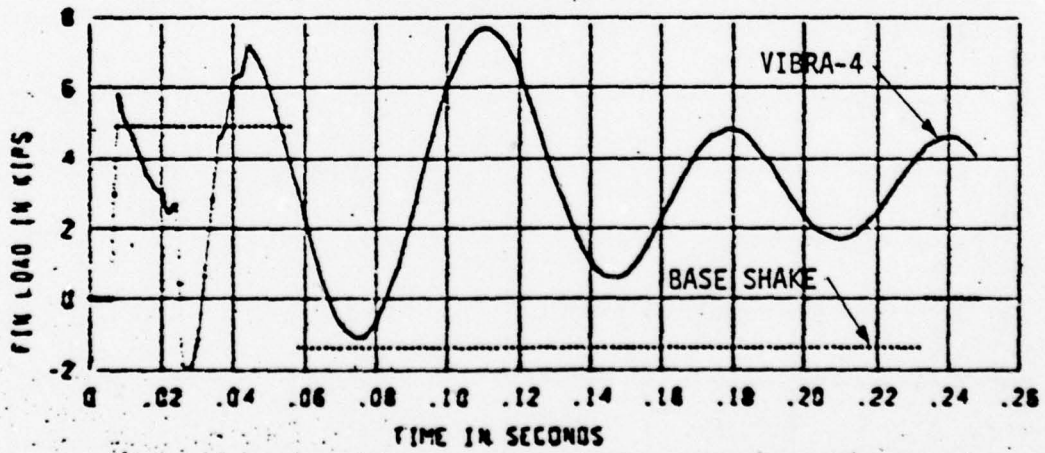
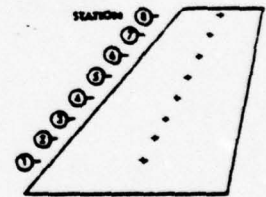


Figure 3-42 Test Loading - Fin Base Shake - Sta. 6

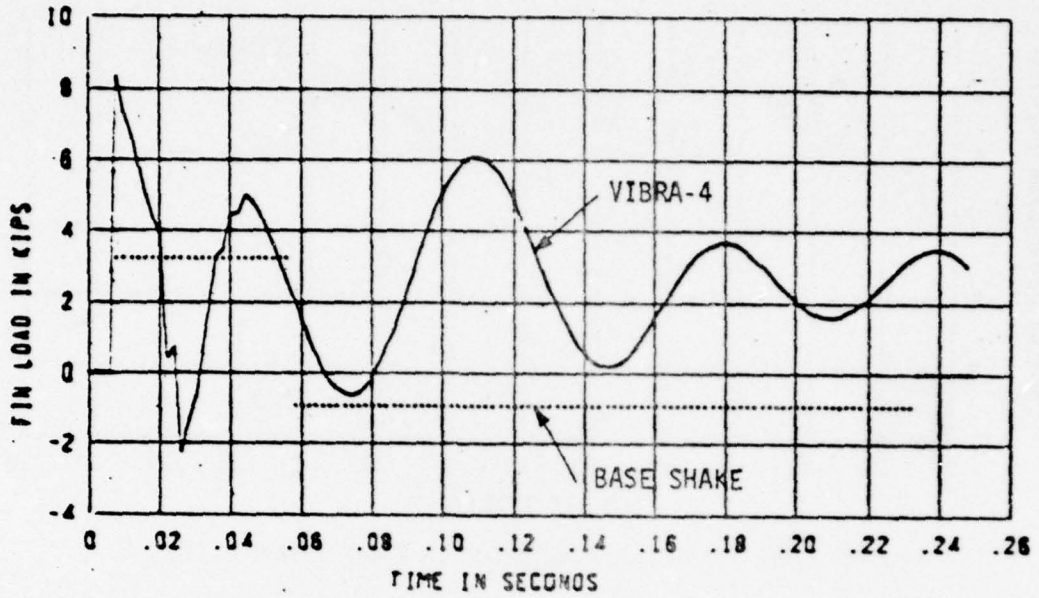


Figure 3-43 Test Loading - Fin Base Shake - Sta. 7

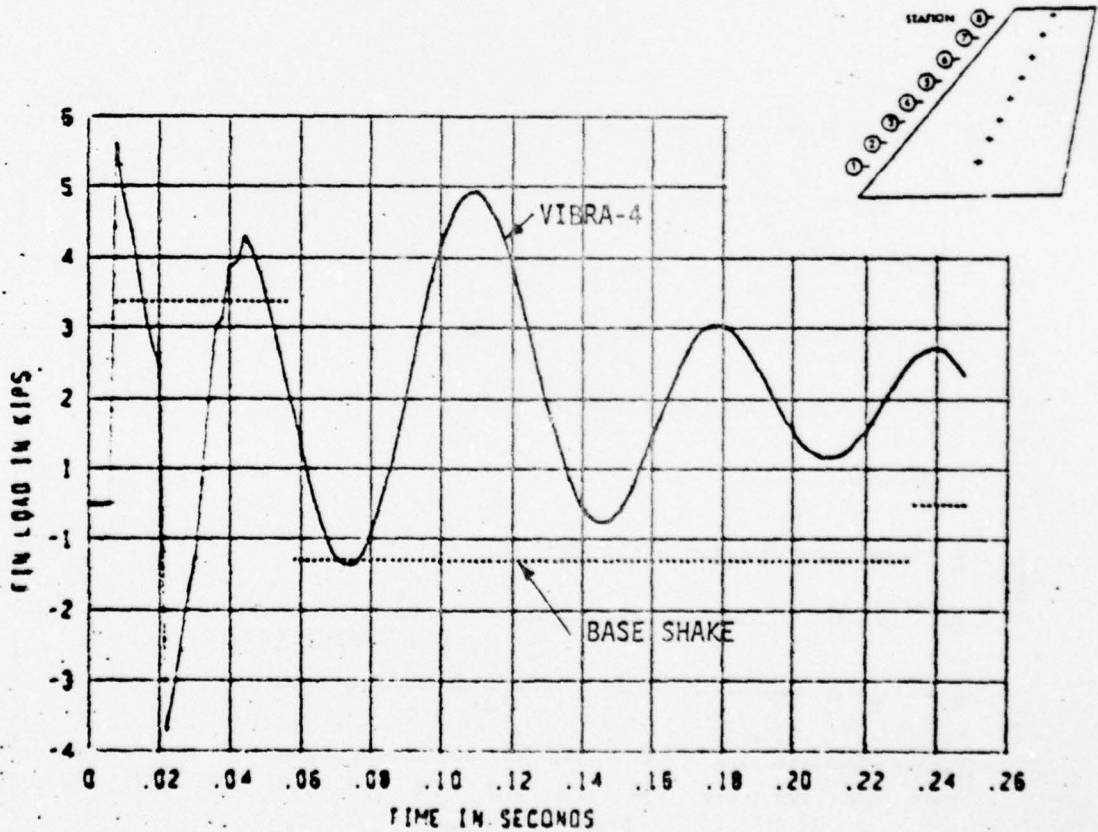


Figure 3-44 Test Loading - Fin Base Shake - Sta. 8

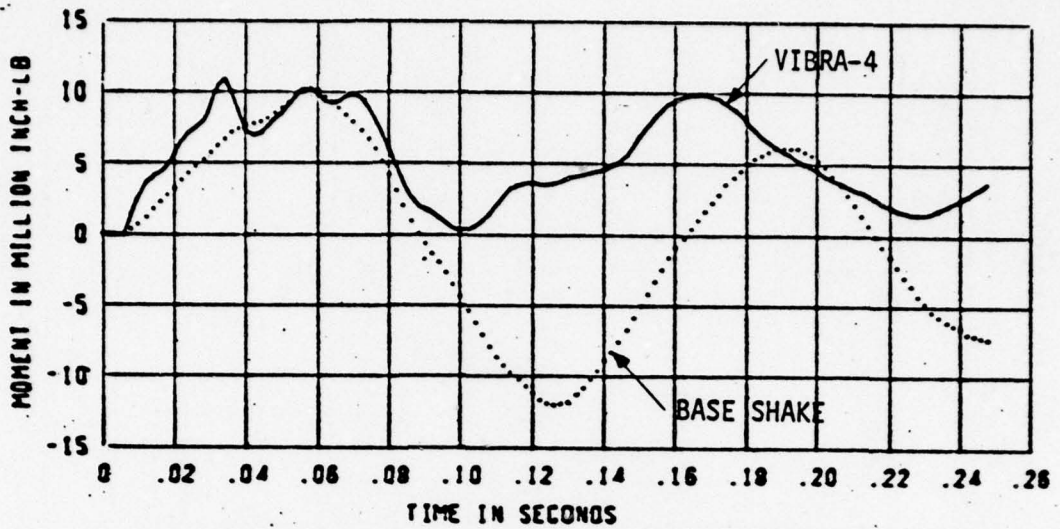


Figure 3-45 Bending Moment - Fin Base Shake - Sta. 1

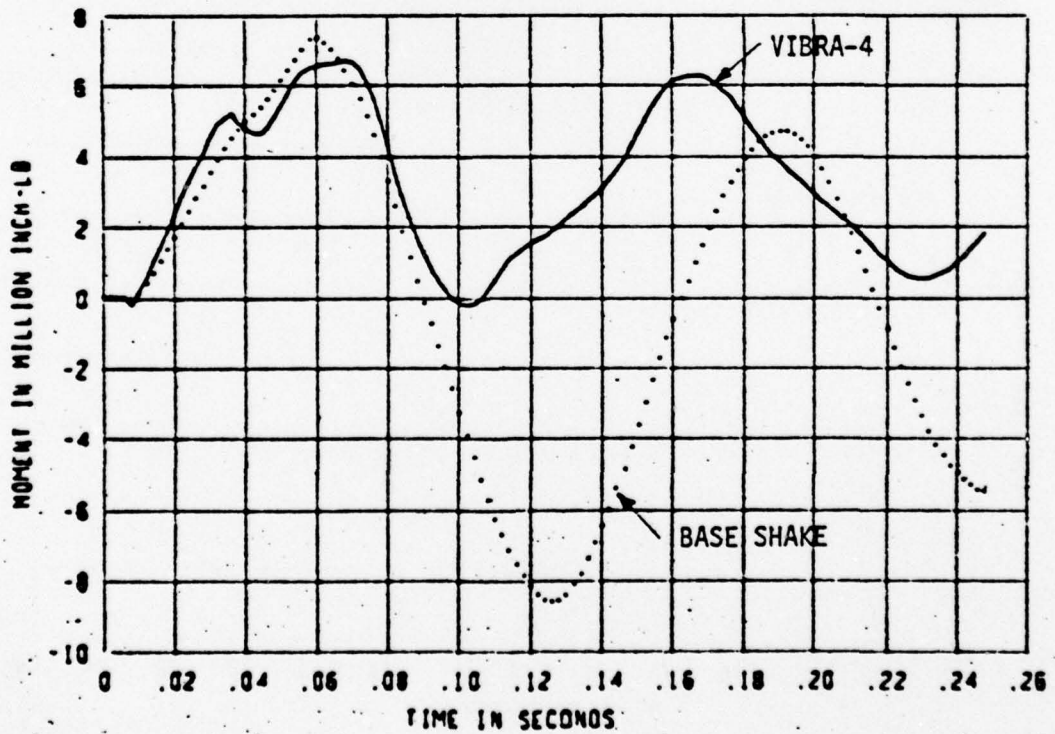
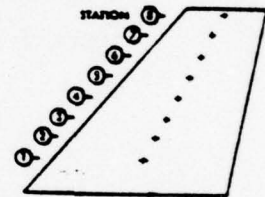


Figure 3-46 Bending Moment - Fin Base Shake - Sta. 2

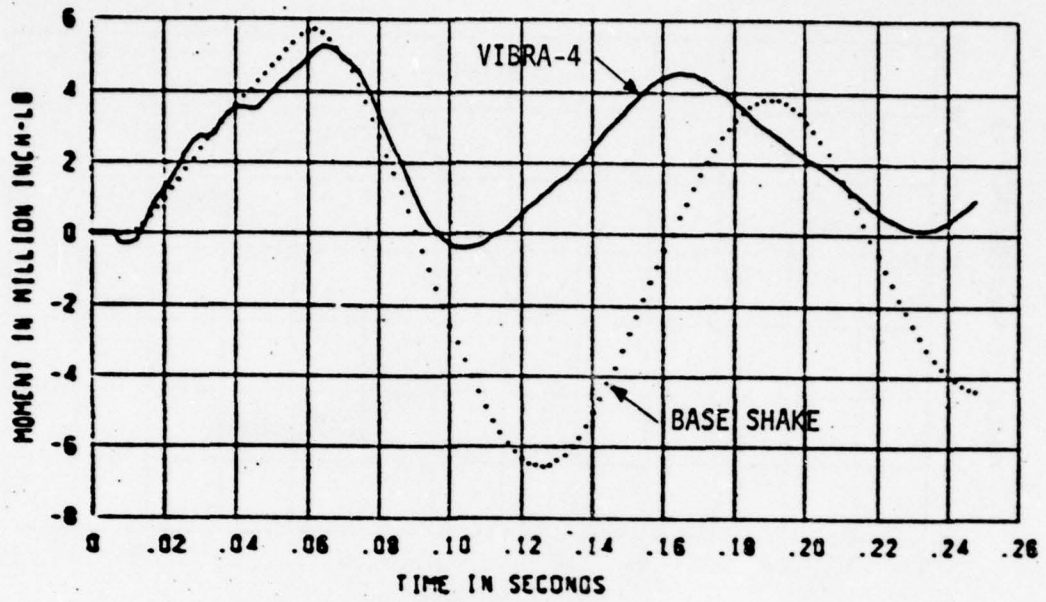


Figure 3-47 Bending Moment - Fin Base Shake - Sta. 3

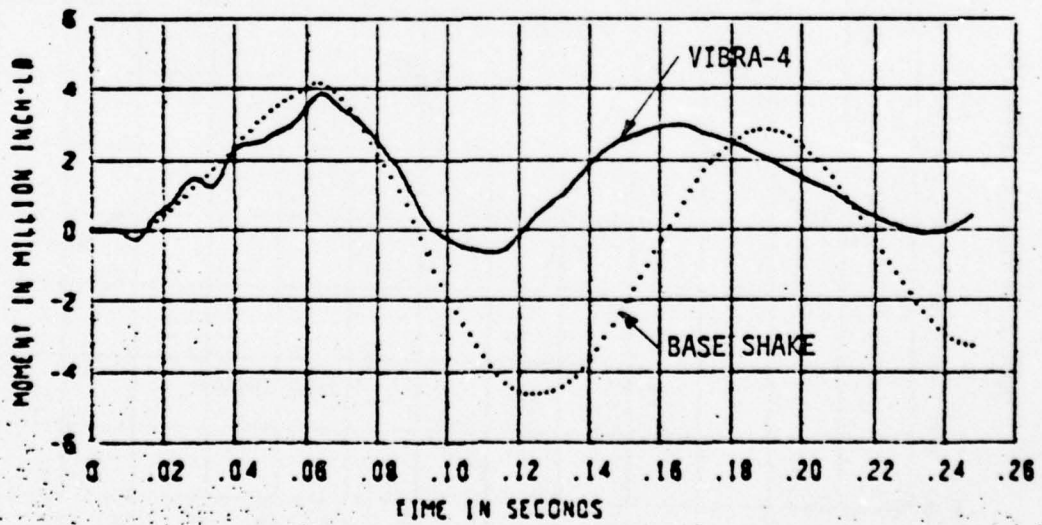
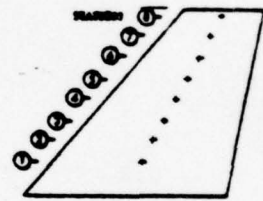


Figure 3-48 Bending Moment - Fin Base Shake - Sta. 4

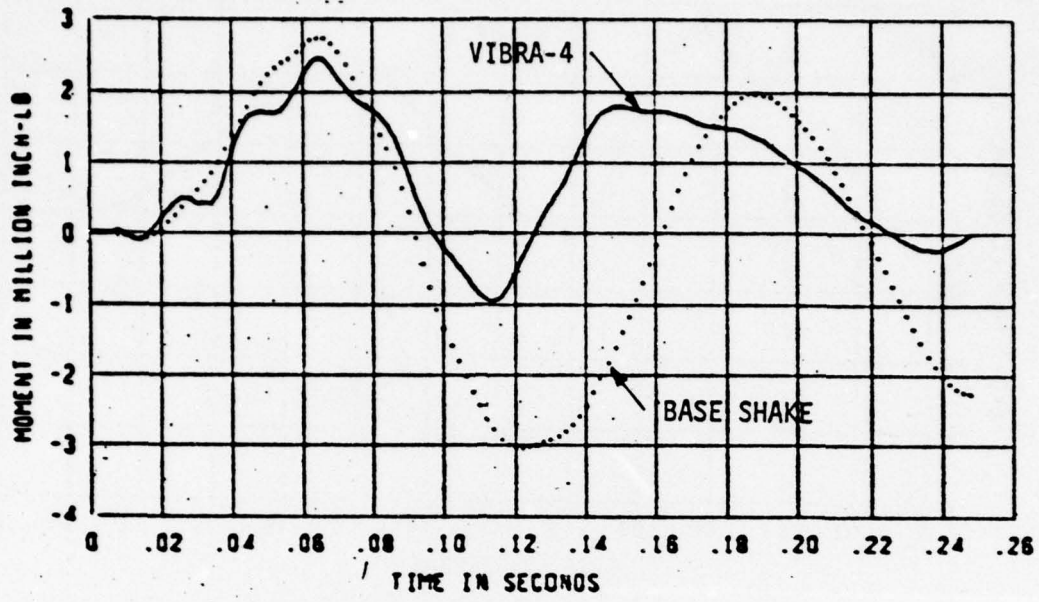


Figure 3-49 Bending Moment - Fin Base Shake - Sta. 5

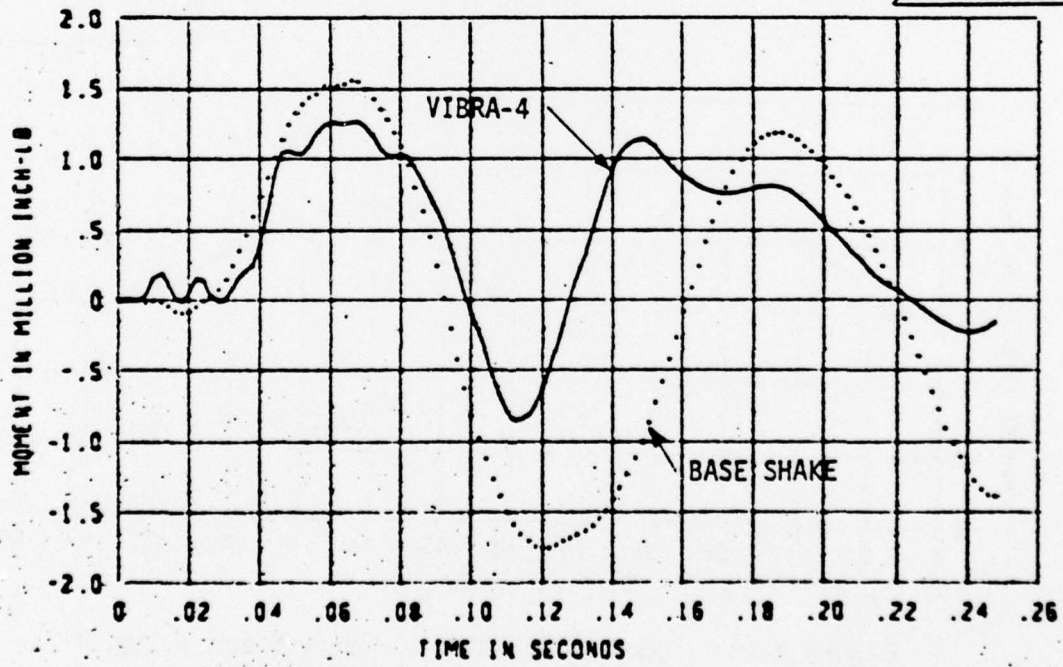
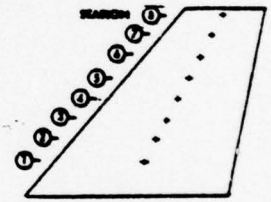


Figure 3-50 Bending Moment - Fin Base Shake - Sta. 6

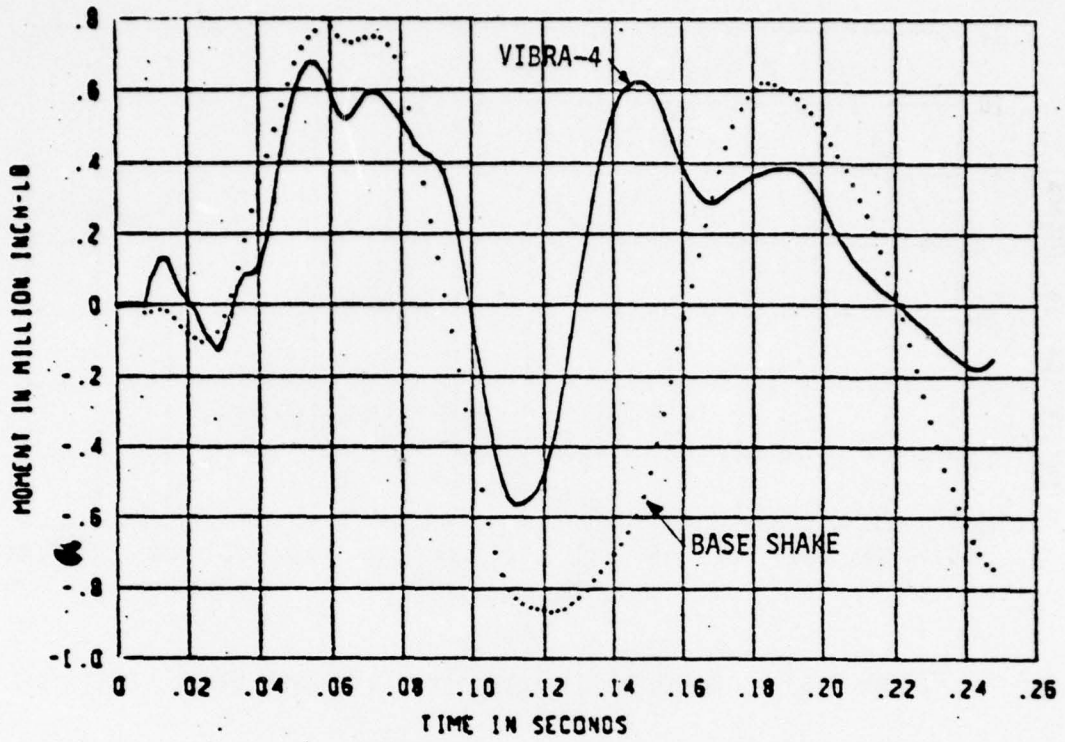


Figure 3-51 Bending Moment - Fin Base Shake - Sta. 7

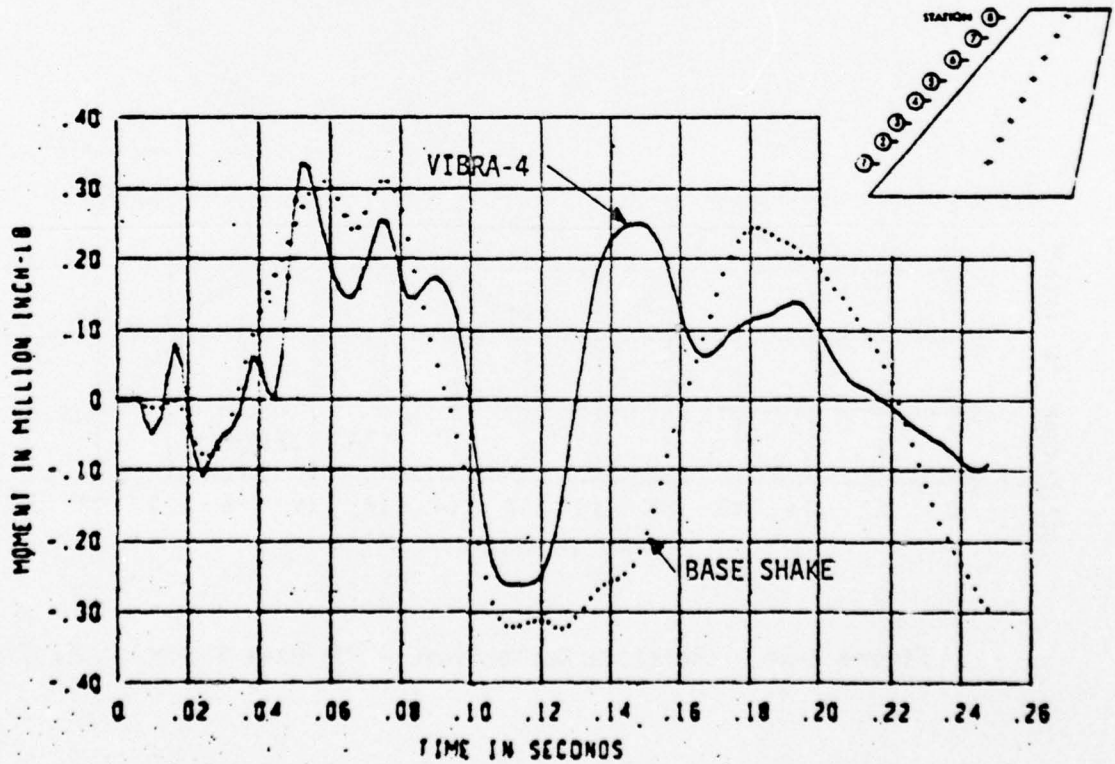


Figure 3-52 Bending Moment - Fin Base Shake - Sta. 8

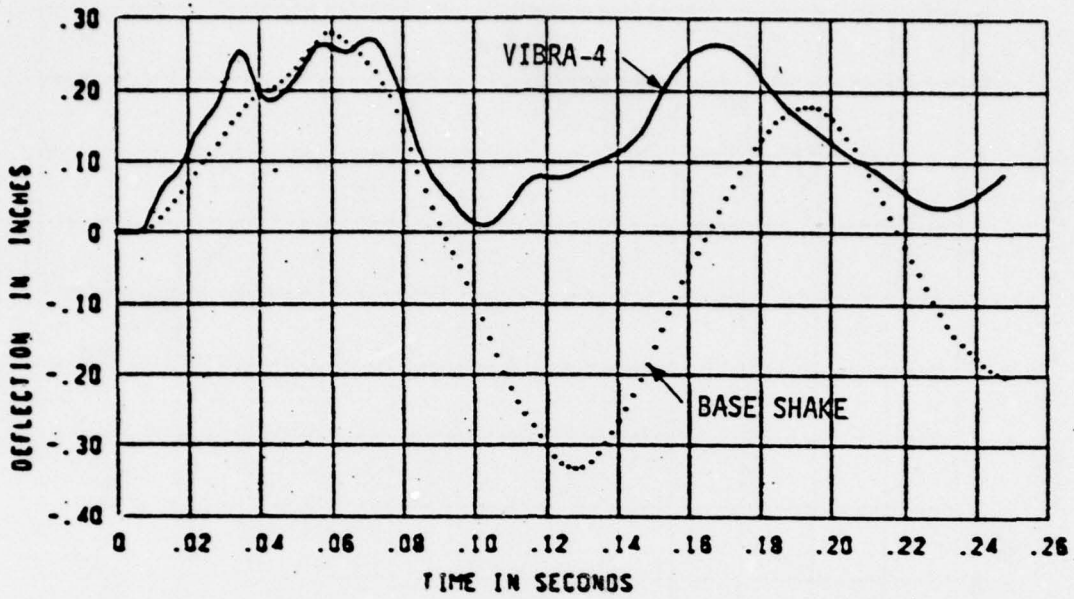


Figure 3-53 Relative Deflections - Fin Base Shake - Sta. 1

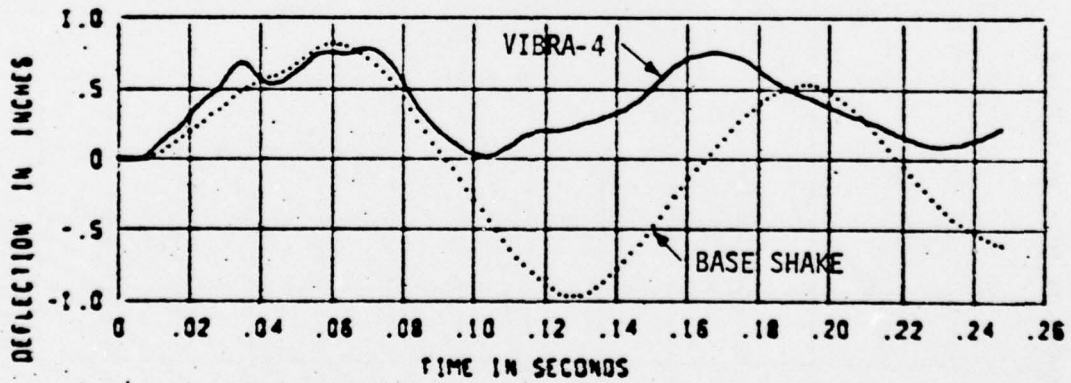
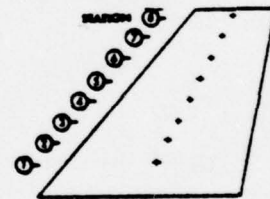


Figure 3-54 Relative Deflections - Fin Base Shake - Sta. 2

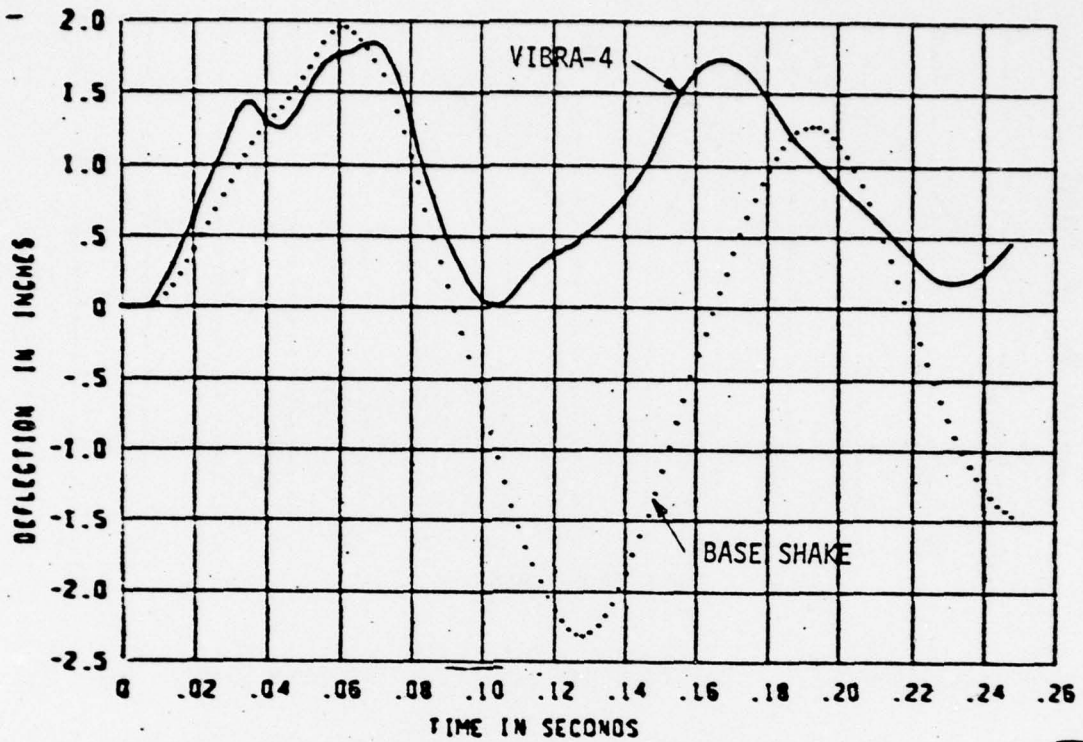


Figure 3-55 Relative Deflections - Fin Base Shake - Sta. 3

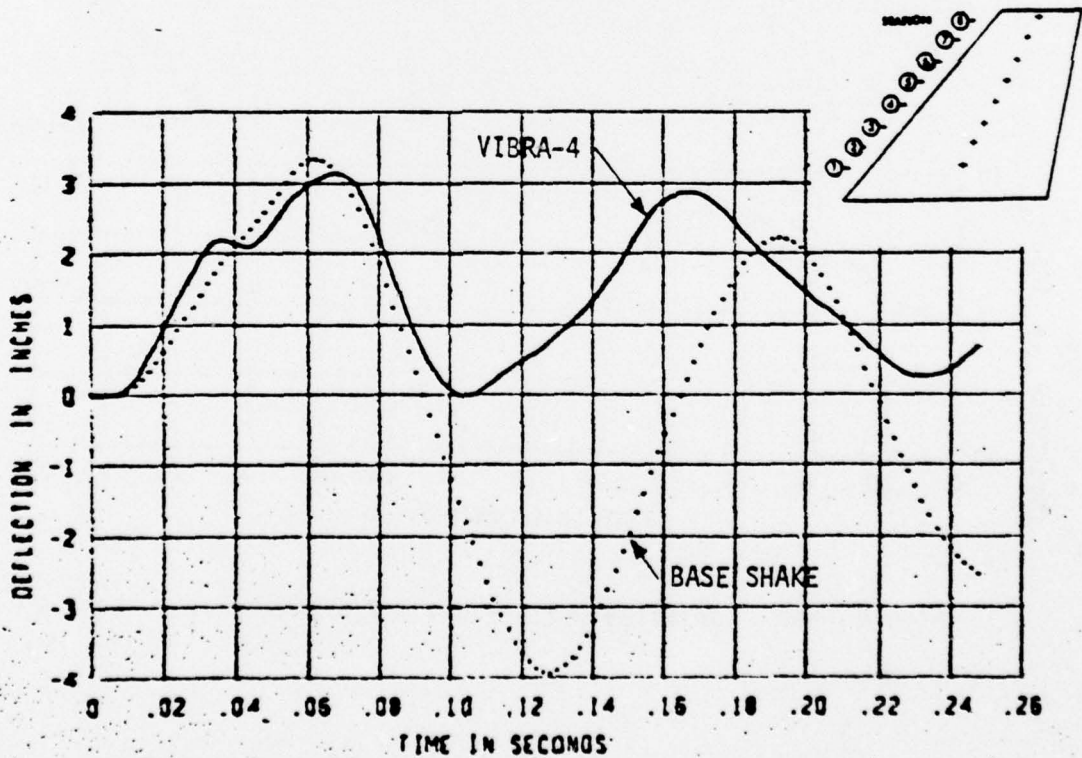


Figure 3-56 Relative Deflections - Fin Base Shake - Sta. 4

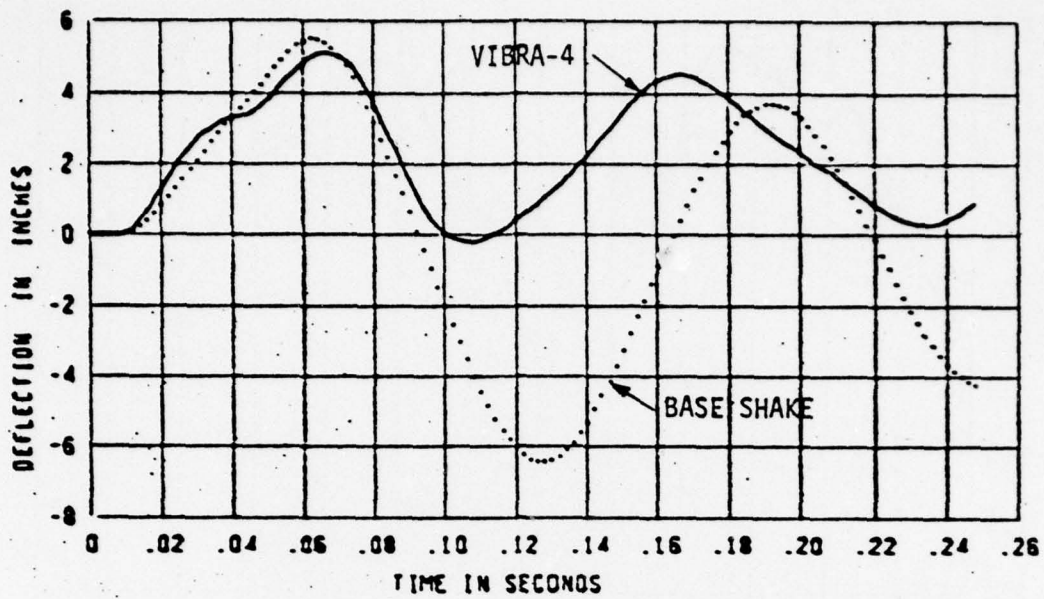


Figure 3-57 Relative Deflections - Fin Base Shake - Sta. 5

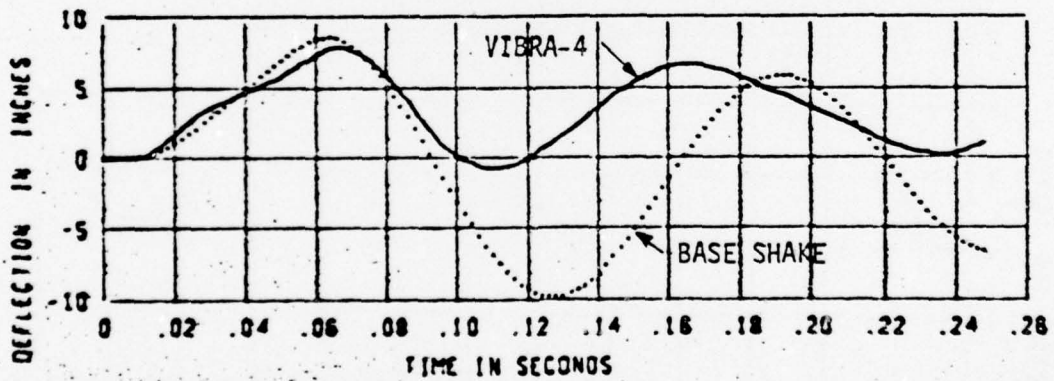
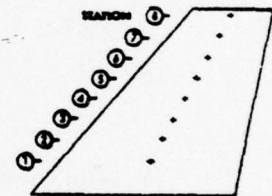


Figure 3-58 Relative Deflections - Fin Base Shake - Sta. 6

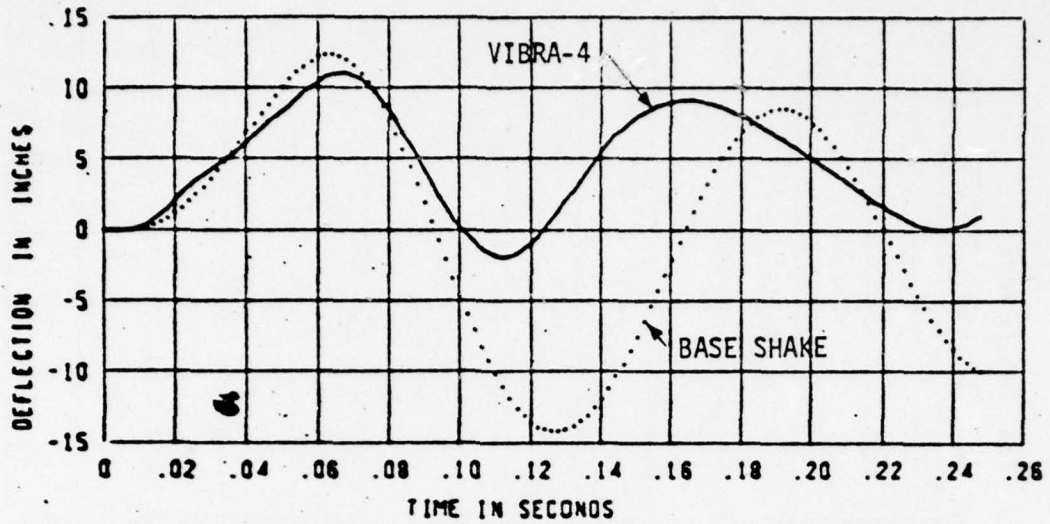


Figure 3-59 Relative Deflections - Fin Base Shake - Sta. 7

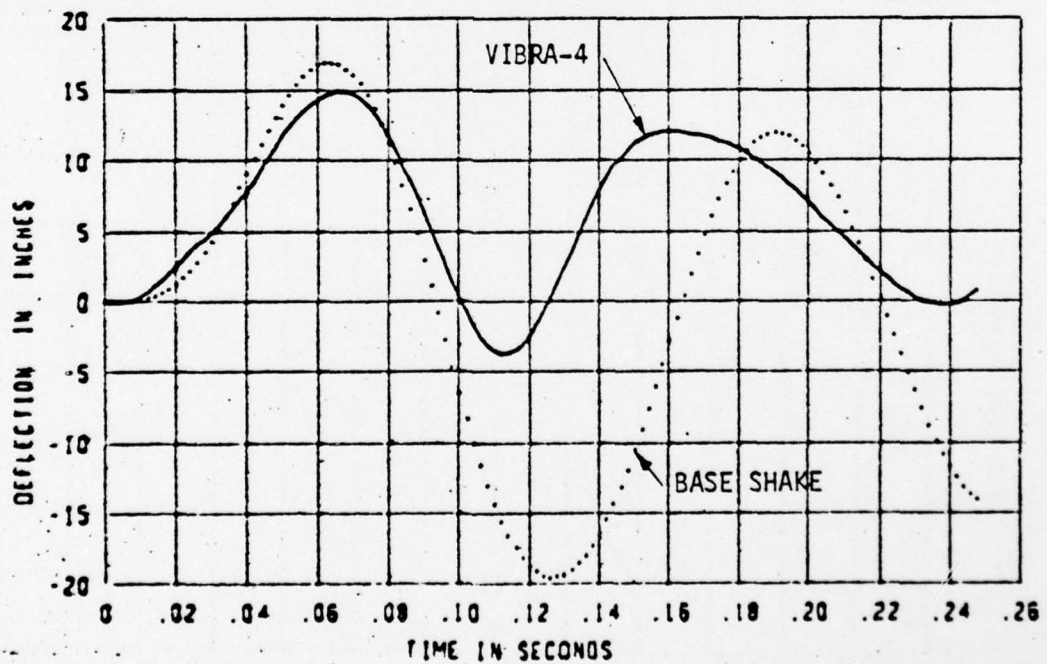
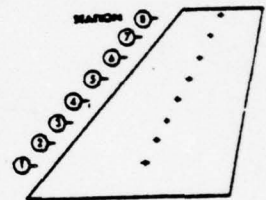


Figure 3-60 Relative Deflections - Fin Base Shake - Sta. 8

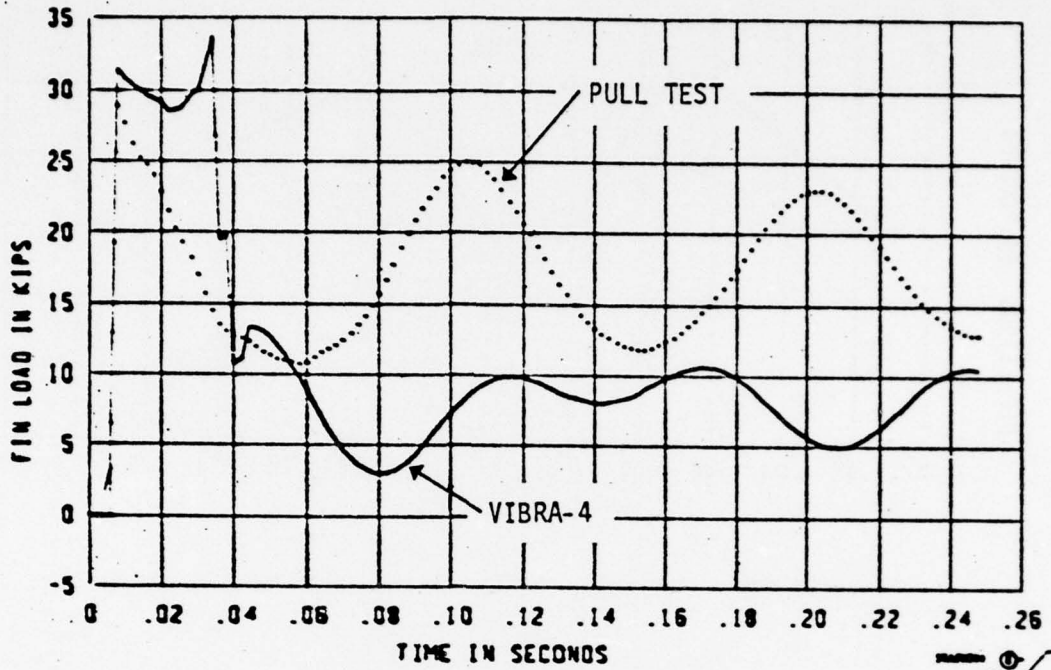


Figure 3-61 Test Loading - Fin Dynamic Pull Test Sta. 1

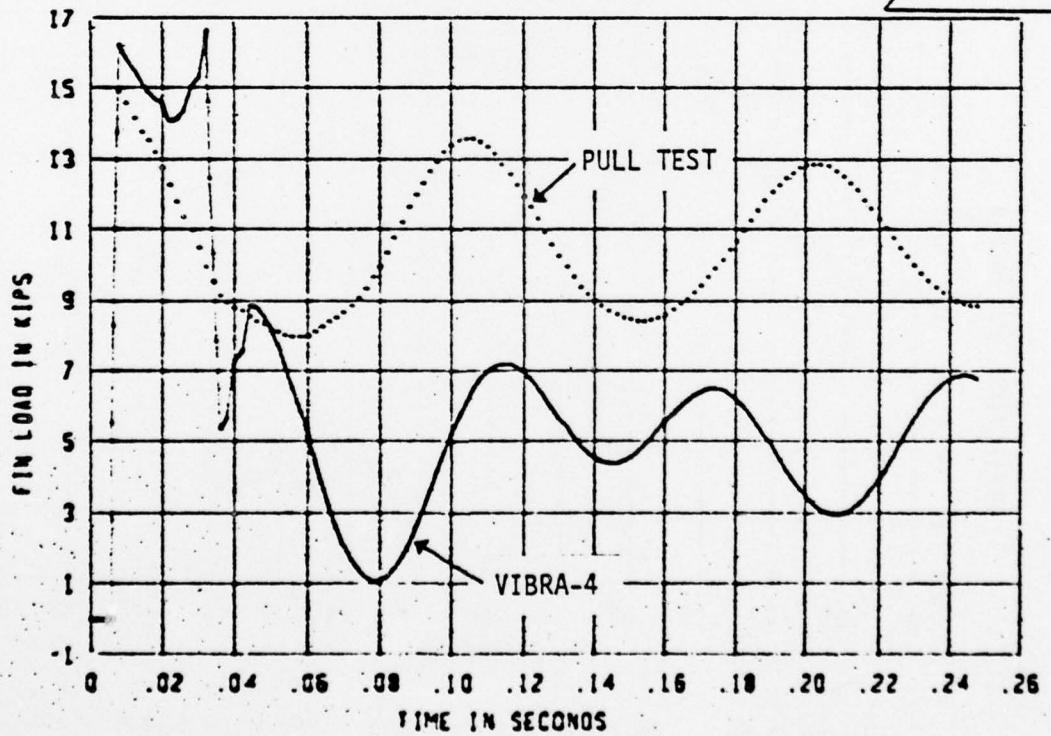
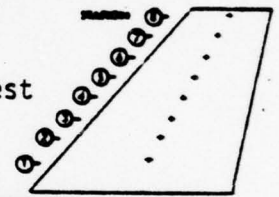


Figure 3-62 Test Loading - Fin Dynamic Pull Test - Sta. 2

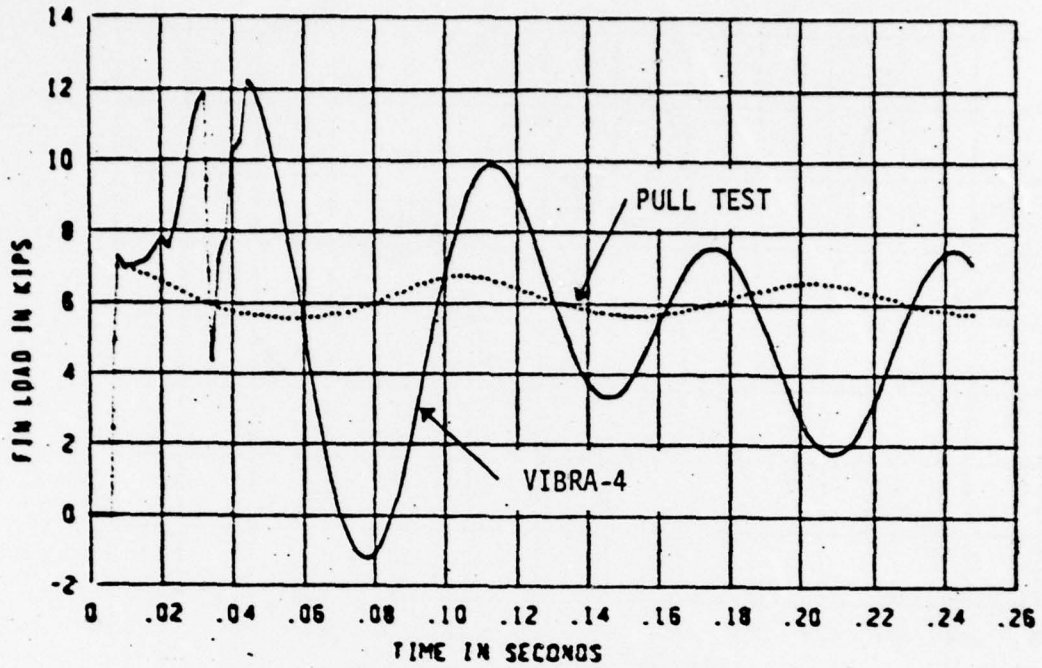


Figure 3-63 Test Loading - Fin Dynamic Pull Test Sta. 3

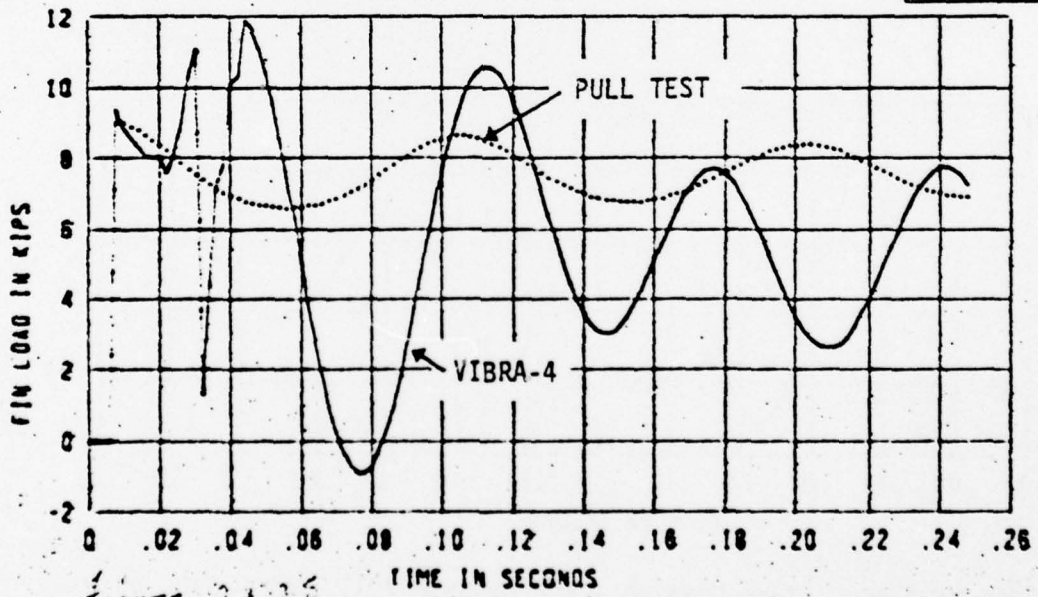
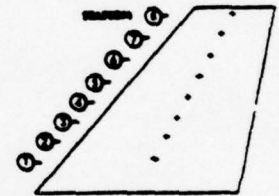


Figure 3-64 Test Loading - Fin Dynamic Pull Test - Sta. 4

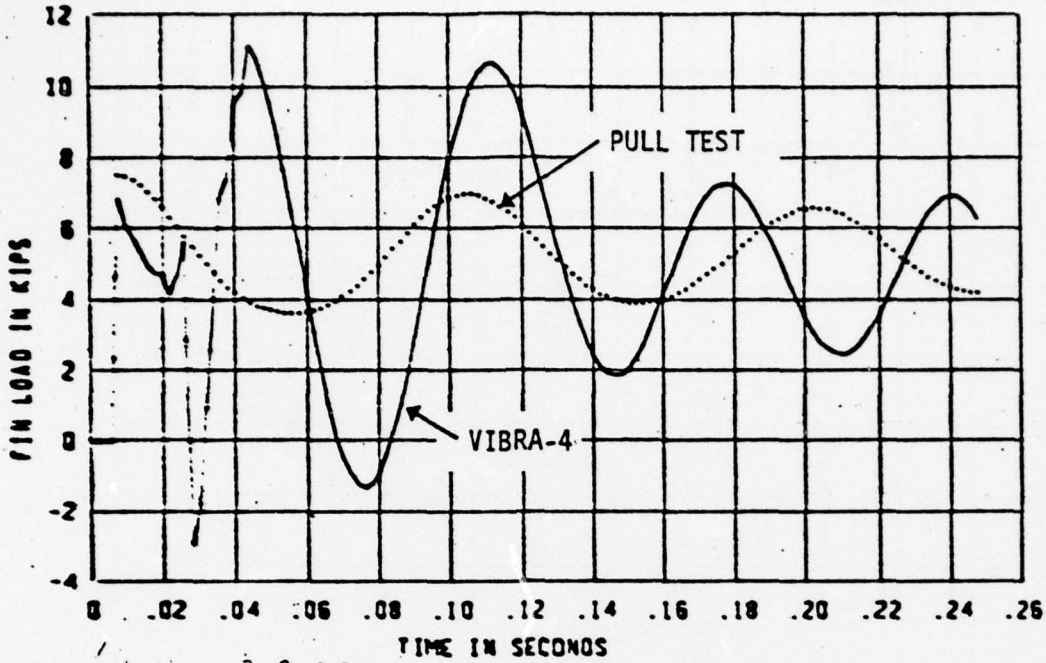


Figure 3-65 Test Loading - Fin Dynamic Pull Test - Sta. 5

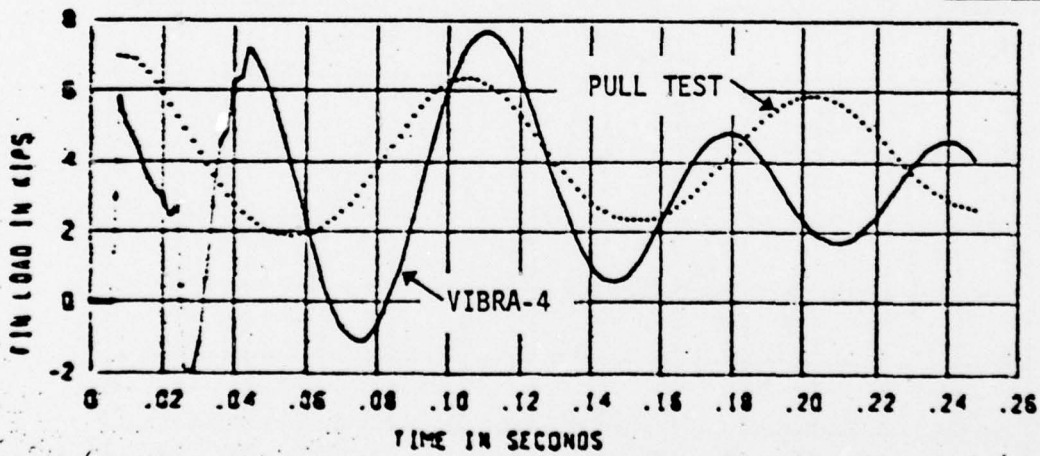
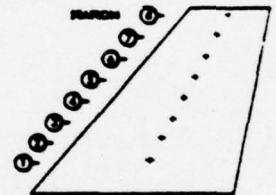


Figure 3-66 Test Loading - Fin Dynamic Pull Test - Sta. 6

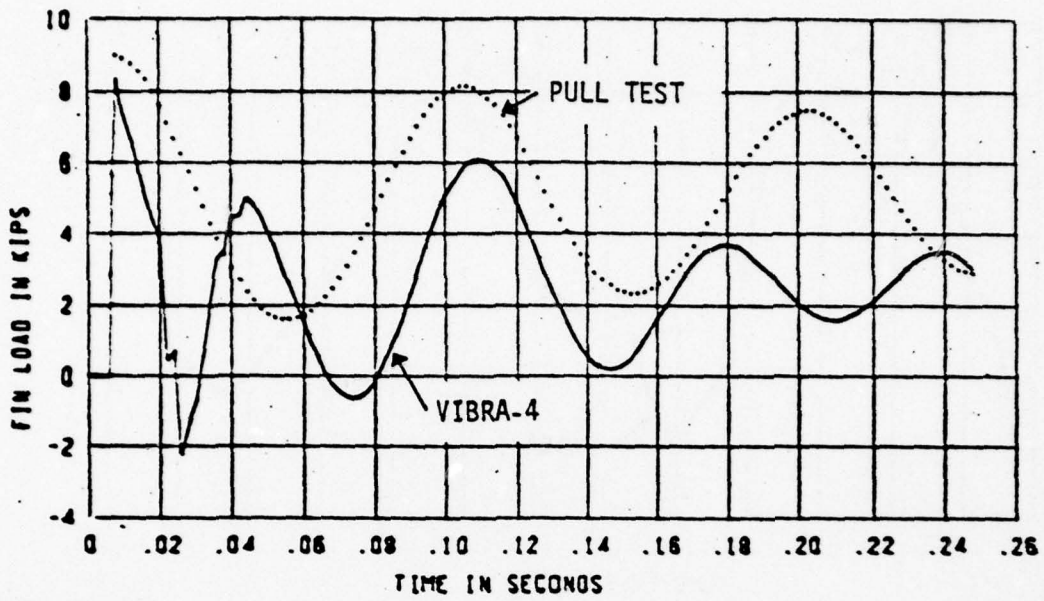


Figure 3-67 Test Loading - Fin Dynamic Pull Test - Sta. 7

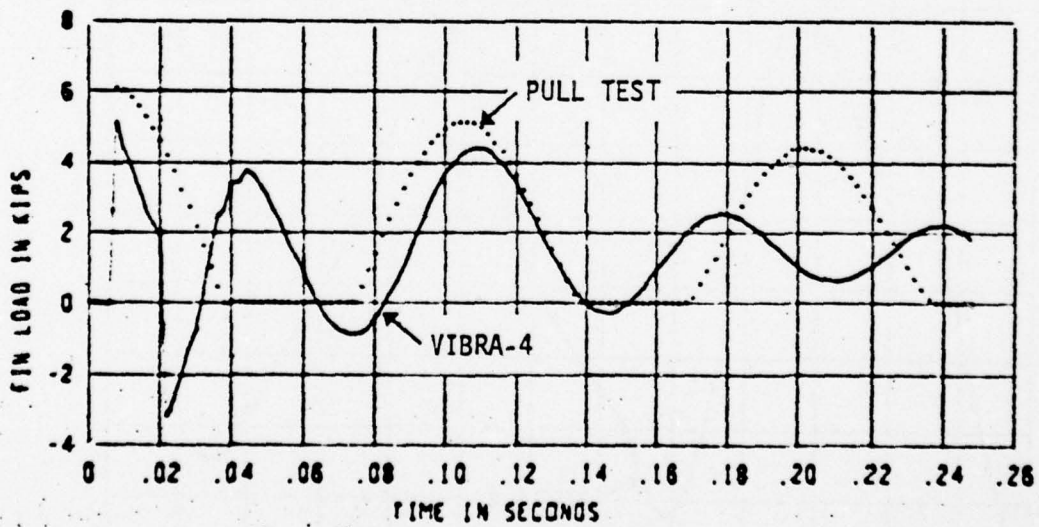
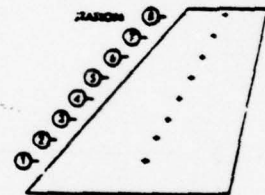


Figure 3-68 Test Loading - Fin Dynamic Pull Test - Sta. 8

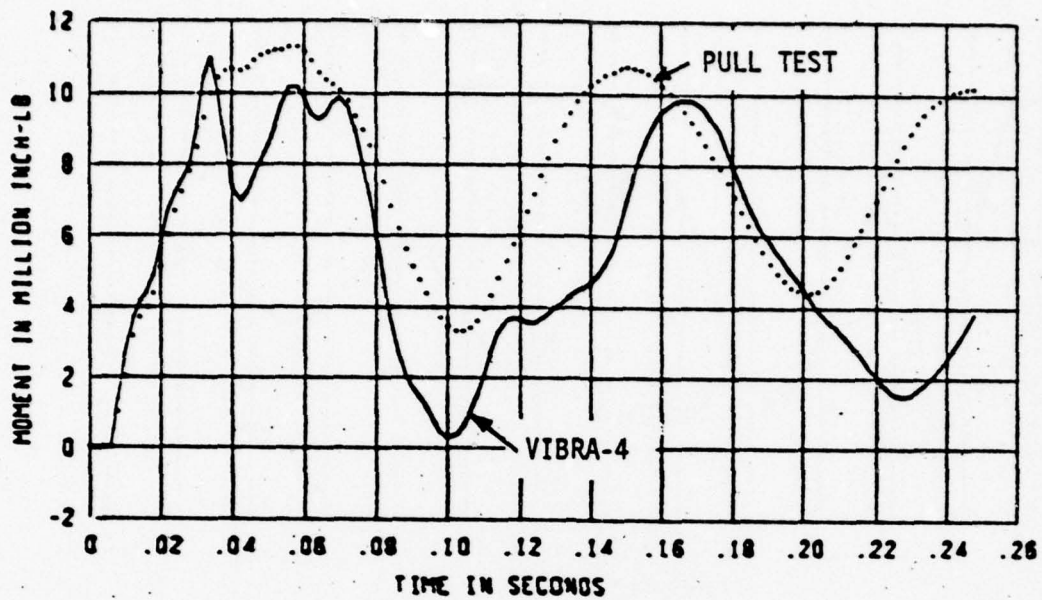


Figure 3-69 Bending Moment - Fin Dynamic Pull Test Sta. 1

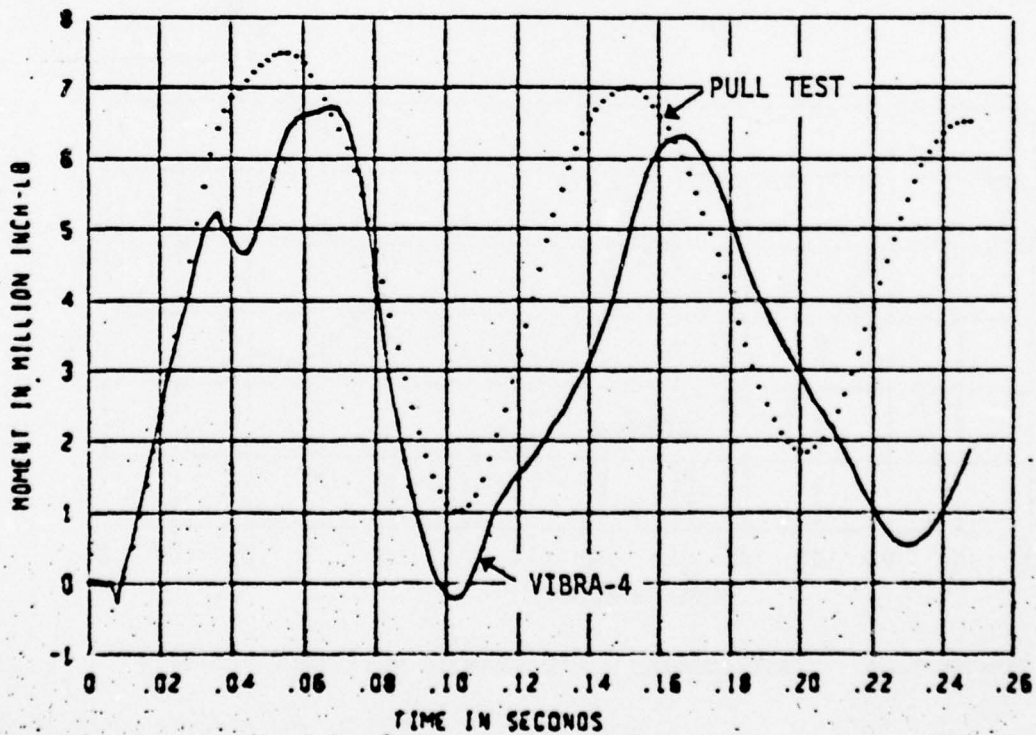
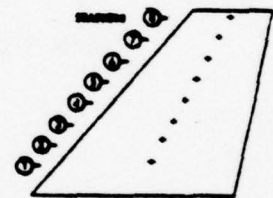


Figure 3-70 Bending Moment - Fin Dynamic Pull Test - Sta. 2

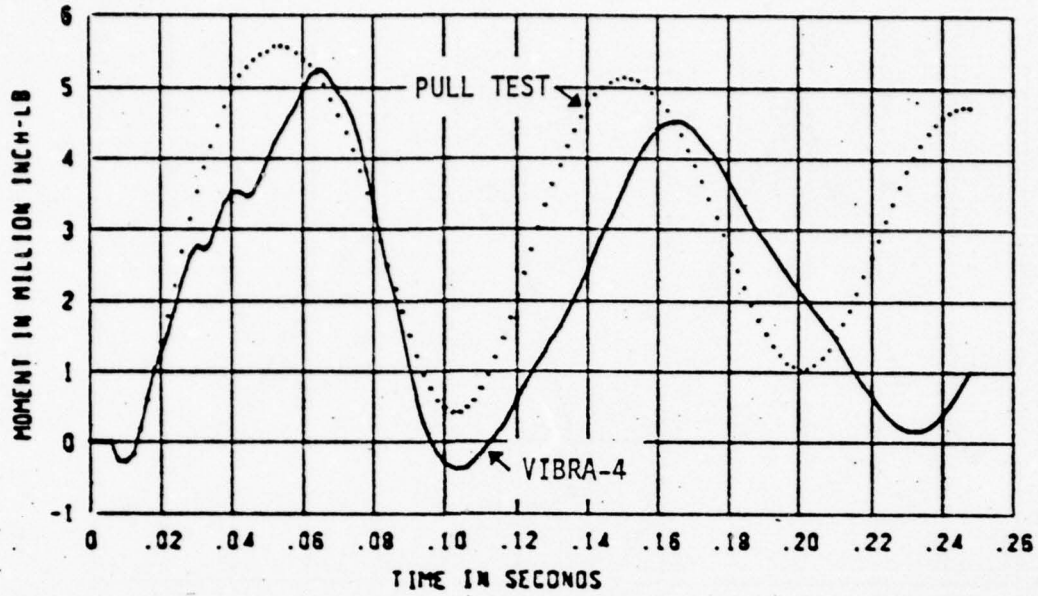


Figure 3-71 Bending Moment - Fin Dynamic Pull Test - Sta. 3

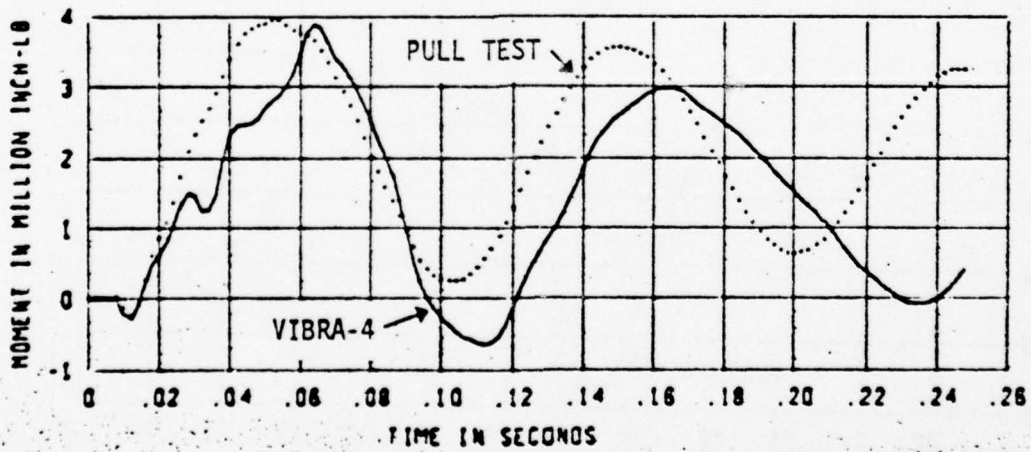
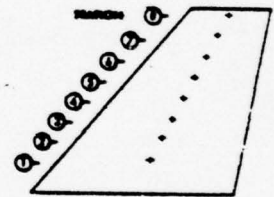


Figure 3-72 Bending Moment - Fin Dynamic Pull Test - Sta. 4

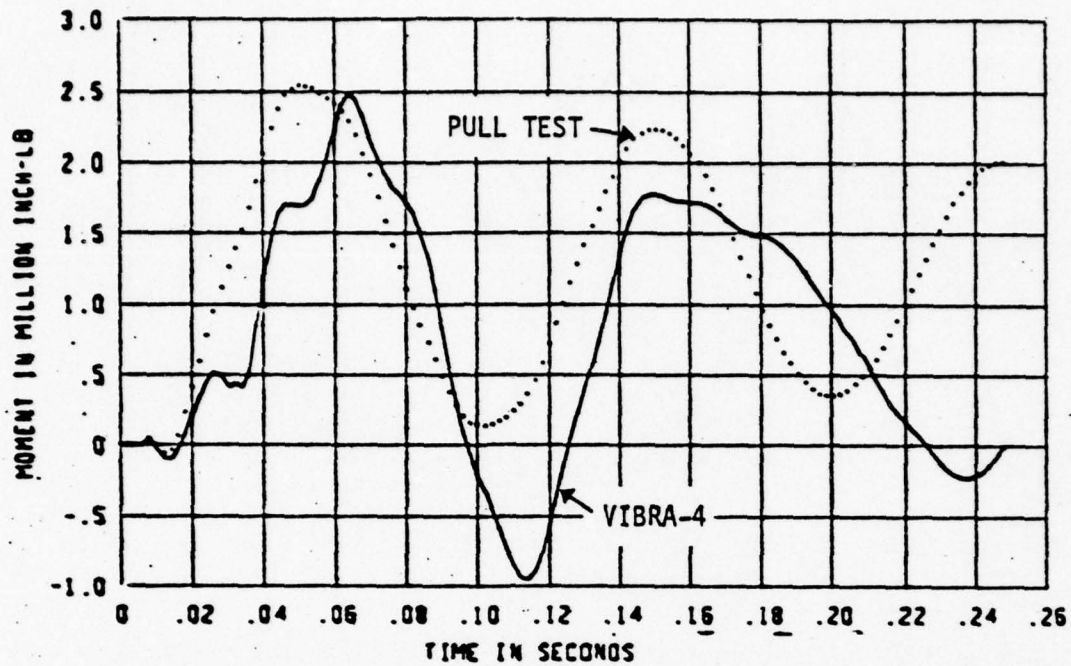


Figure 3-73 Bending Moment - Fin Dynamic Pull Test Sta. 5

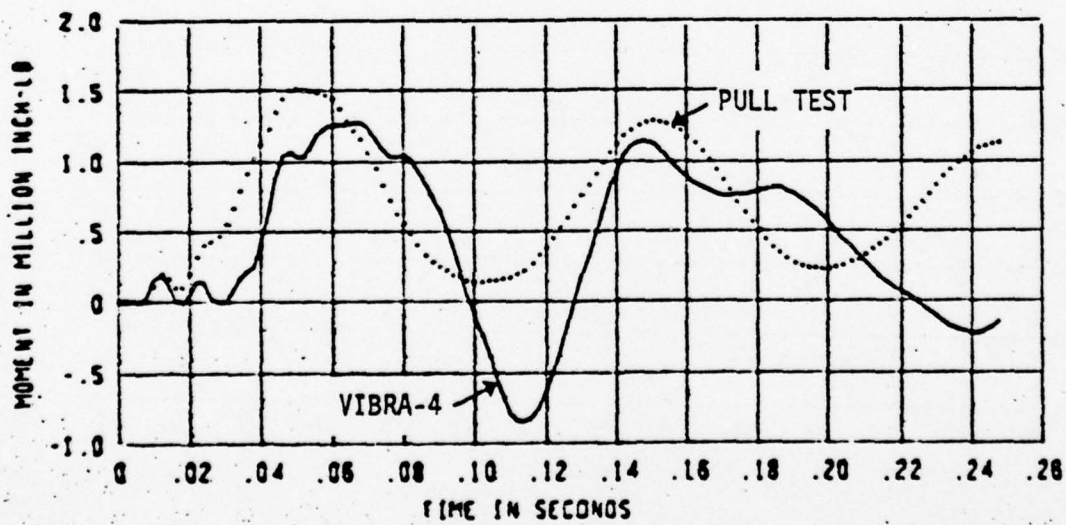
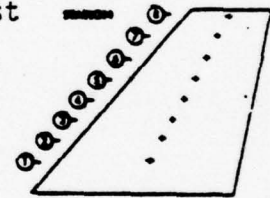


Figure 3-74 Bending Moment - Fin Dynamic Pull Test - Sta. 6

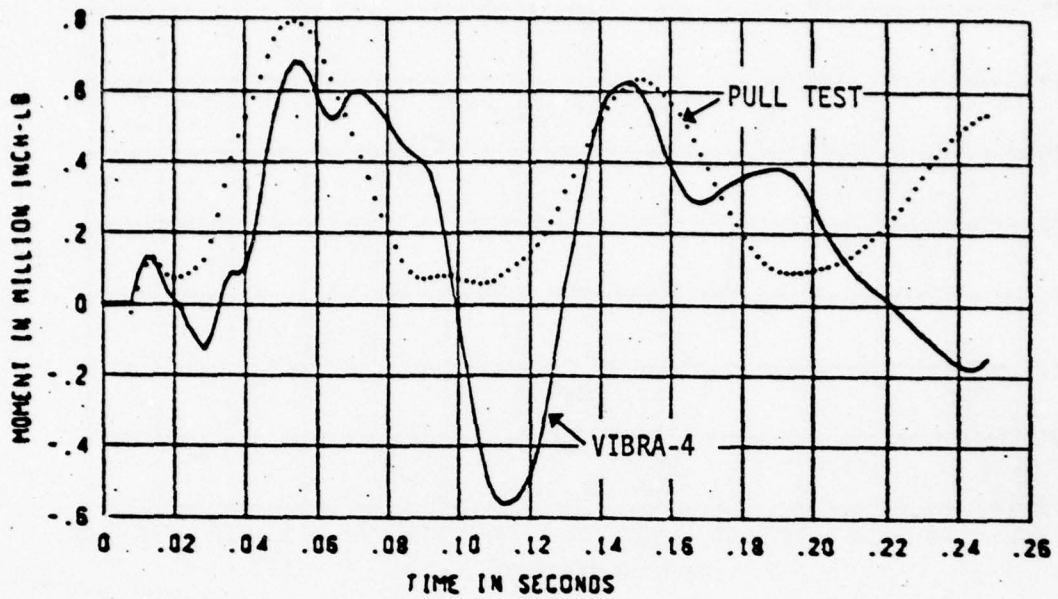


Figure 3-75 Bending Moment - Fin Dynamic Pull Test Sta. 7

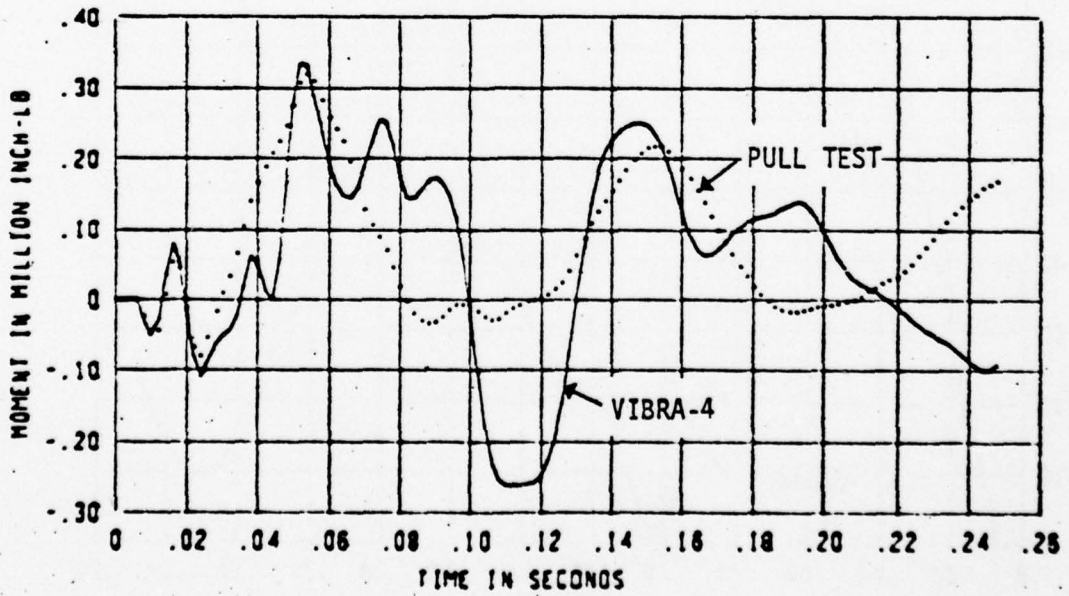
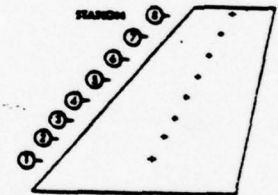


Figure 3-76 Bending Moment - Fin Dynamic Pull Test - Sta. 8

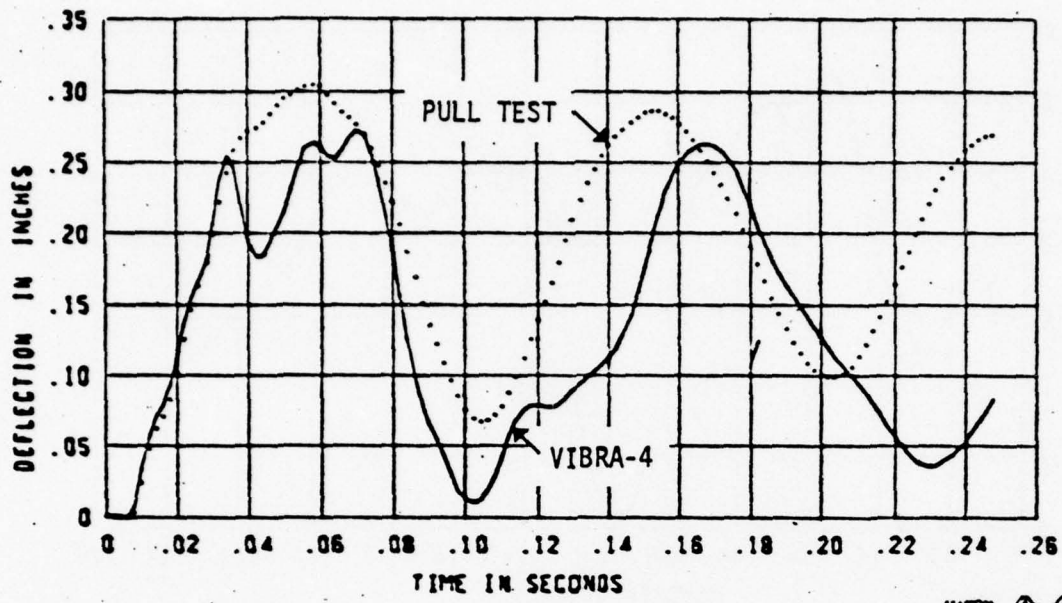


Figure 3-77 Relative Deflections - Fin Dynamic Pull Test - Sta. 1

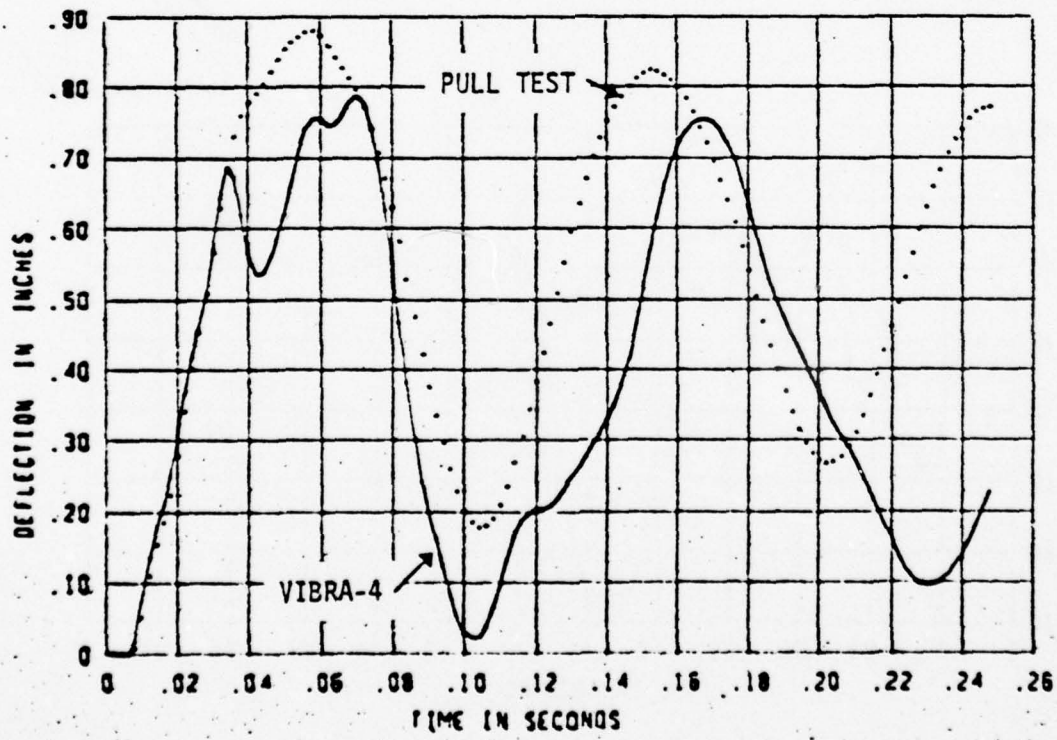
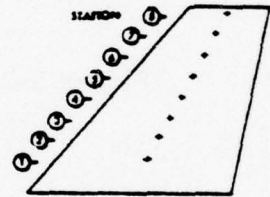


Figure 3-78 Relative Deflections - Fin Dynamic Pull Test - Sta. 2

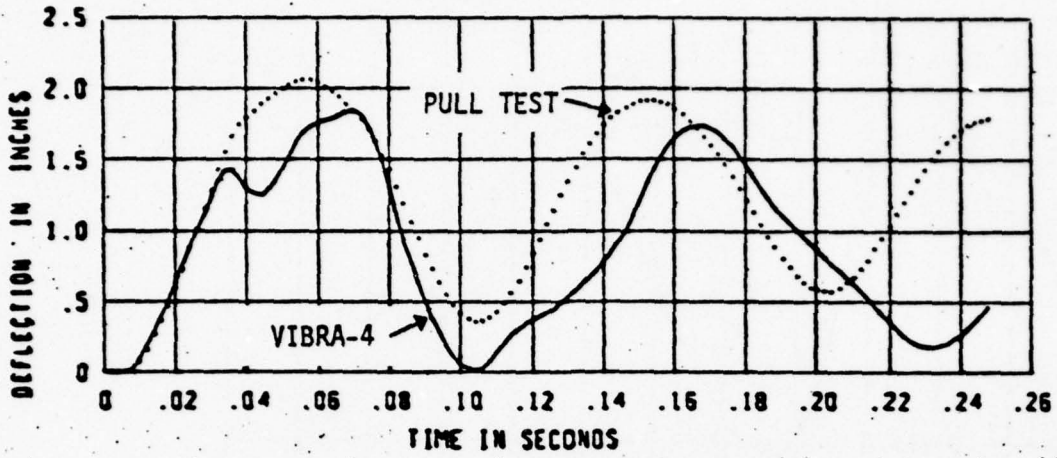


Figure 3-79 Relative Deflections - Fin Dynamic Pull Test - Sta. 3

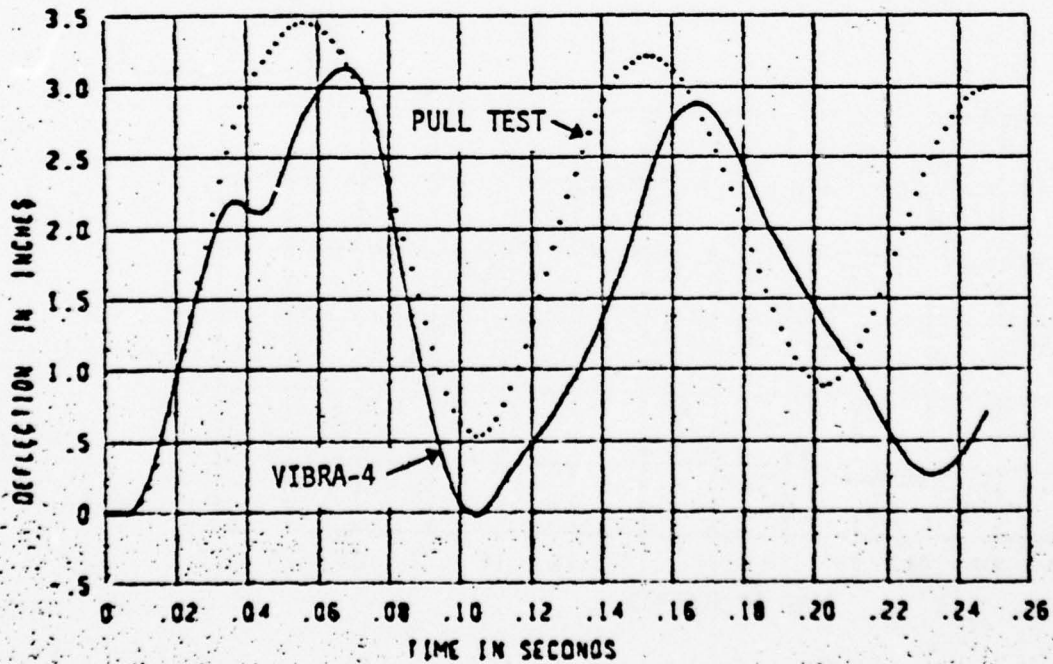
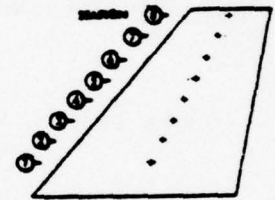


Figure 3-80 Relative Deflections - Fin Dynamic Pull Test - Sta. 4

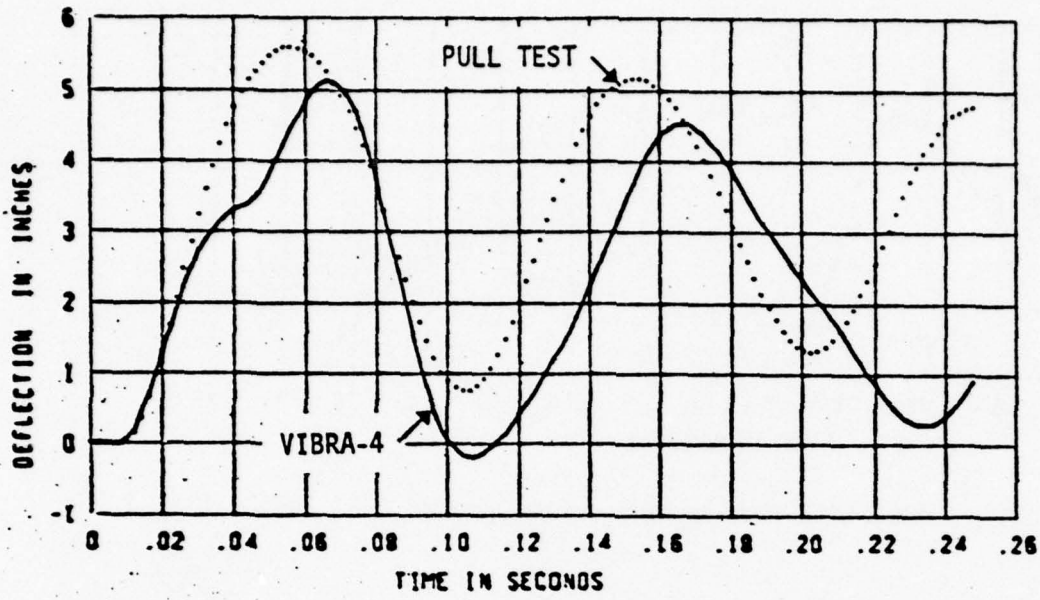


Figure 3-81 Relative Deflections - Fin Dynamic Pull Test - Sta. 5

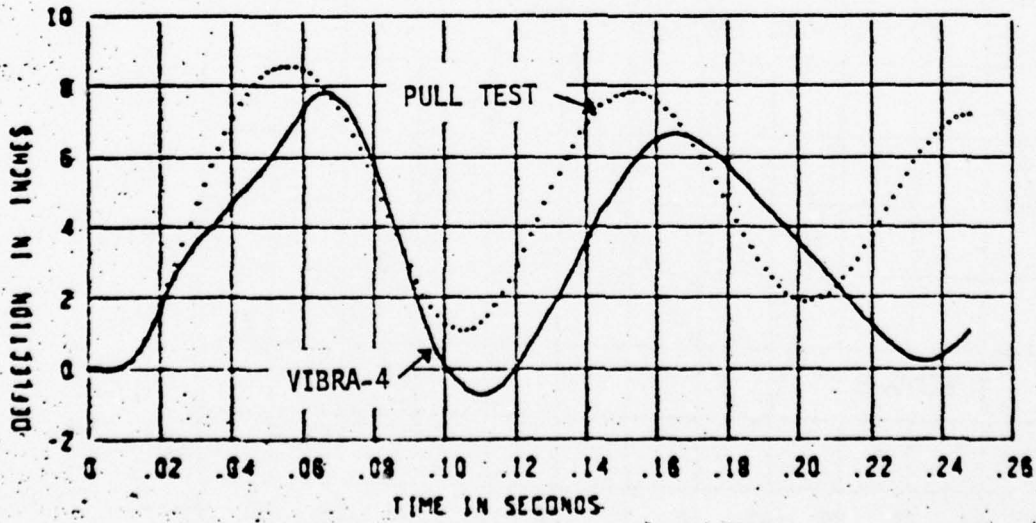
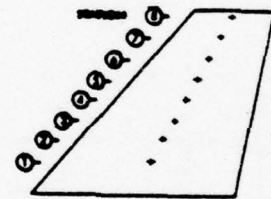


Figure 3-82 Relative Deflections - Fin Dynamic Pull Test - Sta. 6

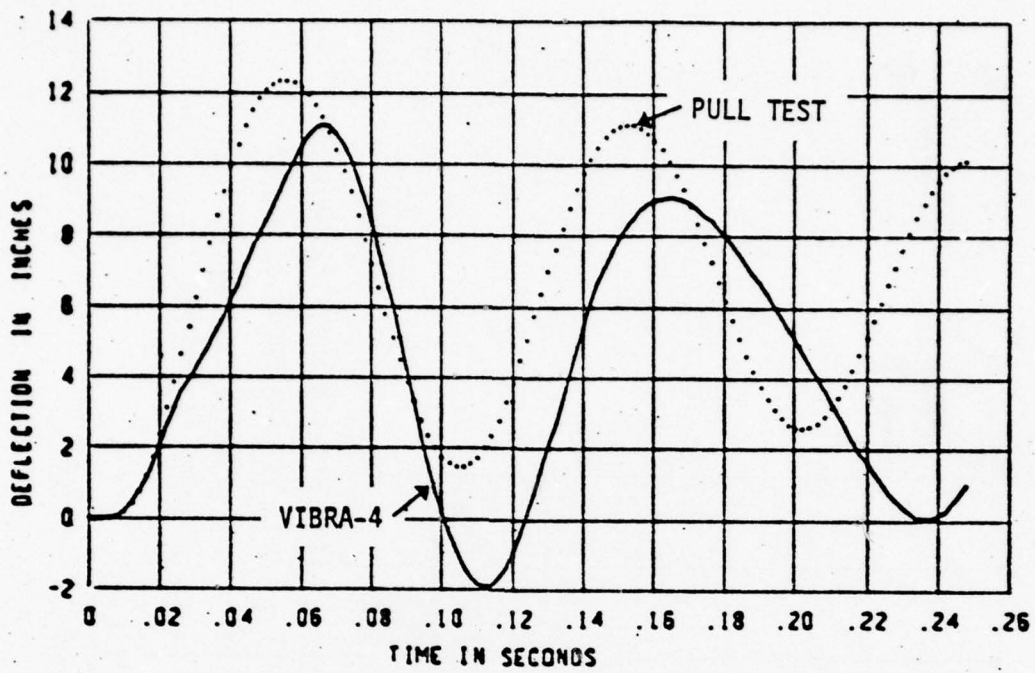


Figure 3-83 Relative Deflections - Fin Dynamic Pull Test - Sta. 7

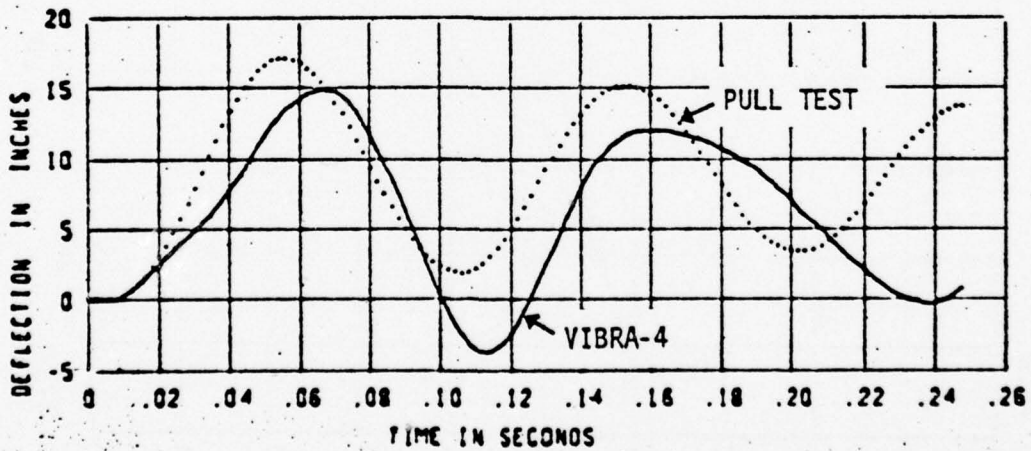
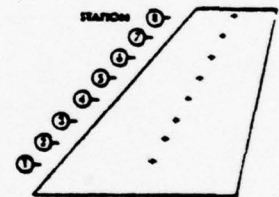


Figure 3-84 Relative Deflections - Fin Dynamic Pull Test - Sta. 8

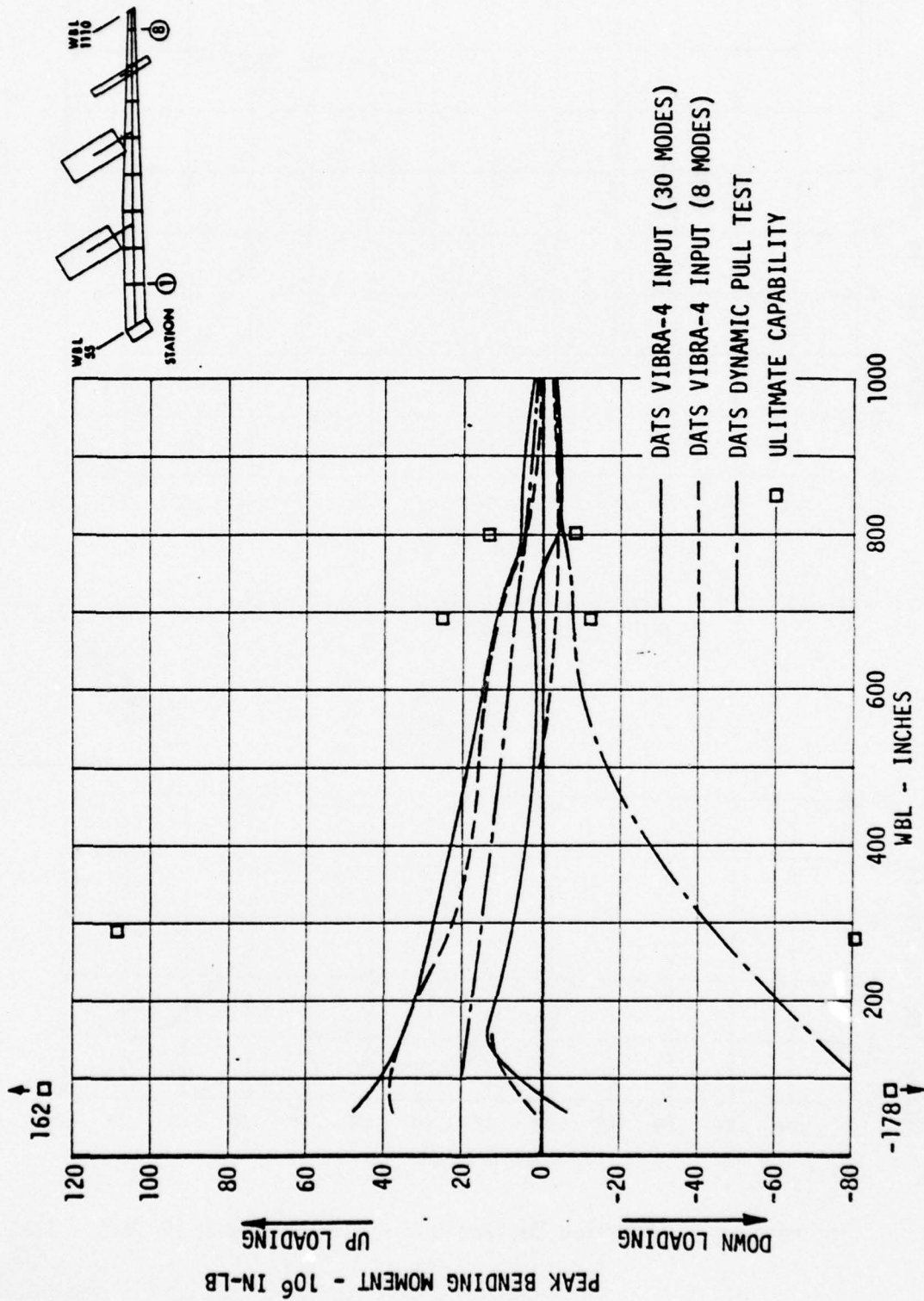


Figure 3-85 VIBRA-4 and DATS Peak Bending Moment Comparison - B-52 H Wing

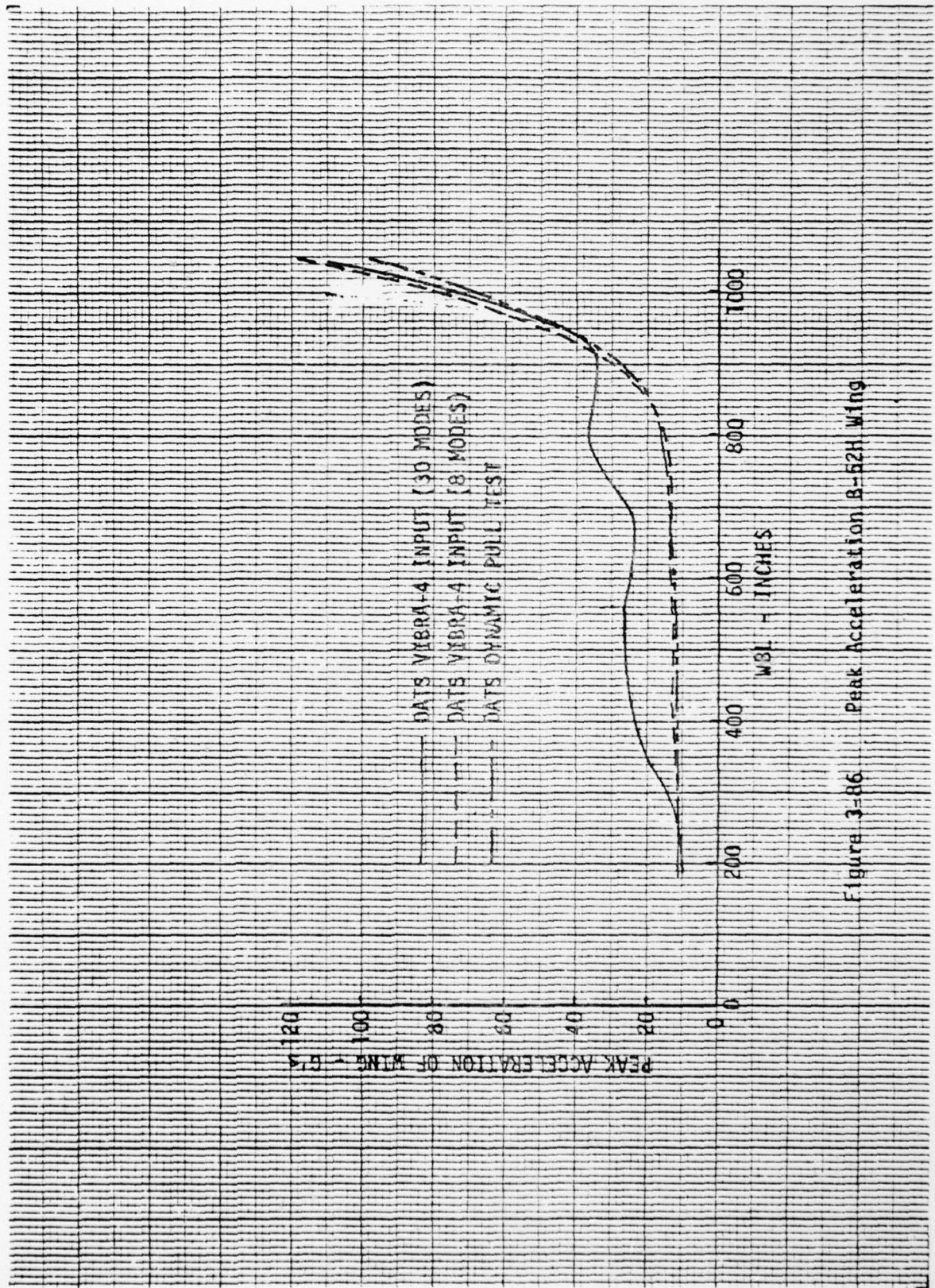


Figure 3-86 Peak Acceleration B-52H Wing

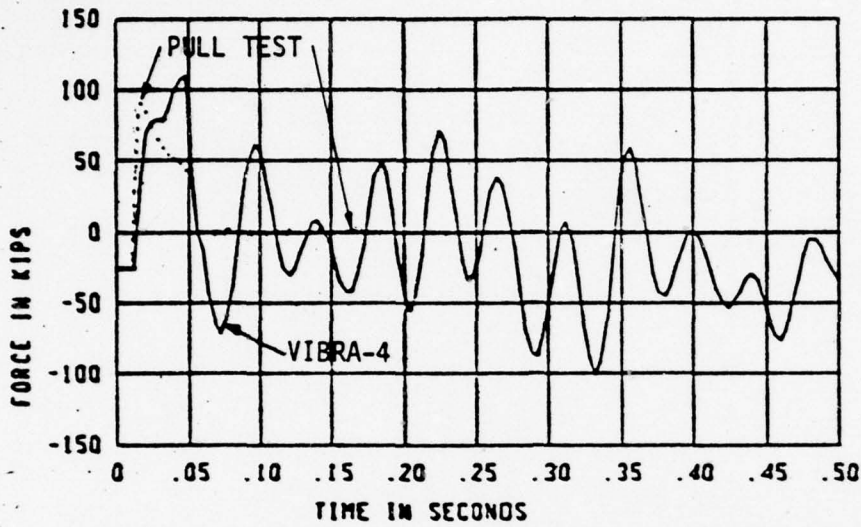


Figure 3-87 Test Loading - Wing Dynamic Pull Test, Sta 1

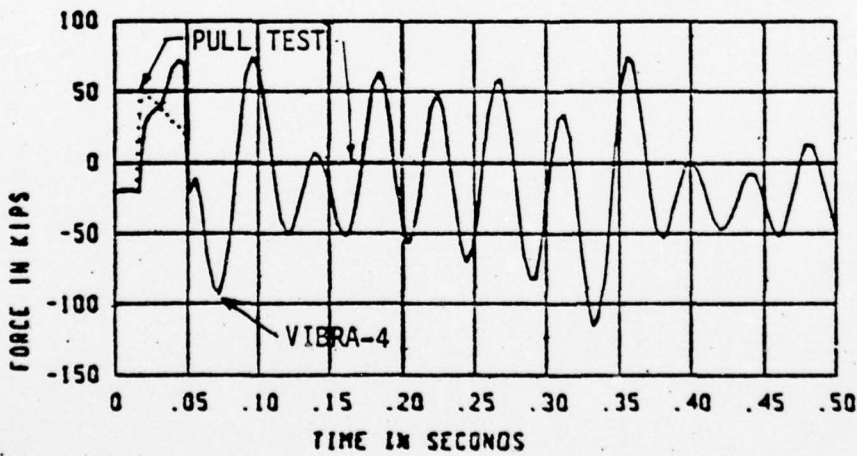
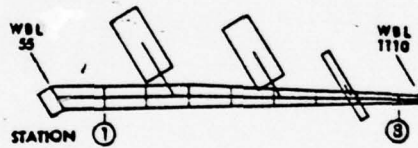


Figure 3-88 Test Loading - Wing Dynamic Pull Test, Sta 2

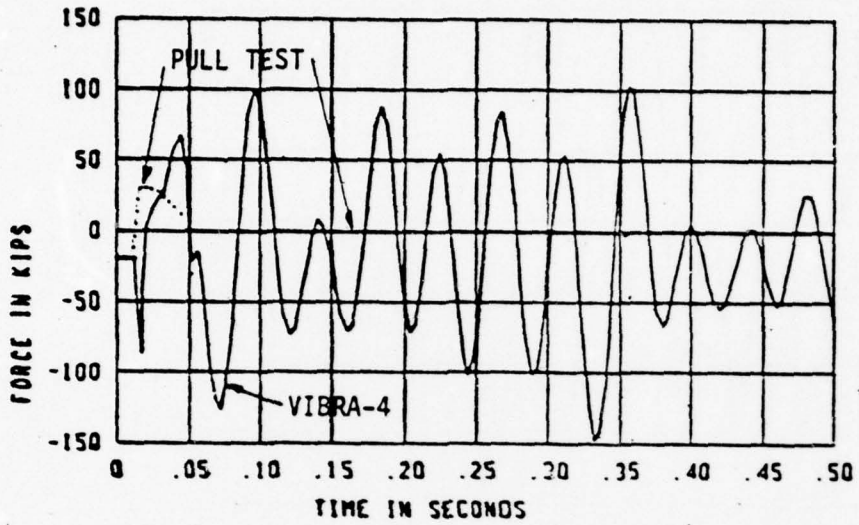


Figure 3-89 Test Loading - Wing Dynamic Pull Test, Sta 3

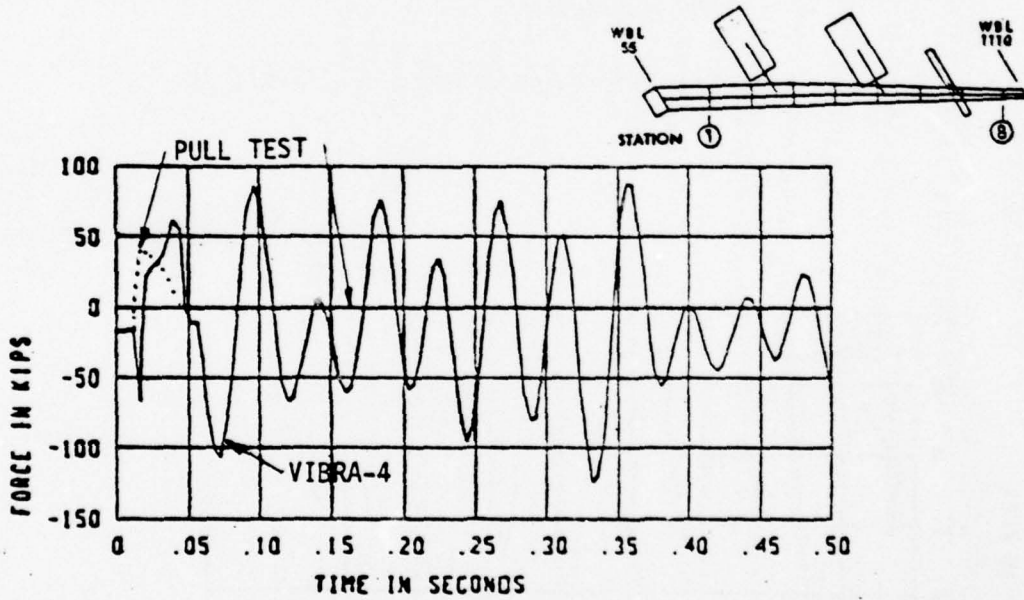


Figure 3-90 Test Loading - Wing Dynamic Pull Test, Sta 4

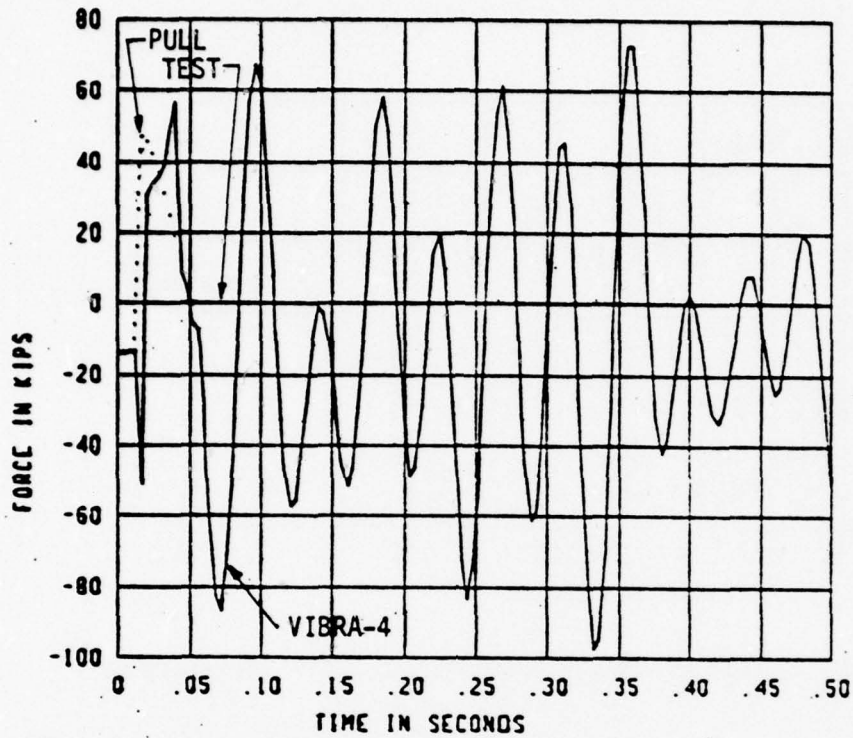


Figure 3-91 Test Loading - Wing Dynamic Pull Test, Sta 5

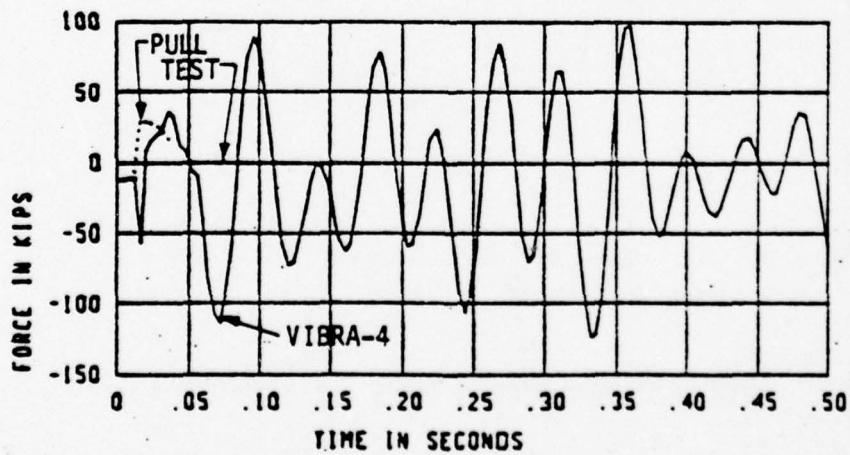
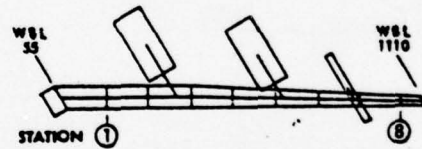


Figure 3-92 Test Loading - Wing Dynamic Pull Test, Sta 6

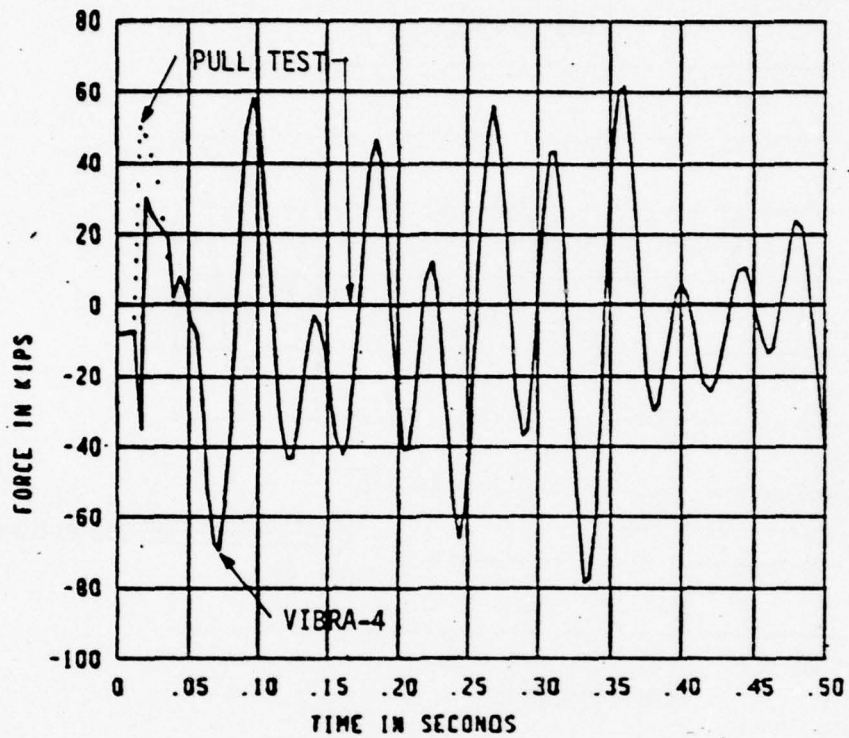


Figure 3-93 Test Loading - Wing Dynamic Pull Test, Sta 7

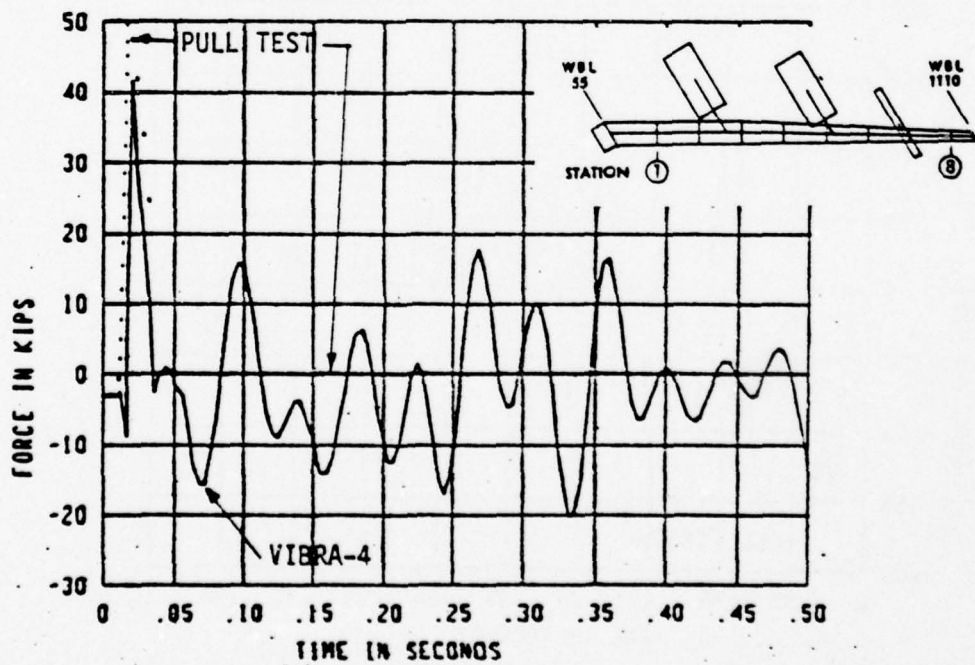


Figure 3-94 Test Loading - Wing Dynamic Pull Test, Sta 8

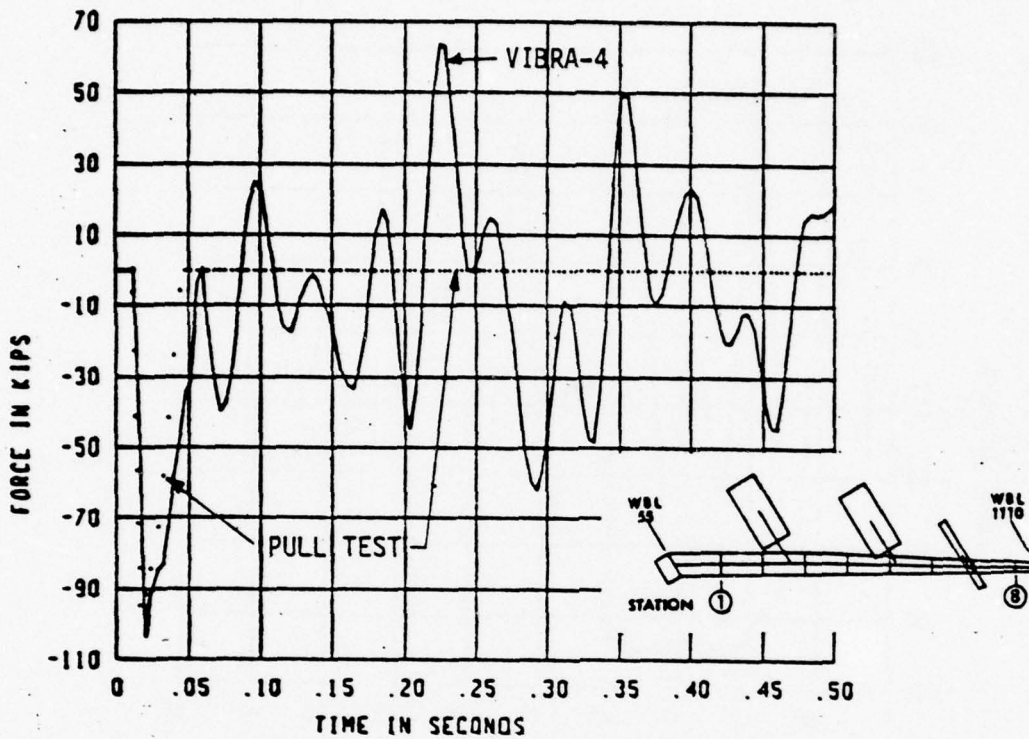


Figure 3-95 Test Loading - Wing Dynamic Pull Test, Sta 9

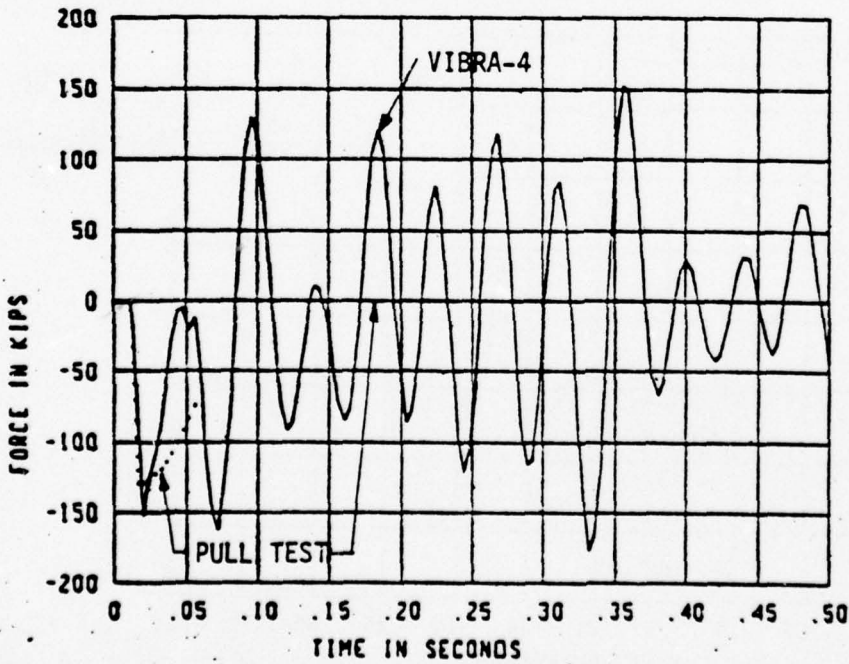


Figure 3-96 Test Loading - Wing Dynamic Pull Test, Sta 10

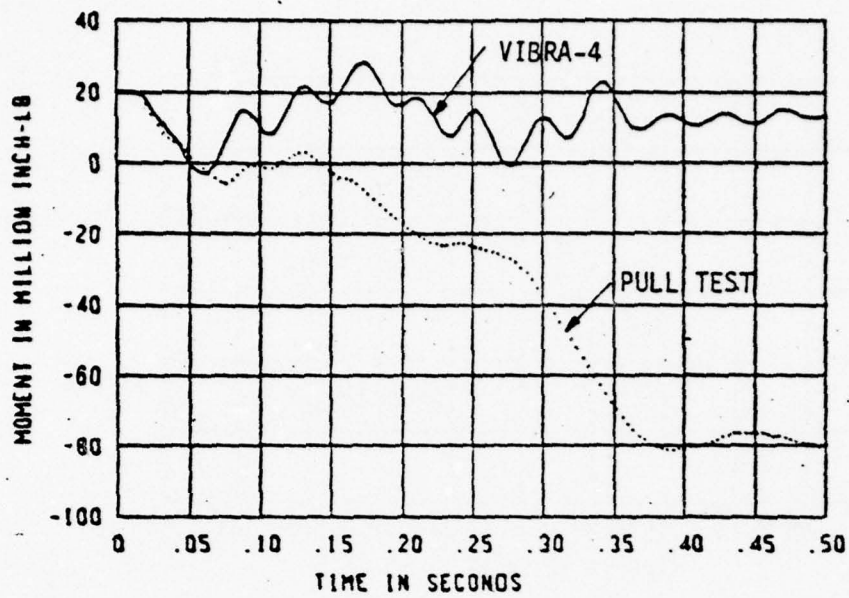


Figure 3-97 Bending Moments - Wing Dynamic Pull Test, Sta 1

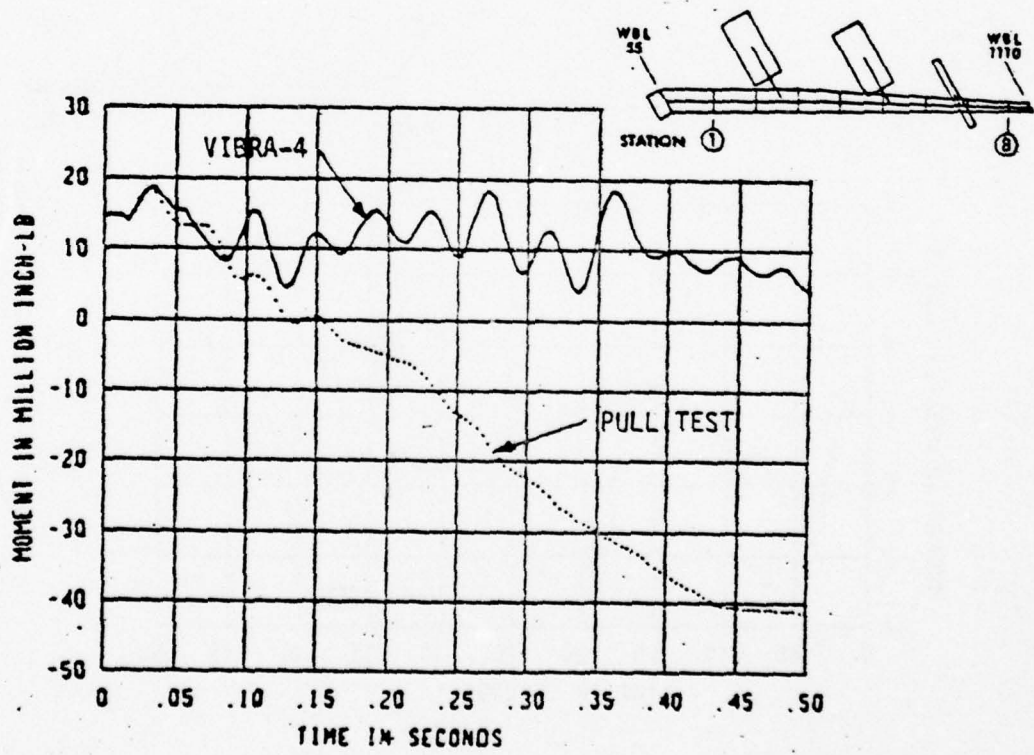


Figure 3-98 Bending Moments - Wing Dynamic Pull Test, Sta 2

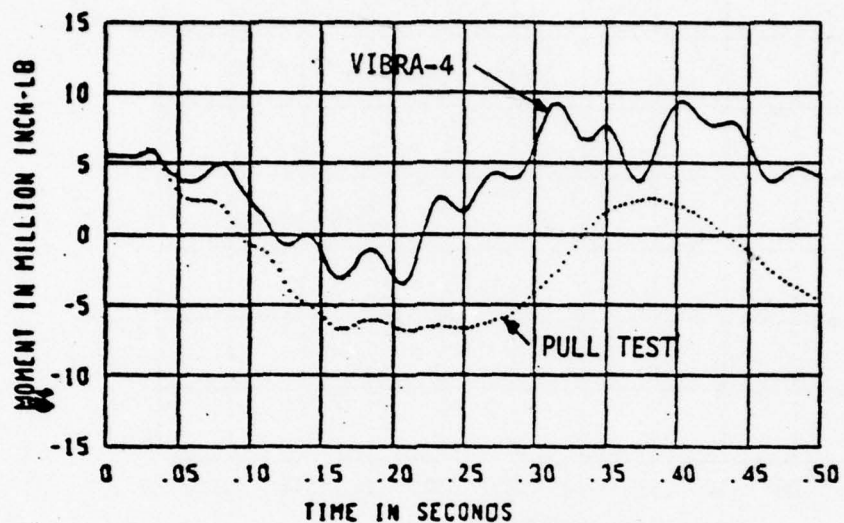


Figure 3-99 Bending Moments - Wing Dynamic Pull Test, Sta 3

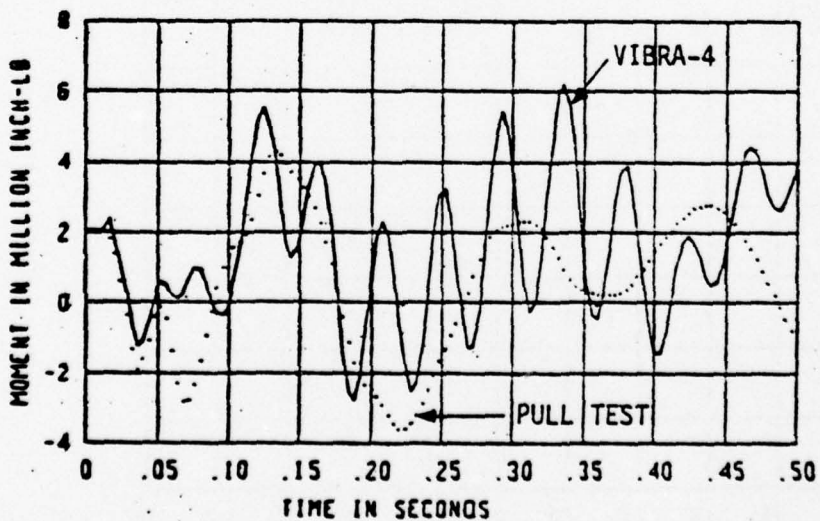
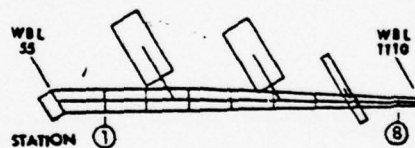


Figure 3-100 Bending Moments - Wing Dynamic Pull Test, Sta 4

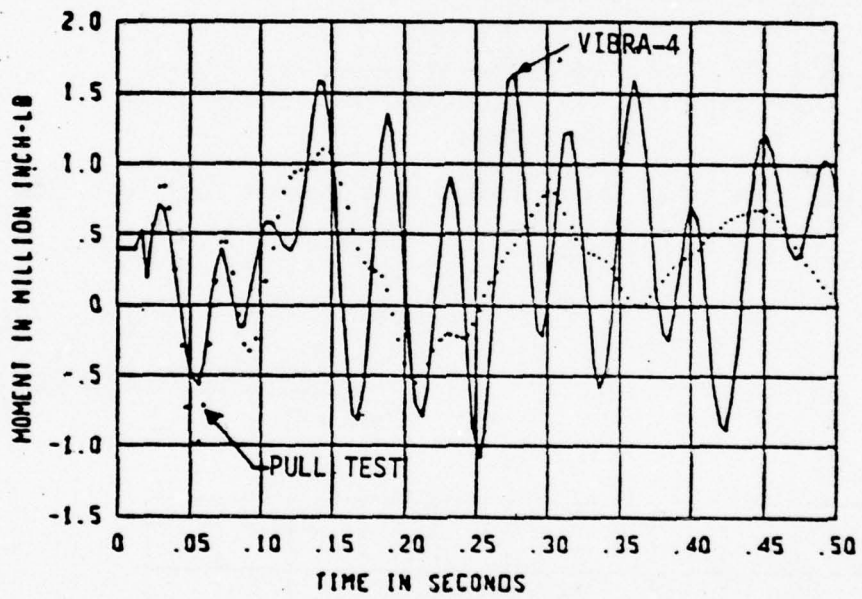
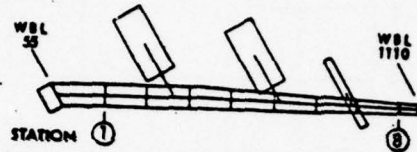


Figure 3-101 Bending Moments - Wing Dynamic Pull Test, Sta 5

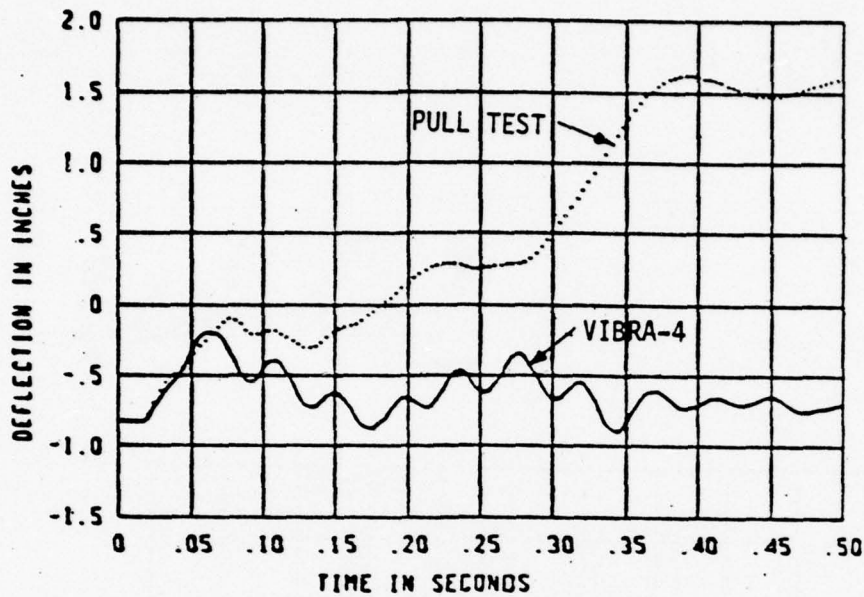


Figure 3-102 Relative Deflections - Wing Dynamic Pull Test, Sta 1

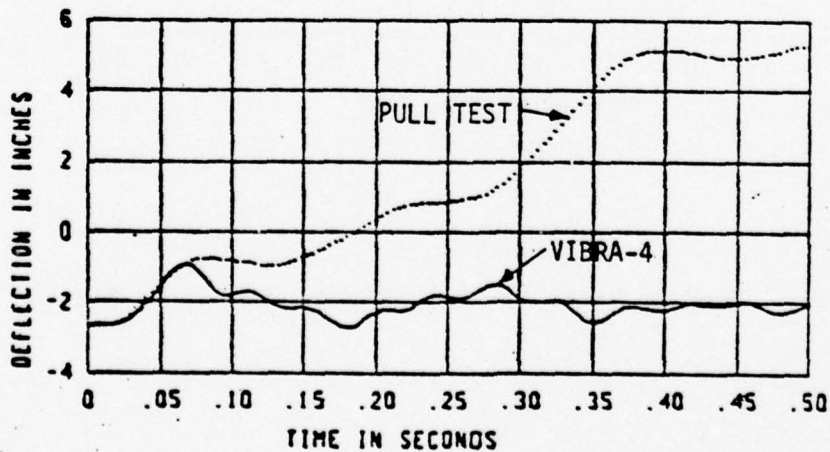
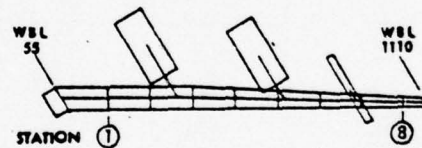


Figure 3-103 Relative Deflections - Wing Dynamic Pull Test, Sta 2

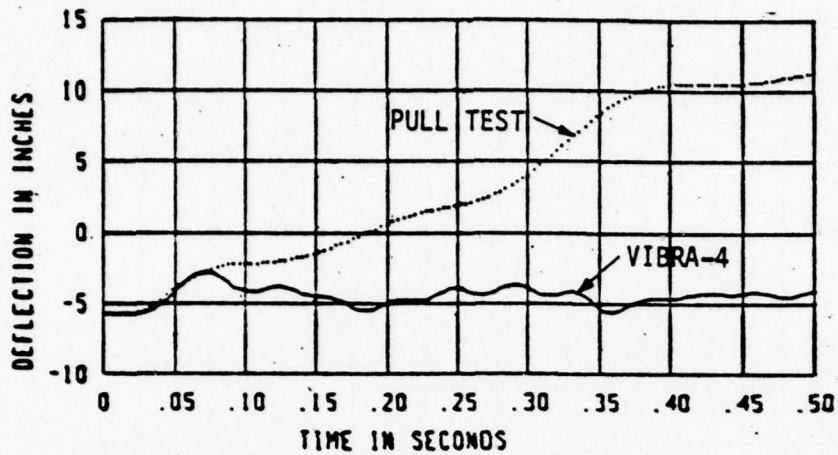


Figure 3-104 Relative Deflections - Wing Dynamic Pull Test, Sta 3

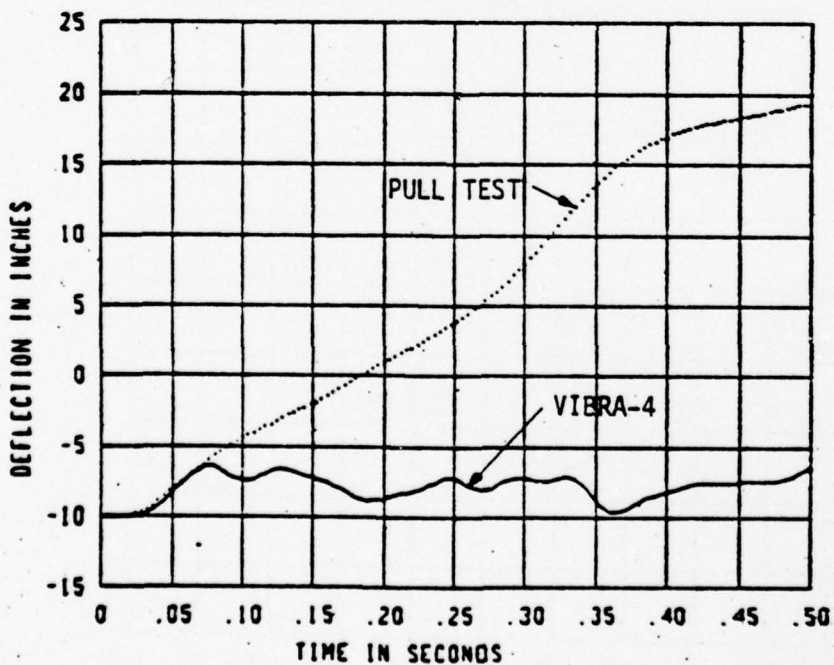
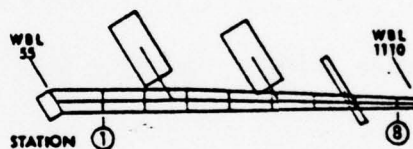


Figure 3-105 Relative Deflections - Wing Dynamic Pull Test, Sta 4

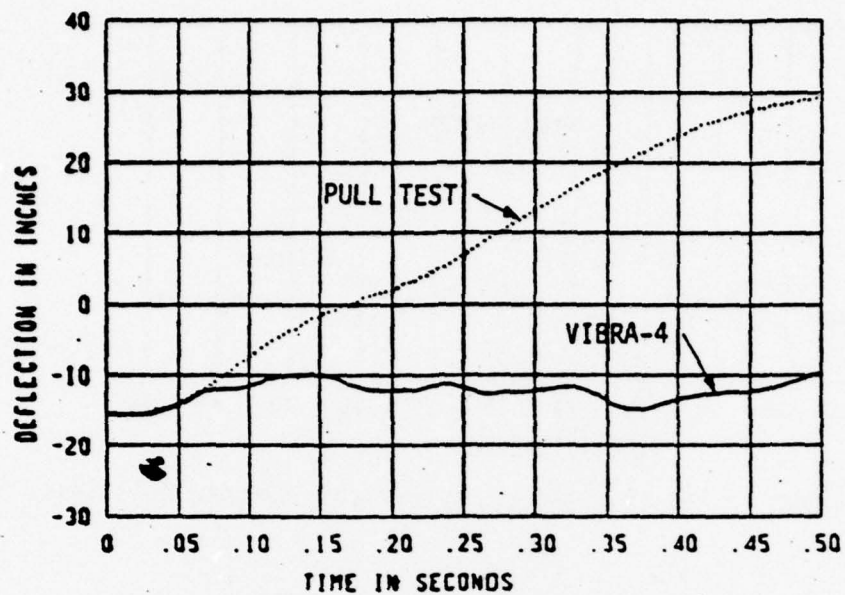


Figure 3-106 Relative Deflections - Wing Dynamic Pull Test, Sta 5

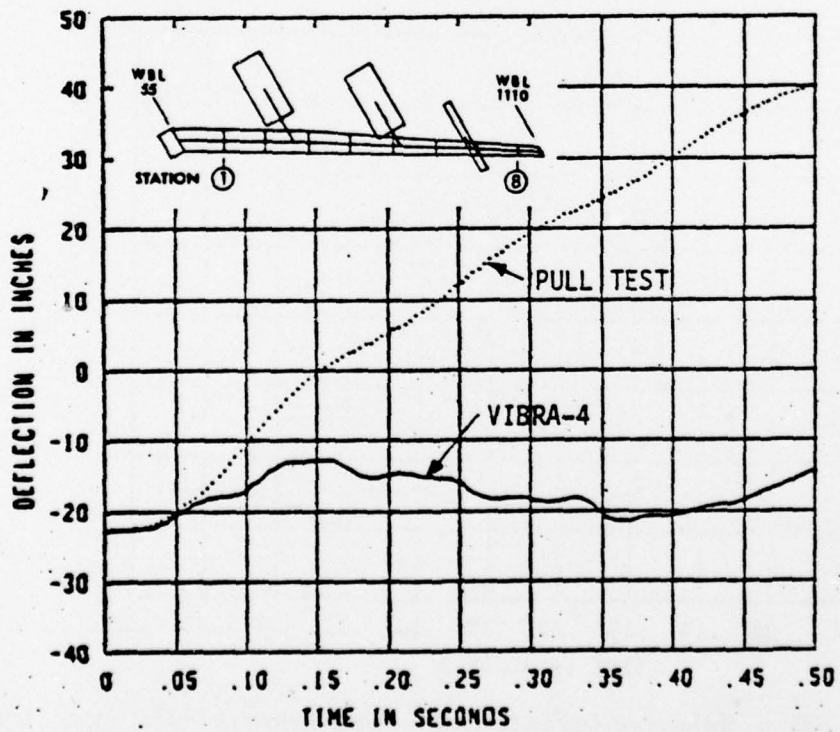


Figure 3-107 Relative Deflections - Wing Dynamic Pull Test, Sta 6

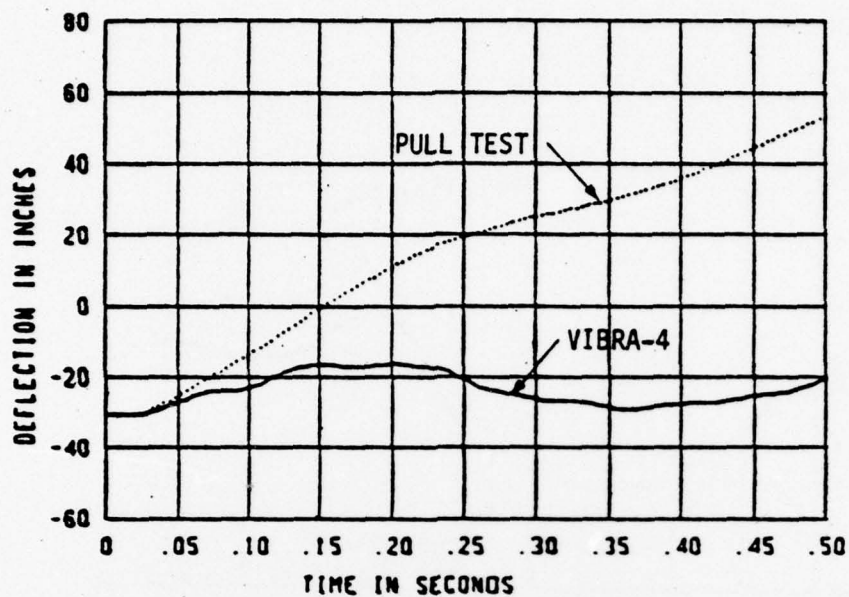


Figure 3-108 Relative Deflections - Wing Dynamic Pull Test, Sta 7

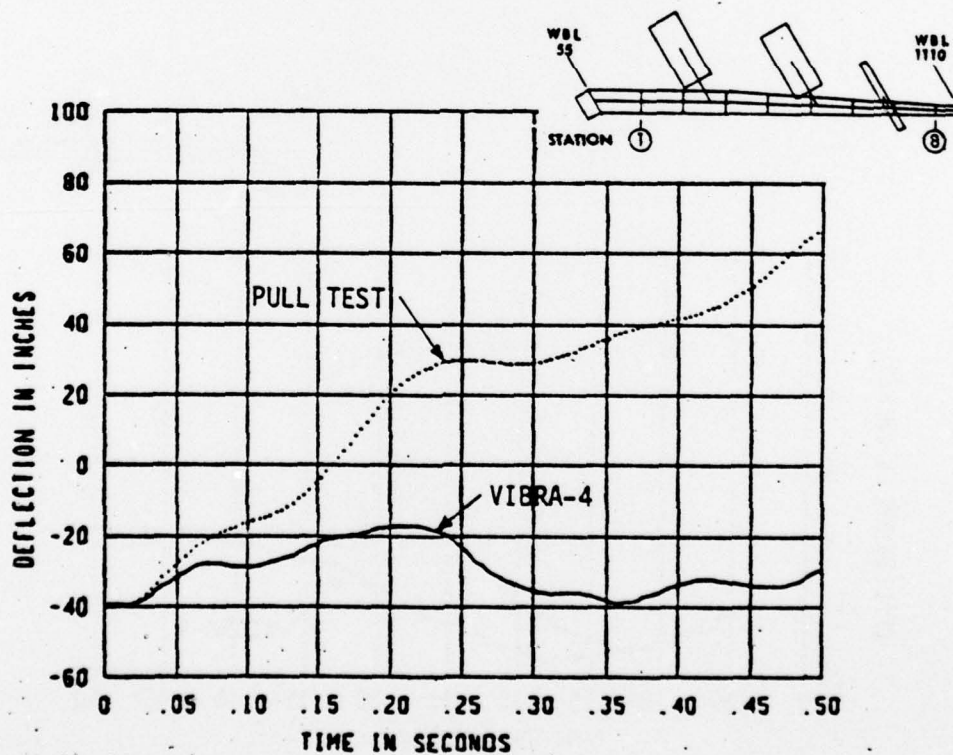


Figure 3-109 Relative Deflections - Wing Dynamic Pull Test, Sta 8

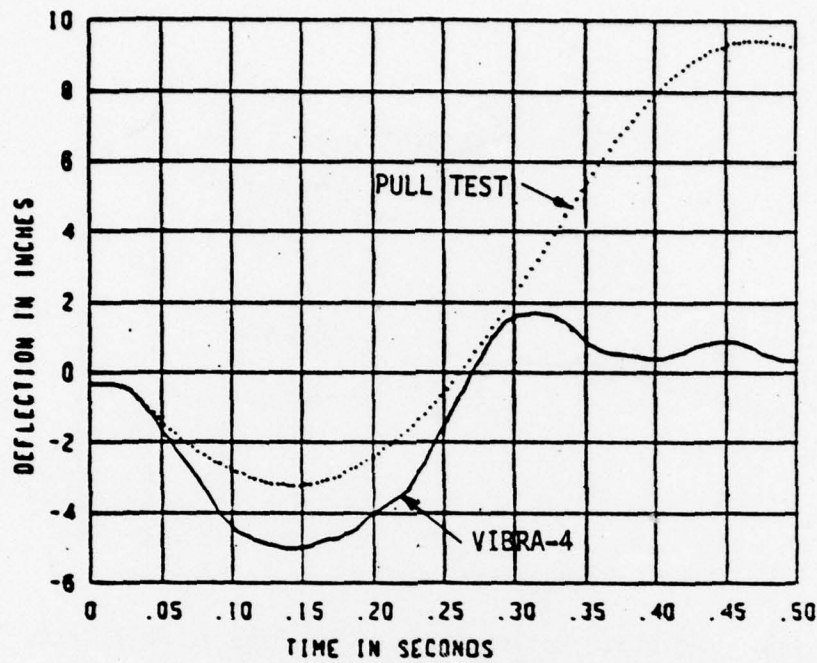


Figure 3-110 Relative Deflections - Wing Dynamic Pull Test, Sta 9

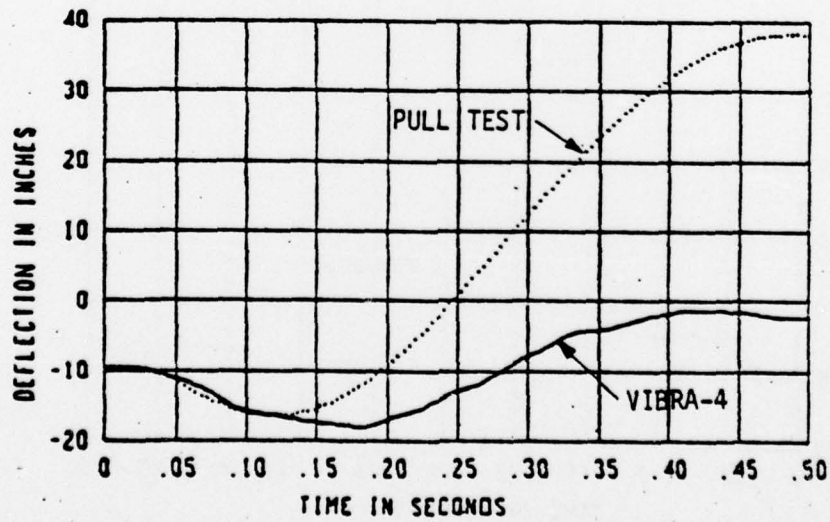
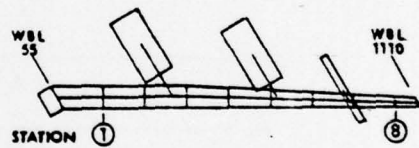


Figure 3-111 Relative Deflections - Wing Dynamic Pull Test, Sta 10

SECTION IV TEST CONFIGURATION

4.0 INTRODUCTION

A description of the physical test setup for both a base shake Fin dynamic test and a dynamic pull test on the fin are described in this section. A description of the dynamic pull test on the B-52H wing shown schematically in Figure 3-15 was not attempted since it appeared further work is required to define that test more completely. It would be similar to the fin dynamic pull test but more complex and larger.

4.1 DYNAMIC PULL TEST SETUP

A series of adjustable pneumatic springs are arranged to apply the simulated nuclear blast pressure loading to a major airplane structural component, i.e., a B-52 fin. See Figure 1-3 for test setup arrangement.

A B-52 fin will be attached to the face of the structural strong back (Bldg. 9-101) by a specially designed attach fitting which accommodates the fin production terminal fittings. The test loading system will consist of a cable sized to react the initial test preload and a pneumatic spring on the opposite side of the fin to apply the dynamic load environment. This arrangement is provided at 8 discrete fin stations. The load reaction system is equipped with a pyrotechnic powered cable cutter which will be energized by a signal from the firing control system. The pneumatic springs are existing hydraulic actuators sized to meet the load and stroke requirements for each fin load point as shown on Figure 4-1. Where necessary, these actuators may be fitted with lightweight rods/pistons to minimize the spring mass. Compressed air to each cylinder will be supplied by a pressure regulator. The remaining elements of the load system, i.e., load cell and connecting linkage, will also be of lightweight design at the fin stations where necessary.

A structural steel test fixture will be erected to react the applied test loads. Each actuator spring will be reacted into the structural floor rails through a load reaction beam.

4.1 (Continued)

In preparation for the tests, the load reaction cable system will be adjusted to position the test fin as required. Initial test loads will be applied through each pneumatic spring by adjusting the charging pressure. Spring rate may be varied by regulating the initial actuator volume.

An instrumentation and control system will provide test event sequence timing, ordnance firing control (cable cutters) and plate and data acquisition system initiation. Signal conditioning, tape and oscillograph recording, and "quick look" instrumentation will be provided to measure and record load, strain, acceleration and displacement on an appropriate time base.

A test setup physically similar to the pneumatic spring arrangement but using electro servo hydraulic controlled actuators to provide the desired load-time histories was examined. Because of the inherently high sensitivity-high flow requirements of the 4 outboard load stations, the approach was considered to be impractical.

4.2 BASE SHAKE-TEST SETUP

One of the 1.5 million pound load "prime movers" designed for Minuteman Missile Suspension System (MSS) testing is employed to provide a single programmable dynamic load input into the root of a B-52 fin. See Figure 1-1 for the test setup arrangement options.

The B-52 fin is mounted to an existing pivot fixture by a specially designed attach fitting which accommodates the fin production terminal fittings. Loading of the fin root is transmitted from the MSS prime mover into the pivot structure through a compression/tension member. This member has become necessary to best utilize the high load reaction capability of the MSS tower and to minimize test setup costs. Two options are possible. One requires the removal of the existing "squish towers" and incorporation of a 40 foot compression member to reach from the prime mover to the fin pivot fixture. The other option requires rotation of the prime mover 90° and addition of a rather short compression member.

The test loading is provided by the 1,500,000 lb. prime mover system. This design is a programmable open loop dynamic load source capable of applying a load-time history environment which may include compression (extension)

4.2 (Continued)

and tension (retraction) loading in sequence. The operation of the prime mover is dictated by a signal(s) from the firing control system.

Preparation for test requires configuring the pulse shaping accumulators and installation of the appropriate number and size of ordnance operated CONAX valves (2 in. or 5 in. dia.) on the prime mover. The start position of the fin is regulated by adjustment of the compression member length.

The instrumentation and control system performs and provides the same function as described in the preceding section; DYNAMIC PULL TEST SETUP. The exception is that the firing control here sequences the CONAX valve operation.

The prime mover dynamic response model described in detail in Ref. 5 was used to predict the motion input to the test fixture and to obtain the detailed actuator configuration (pressure, orifice spacing, valve size, etc.) associated with the input. The predicted velocity history input to the test fixture is compared to the idealized velocity history in Figure 4-2. This figure indicates that the prime mover is capable of providing the desired excitation to the B-52 fin which will result in fin loads consistent with those presented in section 3.3.1. The predicted waveform is characterized by a "scalloped" shape during the deceleration portion which is associated with the fluid flowing through a series of orifice plates with decreasing flow areas. It should be pointed out that the shock capability of the prime mover is much greater than that indicated by Figure 4-2. For example, the initial gaseous nitrogen charging pressure associated with the predicted waveform was only 600 psig compared to the prime mover capability of 5000 psig.

STA.	ACTUATOR*	PRE-LOAD (MAX) (KIP)	ORIG. PRESS P ₁ (PSI)	ORIG. VOL. V ₁ (IN ²)	FINAL PRESS P ₂ (PSI)	FINAL VOL. V ₂ (IN ²)	ROD DIA. (IN)	ACT. BORE (IN)	ROD & PISTON WEIGHT (lbs)
1	HL34-36C	15	2206	114	735	250	1.38	3.25	32
2	HL34-50C	20	2940	191	1618	293	1.38	3.25	38
3	HL34-50C	20	2940	235	2059	303	1.38	3.25	38
4	HL34-52C	20	2940	218	2324	259	1.38	3.25	39
5	HL34-60C	20	2940	239	2529	266	1.38	3.25	42
6	HL34-70C	20	2940	239	2529	266	1.38	3.25	46
7	M82-12	40	2440	96	1951	112	2.00	5.00	51
8	R104-18	60	2885	16	1442	27	3.23	6.07	109

*Actuator Identification No.

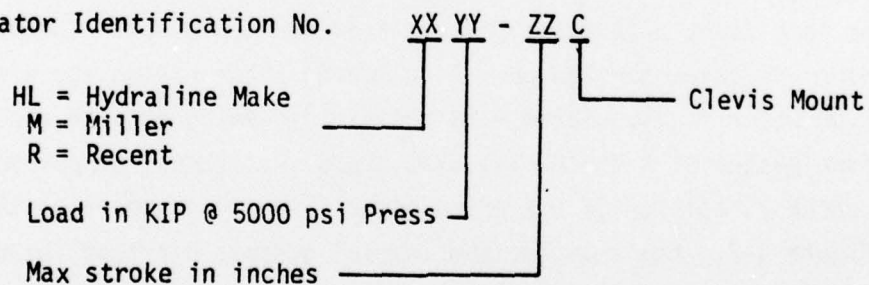


Figure 4-1 Dynamic Pull Test Actuator Data

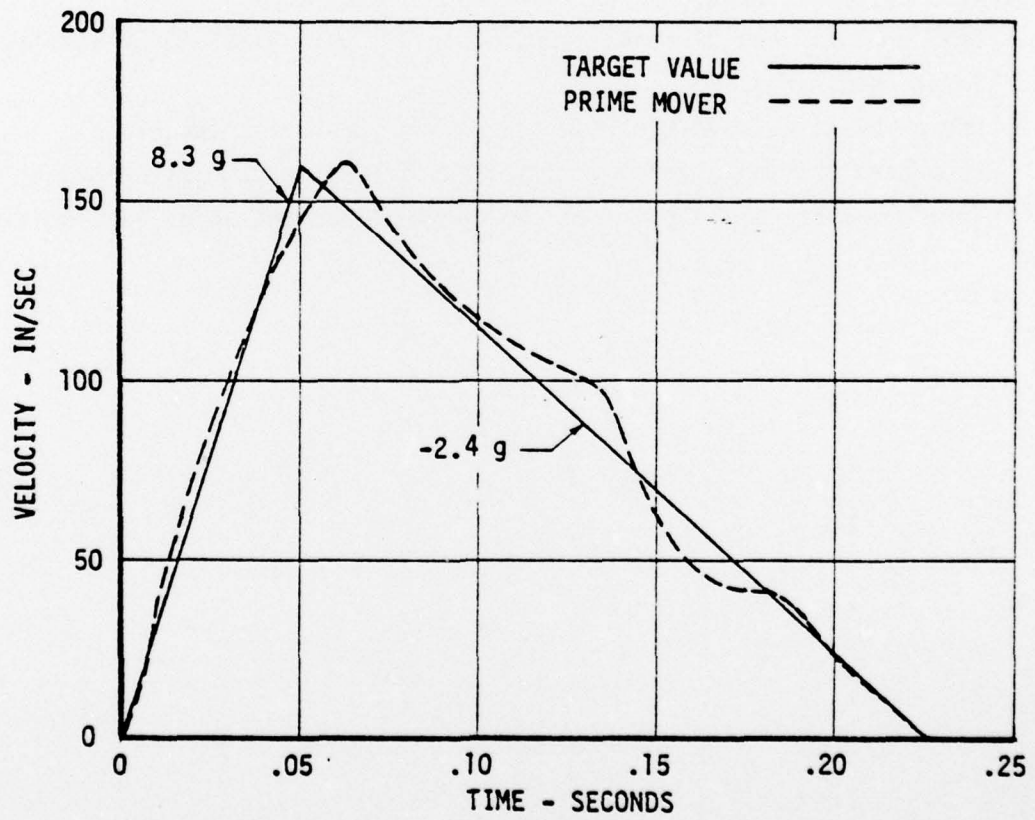


Figure 4-2 Base Shake Prime Mover Performance

SECTION V
CONCLUSIONS

1. Based on calculation results it appears feasible to perform tests on major aircraft structural components to simulate nuclear gust loads.
2. There are two feasible approaches for fin tests, either a base shake or a dynamic pull test. Both give good maximum moment correlation. The dynamic pull test gives a better time history signature.
3. The dynamic pull test appears feasible to test critical areas of the wing. It does not give good bending moment comparison in the less critical inboard areas.
4. DATS analysis calculations compare closely with VIBRA-4 for similar input conditions.
5. Use of blast aerodynamic loading only for test of a structural component produce severe overload, thus, test loads must be modified to account for the structural component attachment point acceleration.

SECTION VI
RECOMMENDATION

1. Develop a better test method for the wing either by testing only the outboard section or refining the dynamic pull test mechanism to give better overall moment correlation.
2. Make trades between a base shake and a dynamic pull test on the fin so a selection can be made between these two methods.
3. Update test method feasibility for simulating VIBRA-6 calculated responses. Modify test methods if required.
4. Conduct a hardware test to demonstrate test feasibility and to evaluate a typical hardware item.

SECTION VII
REFERENCES

1. AFWL-TR-70-140 Vol. 1, "A Digital Computer Program for Calculating The Blast Response of Aircraft to Nuclear Explosions", N. P. Hobbs, G. Zartarian, J. P. Walsh, April 1971, Air Force Special Weapons Center, New Mexico, 87117.
2. AFWL-TR-72-197 Vol. I, "Analytical Models for the B-52H, EC-135A, and 747-200 Aircraft", G. S. Shoup, September 1973, Air Force Weapons Laboratory, New Mexico, 87117.
3. AFWL-TR-72-197 Vol. II, "Analytical Models for the B-52H, EC-135A, and 747-200 Aircraft", G. S. Shoup, July 1973, Air Force Weapons Laboratory, New Mexico, 87117.
4. AFWL-TR-72-197 Vol. III, "Analytical Models for the B-52H, EC-135A, and 747-200 Aircraft", R. D. Miller, June 1973, Air Force Weapons Laboratory, New Mexico, 87117.
5. D2-26571-1, "Minuteman Shock Test Prime Mover - Analysis Model", G. R. Burwell, August 1974, Boeing, Seattle.
6. D3-9271, "Specification - B-52D Wing Proof Load Program CCP 1619", Boeing Structures Staff, November 1974, Wichita.
7. T3-1422, "Static Test Results - B-52 C-F (ECP-1128K) Body and Empennage, and Wing Center Section", J. E. Zimmerman, August 1966, Boeing, Wichita.
8. Private Communication, L. Contreras, R. Mielbrecht, et. al., March 1965, The Boeing Aerospace Company, Seattle.
9. DNA 2048 H-1, Handbook for Analysis of Nuclear Weapon Effects on Aircraft, Volumes I and II, Staff of Kaman Avidyne, March 18, 1976, Burlington, MA 01803.

10. AFWL-TR-76-210, Nuclear Blast Response Computer Program VIBRA-6 Vol. I, J. A. McGrew, et. al., To be Published, Douglas Aircraft Corp. for Air Force Special Weapons Center, New Mexico, 87117.
11. American Defense Preparedness Association Symposium on Vulnerability, Survivability, "Scaling Gust Vulnerability Contours of In-Flight Aircraft", Stephen M. Matthews, October 27, 1976, Lawrence Livermore Laboratory, Livermore, Ca.

DISTRIBUTION LIST

DEPARTMENT OF DEFENSE

Director
Defense Nuclear Agency
ATTN: STSP
ATTN: SPAS
ATTN: DDST
ATTN: TISI Archives
3 cy ATTN: TITL Tech. Library

Under Sec'y of Def. for Rsch. & Engrg.
Department of Defense
ATTN: S&SS (OS)

Commander
FCDNA
ATTN: FCPR

Chief
Livermore Div., FCDNA
ATTN: FCPRL

DDC
Cameron Station
12 cy ATTN: TC

DEPARTMENT OF ARMY

Commander
Harry Diamond Laboratories
ATTN: DRXDO-RBH, James H. Gwaltney
ATTN: DRXDO-NP

Director
U.S. Army Ballistic Research Labs.
ATTN: DRXBR-X, Julius J. Meszaros

Commander
U.S. Army Materiel Dev. & Readiness Cmd.
ATTN: DRCDE-D, Lawrence Flynn

Commander
U.S. Army Nuclear Agency
ATTN: COL Deverill
ATTN: MAJ J. Vecke

DEPARTMENT OF NAVY

Chief of Naval Material
ATTN: Mat. 0323

Chief of Naval Research
ATTN: Code 464, Thomas P. Quinn

Director
Naval Research Laboratory
ATTN: Code 2600, Tech. Lib.

Officer-in-Charge
Naval Surface Weapons Center
ATTN: Ken Caudle

Commanding Officer
Naval Weapons Evaluation Facility
ATTN: Peter Hughes

DEPARTMENT OF NAVY (Continued)

Director
Strategic Systems Project Office
ATTN: NSP-272

DEPARTMENT OF THE AIR FORCE

AF Materials Laboratory, AFSC
ATTN: MBC, Donald L. Schmidt
ATTN: MBE

AF Weapons Laboratory, AFSC
ATTN: DYV, Lt Col Rensvold
ATTN: SUL

Commander
ASD
4 cy ATTN: ENFS, D. Ward

Commander
Foreign Technology Division, AFSC
ATTN: PDBF, Mr. Spring

Commander In Chief
Strategic Air Command
ATTN: XPFS

DEPARTMENT OF ENERGY

Sandia Laboratories
ATTN: Doc. Control for D. McCloskey

DEPARTMENT OF DEFENSE CONTRACTORS

Aerospace Corporation
ATTN: W. Barry

Avco Research & Systems Group
ATTN: William Broding
ATTN: J. Patrick

The Boeing Company
ATTN: Ed York
ATTN: Robert Dyrdaahl
ATTN: David M. Eckbiad
ATTN: Nelson E. Funston

Boeing Wichita Company
ATTN: R. Syring
ATTN: D. Pierson

Effects Technology, Inc.
ATTN: Richard Parris

General Dynamics Corp.
Fort Worth Division
ATTN: R. Shemensky

General Electric Company
TEMPO-Center for Advanced Studies
ATTN: DASIAC

Kaman Avidyne
Division of Kaman Sciences Corp.
ATTN: Norman P. Hobbs

DEPARTMENT OF DEFENSE CONTRACTORS (Continued)

Kaman Sciences Corporation
ATTN: Donald C. Sachs

Martin Marietta Corporation
Orlando Division
ATTN: Gene Aiello

McDonnell Douglas Corporation
ATTN: J. McGrew

Northrop Corporation
ATTN: Don Hicks

Prototype Development Associates, Inc.
ATTN: John McDonald

DEPARTMENT OF DEFENSE CONTRACTORS (Continued)

R & D Associates
ATTN: Albert L. Latter
ATTN: F. A. Field
ATTN: Jerry Carpenter

Rockwell International Corporation
ATTN: R. Sparling

Science Applications, Inc.
ATTN: Dwane Hove

SRI International
ATTN: George R. Abrahamson